NOAA OAR Special Report

PMEL Tsunami Forecast Series: Vol. NN

A Tsunami Forecast Model for Portland, Maine

Michael C. Spillane[1,2]

[1]Joint Institute for the Study of the Atmosphere and Ocean (JISAO), University of Washington, Seattle, WA

[2]NOAA/Pacific Marine Environmental Laboratory (PMEL), Seattle, WA

April 22, 2015

NOTICE from NOAA

Mention of a commercial company or product does not constitute an endorsement by NOAA/OAR. Use of information from this publication concerning proprietary products or the tests of such products for publicity or advertising purposes is not authorized. Any opinions, findings, and conclusions or recommendations expressed in this material are those of the authors and do not necessarily reflect the views of the National Oceanic and Atmospheric Administration.

Contribution No. 3387 from NOAA/Pacific Marine Environmental Laboratory
Contribution No. 2086 from Joint Institute for the Study of the Atmosphere and Ocean (JISAO)

Also available from the National Technical Information Service (NTIS)
(http://www.ntis.gov)

Contents

List of Figures

List of Tables

Foreword

Tsunamis have been recognized as a potential hazard to United States coastal communities since the mid-twentieth century, when multiple destructive tsunamis caused damage to the states of Hawaii, Alaska, California, Oregon, and Washington. In response to these events, the United States, under the auspices of the National Oceanic and Atmospheric Administration (NOAA), established the Pacific and Alaska Tsunami Warning Centers, dedicated to protecting United States interests from the threat posed by tsunamis. NOAA also created a tsunami research program at the Pacific Marine Environmental Laboratory (PMEL) to develop improved warning products.

The scale of destruction and unprecedented loss of life following the December 2004 Sumatra tsunami served as the catalyst to refocus efforts in the United States on reducing tsunami vulnerability of coastal communities, and on 20 December 2006, the United States Congress passed the "Tsunami Warning and Education Act" under which education and warning activities were thereafter specified and mandated. A "tsunami forecasting capability based on models and measurements, including tsunami inundation models and maps..." is a central component for the protection of United States coastlines from the threat posed by tsunamis. The forecasting capability for each community described in the PMEL Tsunami Forecast Series is the result of collaboration between the National Oceanic and Atmospheric Administration office of Oceanic and Atmospheric Research, National Weather Service, National Ocean Service, National Environmental Satellite, Data, and Information Service, the University of Washington's Joint Institute for the Study of the Atmosphere and Ocean, National Science Foundation, and United States Geological Survey.

PMEL Tsunami Forecast Series: Vol. NN

A Tsunami Forecast Model for Portland, Maine

M. C. Spillane [1, 2]

Abstract. Operational tsunami forecasting by NOAA's Tsunami Warning Centers relies on the detection of tsunami wave trains in the open ocean, the inversion of these data (telemetered via satellite) to quantify their source characteristics, and real-time modeling of the impact on threatened coastal communities. For each such community the latter phase of the process involves a pre-tested forecast model capable of predicting the impact, in terms of inundation and dangerous inshore currents, with sufficient resolution and within the time constraints appropriate to an emergency situation.

In order to achieve this goal, considerable advance effort is required to tune each forecast model to the specific bathymetry and topography, both natural and manmade, of the impact area, and to validate its performance with a complete set of potential tsunami sources. Where possible the validation runs should replicate observed responses to historical events, but the sparse instrumental record of these rare but occasionally devastating occurrences dictates that comprehensive testing should include a suite of scenarios that represent potential future events.

During the forecast model design phase, and in research mode outside the pressures of an emergency situation, more detailed and slower-running models can be investigated. Such a model (referred to as a reference model) represents the most credible numerical representation of tsunami response for the study region, using the most accurate bathymetry available and without the run time constraint of operational use. Once a reference model has been developed, the process of forecast model design is to determine where efficiencies can be gained, through reducing the grid resolution and increasing the model time step, while still adequately representing the salient features of the more detailed (but not operationally feasible) solution.

This report documents the reference and forecast model development for Portland, which is the major metropolitan area in the state of Maine. At the time of writing, Portland has not experienced a tsunami. This is the result both of the sparse history of events along the eastern U.S. seaboard, and the presence of a broad shallow shelf that isolates the Gulf of Maine from the open Atlantic; Portland itself lies in a sheltered embayment of the Gulf called Casco Bay. The absence of a historical record eliminates the option of model validation based on observations, but the investigation of realistic event scenarios, involving seismic activity north of Puerto Rico or, more remotely, in the south and east Atlantic, suggests that the study area is not immune to impact.

[1]Joint Institute for the Study of the Atmosphere and Ocean (JISAO), University of Washington, Seattle, WA
[2]NOAA/Pacific Marine Environmental Laboratory (PMEL), Seattle, WA

Chapter 1

Background and Objectives

1.1 The setting of Portland, Maine

Portland is a harbor city at the southwest corner of Casco Bay, an inlet of the Gulf of Maine. The city lies on a neck of land between Back Cove to the north and the Fore River estuary to the south (Figure 1), with deep anchorages sheltered by offshore islands, just three and a half miles from the Gulf. Figure 2 is an extract from NOAA Chart 13292. Portland's natural setting has fostered a long history of permanent settlement extending back to 1633 (Conforti, 2005). Its principal exposure is to gales from the northeast and the area has been impacted by numerous storm surge events as well as several hurricanes and tropical storms over the years, as recorded by Cotterly (1996) and Budd (1980).

The city with its neighboring communities, including South Portland on the southern bank of the Fore River (and Biddeford further south), has a large and growing population (514,098, Census Bureau (2010)). It lies within a state whose coastline is extremely rugged, with numerous islands and inlets. This physical beauty makes it a desirable vacation destination (with an estimated 3.6 million visitors per year) for which Portland is a hub, thereby adding a sizeable non-resident population. While outlying coastal communities, on the mainland and nearby islands, are also exposed to some tsunami risk, the focus of the forecast model is on the main population and infrastructure centers of Portland and South Portland. Figure 3 serves to identify features and locations within the study area that arise in subsequent discussion.

1.2 Natural hazards

As noted earlier, tsunami impact is low on the spectrum of natural hazards to Maine, as indeed it is for the entire eastern seaboard of the United States. Low, that is, in terms of frequency of occurrence. The area is not immune, however; potential sources have been compiled and discussed (AMTHAG, 2008; ten Brink et al., 2009). Historically, however, the compilation of tsunami data by Lander and Lockridge (1989) has scant mention of Maine. The largest, most widespread, recorded tsunami in the Atlantic to date was associated with the Lisbon earthquake of 1755, originating in the Gulf of Cadiz. Despite the numerous population centers in colonial America, observations of the event in the western Atlantic were mainly from the Caribbean, with one from Bonavista, Newfoundland (see Figure 4). Barkan et al. (2009) have attributed this to the orientation of the source; other source geometries in future events might

pose a greater threat to the U.S. mainland. The largest local earthquake for the east coast, estimated at magnitude 6.3, occurred in the same year (1755) and was centered east of Cape Ann, Massachusetts. Lander and Lockridge (1989), however, report only confused accounts of wave activity.

Another significant source mechanism for damaging tsunami waves is submarine landslide (Driscoll et al., 2000). Portland, and a number of other Maine locations are listed as having experienced "high tides" following the submarine landslide-induced tsunami of 1929 whose source was on the Grand Banks, south of Newfoundland, and led to serious loss of life and damage there. A study of the event by Fine et al. (2005) and an extensive search by Wigen (1989) revealed no instrumental records of water level response from Maine, though the tsunami signal was evident in the Atlantic City, New Jersey tide gauge. Figure 4, in addition to locating Portland, identifies other potential tsunami sources. The South Sandwich Trench is a remote though active subduction zone in the South Atlantic. Potential flank collapse of the Cumbre Vieja volcano in the Canary Islands has been discussed by Ward and Day (2012). The locations of the BPR instruments of the U.S. DART (Deep-ocean Assessment and Reporting of Tsunami) tsunameter array, capable of detecting propagating tsunami waves in the open ocean, are marked. By transmitting direct observations via satellite, DARTs initiate the process culminating in real time forecasts. A forecast model has also been developed for the community of Bar Harbor, Maine.

The Lander and Lockridge (1989) tsunami catalog includes a number of unexplained events. In 1872 Penobscot Bay experienced waves of up to 50 cm for which a seismic source has not been identified. On January 9, 1926 Bass Harbor on Mt. Desert Island, Maine emptied suddenly then a 3 m inrush of water followed; a lesser wave was observed the same day at Vinalhaven in Penobscot Bay. On October 28, 2008 anomalous harbor oscillations, reminiscent of Bass Harbor 1926, were experienced at Boothbay, Southport, and Bristol, Maine, as reported in the Boston Globe (2008). Speculation about the origin of the latter occurrence includes the possibility that it might be meteorological. Several tide gauges between New Jersey and Maine show weaker but consistent oscillations associated with the passage of an offshore weather system. A squall-line surge was posited (Sallenger et al., 1995) as the source of an unusual wave in Daytona, Florida in July 1992. Other areas of the world are prone to meteorologically-forced tsunamis, referred to locally as "šćiga" in the Adriatic or "rissaga" in the Balearic Islands The theory of such waves is described by Monserrat and Rabinovich (2006) where some dramatic images of their effects are shown.

1.3 Tsunami warning and risk assessment

The forecast model development, described here, permitted Portland, Maine, to be incorporated into the tsunami forecasting system SIFT (Short-term Inundation Forecasting for Tsunamis), developed at NCTR (NOAA Center for Tsunami Research) for use by the U.S. Tsunami Warning Centers (TWC). Currently that system is focused on seismically-generated tsunamis but the existence of a tested model for Portland, Maine should allow non-seismic sources, landslide or meteorological, to be added as methodologies to simulate them become available.

As noted earlier, a more frequently recurrent natural hazard for Portland, and other communities in the Gulf of Maine, is storm surge. Forecast and warning tools are available, through the Northeastern Regional Association of Coastal and Ocean Observing Systems (neracoos.org), to inform emergency managers when the threat of such an event is perceived. The amplitudes

(~ 1 m) of the largest tsunami waves simulated in this report may not sound overly serious, compared with the surges that are not uncommon for the area. However, the sudden onset and rapidly varying and damaging currents of a tsunami make their inclusion in a comprehensive warning capability important in an area of extensive waterfront infrastructure. In this regard the forecast model, and its associated tools, will be of benefit in ongoing risk assessment; adjustments to the bathymetric files can be made to mimic proposed developments, such as dredging or near shore construction, to investigate how they might alter the harbor response. This report does not constitute a tsunami risk assessment for Portland, Maine though the suite of test cases employed during model testing do provide some insight into the relative impact potential of different source areas.

Chapter 2

Forecast Methodology

2.1 The tsunami model

In operational use, a tsunami forecast model is used to extend a pre-computed deep-water solution into the shallows, and onshore as inundation if appropriate. The model consists of a set of three nested grids named A (outermost with coarse resolution), B (intermediate), and C (innermost). The latter provides fine resolution that, in a real-time application of the MOST model (Method of Splitting Tsunami, Titov and Synolakis (1998); Titov and González (1997)), permits forecasts at spatial scales (as little a few tens of meters) relevant to local emergency management. The validity of the MOST model applied in this manner, and the operational effectiveness of the forecast system built around it, has been demonstrated during unplanned tests in the Pacific Basin triggered by several mild to severe tsunami events in the years since the 2004 Indian Ocean disaster (Wei et al., 2008). Successful hindcasting of observed historic events, even mild ones, during forecast model development lends credence to the ability of accurately forecasting the impact of future events. Such validation of tsunami modeling procedures is documented in other volumes of this series, but is largely unavailable for Atlantic models. Before proceeding to a description of the forecast model development for Portland, it is useful to describe the steps in the overall forecast process.

2.2 NOAA‘s tsunami forecast system

Operational tsunami forecasts are generated at Tsunami Warning Centers, staffed 24/7 in Alaska and Hawaii, using the SIFT tool, developed at NCTR. The semi-automated process facilitates the steps by which TWC operators assimilate data from an appropriate subset of the DART tsunami sensors, “invert” the data to determine the linear combination of pre-computed propagation solutions that best match the observations, then initiate a set of forecast model runs if coastal communities are threatened or, if warranted, cancel the warning. Steps in the process are as follows:

- When a submarine earthquake occurs the global network of seismometers registers it. Based on the epicenter, the unit sources in the propagation database (Gica et al., 2008) that are most likely to be involved in the event, and the DART array elements (Spillane et al., 2008) best placed to detect the waves passage are identified. TWC operators can

trigger DARTs into rapid sampling mode in the event that this did not occur automatically in response to the seismic signal.

- There is now an unavoidable delay while the tsunami waves are in transit to the DARTs; at least a quarter of a cycle of the first wave in the train must be sampled before moving to the "inversion" step.

- When sufficient data have accumulated, at one or more DARTs, the observed time series are compared with the model series from the candidate unit sources. Since the latter are pre-computed (using the MOST code), and the dynamics of tsunami waves in deep water is linear, a least squares approach taking very little time can identify the unit sources (and the appropriate scale factors for each), that best fit the observations. The "inversion" methodology is described by Percival et al. (2011).

- Drawing again on the propagation database, the scale factors are applied to produce a composite basin-wide solution with which to identify the coastal regions most threatened by the radiating waves.

- It is at this point that one or more forecast models are run. The composite propagation solution is employed as the boundary condition to the outermost (A grid) domain of a nested set of three real-time MOST model grids that telescope with increasingly fine scale to the community of concern. A grid results provide boundary conditions to the B grid, which in turn forces the innermost C grid. Non-linear processes including inundation are modeled so that, relying on the validation procedures during model development, credible forecasts of the current event are available.

- Each forecast model provides quantitative and graphic forecast products with which to inform the emergency response, or to serve as the basis for canceling or reducing the warnings. Unless the tsunami source is local, the forecast is generally available before the waves arrive but, even when lead-time cannot be provided, the several hour duration of a significant event (in which the first wave may not be the most damaging) give added value to the multi-hour forecasts provided.

Because multiple communities may be potentially at risk, it may be necessary to run simultaneously, or in a prioritized manner, multiple forecast models. Each must be optimized to run efficiently in as little time as possible; the current standard is that an operational forecast model should be capable of simulating 4 hr of real time within about 10 min of CPU time on a fast workstation computer. Due to the presence of a broad and shallow shelf between Portland and the deep ocean south of Georges Bank, which slows the waves, this standard is difficult to attain. The slow passage across the shelf requires that 8–12 hr be simulated from the time when the wave train enters the A grid domain. On the other hand by delaying the arrival and reducing the waves amplitude, the broad shelf reduces the urgency of producing a forecast. Should estimates and observations from more exposed sections of coast be mild, a decision to terminate the Portland model run may be justified. It should be noted that future versions of the MOST code will permit models for adjacent communities to share the results from the outermost grid, thereby reducing the overall computational burden of regional forecasting.

Chapter 3

Forecast Model Design for Portland, Maine

3.1 Digital elevation models

Water depth determines local tsunami wave speed and sub-aerial topography determines the extent to which tsunami waves inundate the land. Thus a prerequisite for credible tsunami modeling is the availability of accurate gridded bathymetric and topographic datasets, termed digital elevation models (DEM). Given their expertise in this area, and the number of coastal communities needing tsunami forecast capability, NCTR relies heavily on the National Geophysical Data Center (NGDC) to provide the DEMs required. In the case of Portland Maine, the DEM, a composite of multiple data sources merged and converted to a common datum of Mean High Water (MHW), was produced and documented by Lim et al. (2008). The use of MHW as the "zero level" for forecast results is standard. The MOST model does not currently include tidal fluctuations and, since a tsunami may arrive at any stage of the tide, it is best to employ a "worst-case" approach by assuming high tide when forecasting impacts.

The DEM provided by NGDC for Portland is illustrated in Figure 5. For a thorough description of the data sources and methods employed in constructing it, see Lim et al. (2008) whose Table 1 is reproduced below. With one-third arc sec ($\sim$ 10 m) resolution the DEM provides the basis for the B and C grids for both reference and forecast model usage. NCTR maintains an atlas of lower resolution gridded bathymetries, which can be used for the A grids, as described later. All of the DEMs employed were verified for consistency with charts, satellite imagery, and other datasets during the course of MOST grid development.

The elevations and depths used in the development of this forecast model were based on the digital elevation model provided by the NGDC and the author considers it to be a good representation of the local topography and bathymetry. As new digital elevation models become available, forecast models will be updated and report updates will be posted at nctr.pmel.noaa.gov/forecast_reports/ .

3.2 Tides and sea level variation

Portland has a history of tidal observations dating back to 1910. The tide station (8418150) is located at the south end of State Pier and the instrumentation has been upgraded to include

a tsunami-capable gauge sampling at 1-min intervals. Station characteristics are provided in Table 2, based on the wealth of online tidal information available at NOAA's CO-OPS (Center for Operational Oceanographic Products and Services) website (tidesandcurrents.noaa.gov). Note the sizeable diurnal range of over 3 m and that, while the rate of change in sea level is low (compared to more seismically active areas), there is substantial seasonal, interannual and short-term variability.

A sample section of the tide gauge record, again extracted from the CO-OPS website is reproduced in Figure 6. Deviations (or residuals) from the astronomically predicted tide can be several tens of centimeters. In a NOAA Technical Report, Sweet et al. (2009) have studied the widely reported anomalous sea level elevations along the U.S. East Coast during June-July 2009. They attribute the anomalies (which when smoothed were as much as 10 mm above seasonally adjusted levels in the case of Portland) to northeasterly wind forcing and changes in Gulf Stream transport. The final rows of Table 2 refer to the threshold for coastal flooding employed in producing storm surge warnings for the coast of Maine. Since MHW is 2.886 m above MLLW and the threshold (of 3.658 m) used in storm surge modeling has been exceeded about 37 times since 1980 (Cannon, 2007), the use of MHW as the zero level of modeled sea level may not be the truly worst case. While the simultaneous arrival of the crest of a large tsunami at high tide during a storm surge has low probability, a recent study (Sweet and Park, 2014) shows how rising sea levels are increasing the frequency of "nuisance" flooding, thereby extending periods of vulnerability for coastal communities. Sustained harbor oscillations at a resonant period (a mild instance in the Portland tidal record is shown in Figure 6) may also extend the threat duration. This frequently occurs at Crescent City, California (as discussed later using Figure 19.)

To look for resonances in sea level in the Portland area, a five lunar month record (Jul. 29, 2008 to Feb. 1, 2009) of 1-min data was down-loaded from the CO-OPS website. Several short gaps in the record were patched by interpolation of the 6-min instruments and the predicted tidal signal was subtracted. A spectral analysis using the FFT (Fast Fourier Transform) of the residuals produced the spectrum shown in red in Figure 7. Several peaks, at frequencies associated with tidal constituents are evident (particularly M2) when the results are band-averaged, indicating that a low level of tidal energy has not been eliminated by the predictions. Beyond the shallow water tidal constituents is where our interest lies. Here a clear peak with a period about 94 min and several lesser peaks appear; one of these, near 12 min is apparent in the sample record shown in Figure 6. Oscillations at this and other periods were observed visually during the downloading of the tidal data but appeared quite episodic and the noisiness of the spectrum is not surprising. From the synthetic time series at the tide gauge site, generated from numerous forecast model runs (see Section 4), an ensemble average spectrum drawn in blue in Figure 7 was constructed and the correspondence between several of its peaks with those in the observed spectrum will be discussed later.

3.3 The CFL condition and other considerations for grid design

Water depth dependent wave speed, in conjunction with the spacing of the spatial grid representation, places an upper limit on the time step permissible for stable numerical solutions employing an explicit scheme. This is the CFL (Courant-Friedrichs-Levy) limit, which requires careful consideration when the grids employed for a reference or forecast model are being designed. Finer-scale spatial grids, or greater water depths, require shorter time steps thereby increasing the amount of computation required to simulate a specific real time interval.

Another feature of the application of gridded numerical solutions to the tsunami wave problem is the shortening that the wave train encounters in moving from deep water onto the shelf. In deep water a grid spacing of 4 arc sec (of latitude and longitude, corresponding to ~ 7 km) is normally used to represent propagating wave trains whose wavelength is typically of the order of a few hundred kilometers. The stored results of such propagation model runs are typically decimated by a factor of 4, resulting in a database of ~ 30 km spacing (and 1-min temporal sampling) with which to generate the boundary conditions for the outermost of the nested grids in a model solution. The extraction of the boundary conditions (of wave height and the two horizontal velocity components) is achieved by linear interpolation in space and time. To provide realistic interpolated values the stored fields for these variables must be smoothly varying, and have adequate sampling in space and time to resolve their structure. As seen in Figure 8, the steep rise of the seafloor along a north south transect (68°W) from the abyss to Georges Bank is likely to preclude the use of coarsely resolved grids. After some experimentation, placing the southern boundary of the A grid at 37°N was found to permit adequate interpolation.

Figure 9 is used to illustrate the shortening and slowing that a wave train encounters as it moves onto the continental shelf, Ideally an animation of model waves would be provided but this is not possible in a printed report. Instead travel time contours (isochrons), based on the TTT (Tsunami Travel Time) application (Wessel, 2008), are drawn at 10-min intervals for waves originating near Puerto Rico. The isochrons, which mimic wave fronts, become compressed drastically as they "move" onto the shelf. Another benefit of this presentation is that it illustrates the extended duration of the simulation time required; waves traversing the broad shallow shelf take approximately 4 hr (after first encountering the model domain boundary) to reach the interior of Portland harbor, shown in the inset (where the contour interval has been reduced to 1-min). As the forecast model results will illustrate, the tsunami wave train, and the harbor oscillations it excites, persist for several hours so that at least 8 to 12 hr of simulation are required.

The isochrons in the inset panel of Figure 9 show the possibility of waves entering the C grid by the shallower northern entrance. However, the TTT calculation is strictly geometric, based on water depth alone, and does not indicate the importance of this mode of entry. A hydrodynamic model, such as MOST, is needed to elucidate the energetics.

In consequence of the above discussion, the outer boundary through which the waves enter the study region should be placed in the deep water off the shelf in order to allow the propagation database-derived boundary values to transition smoothly into the model interior. The outermost of the nested grids (A) needs to have fine enough resolution to adequately represent the compressed waves as they move onto the shelf to become the boundary condition forcing the intermediate (B) grid. Another feature illustrated by Figure 9 is the wave refraction associated with depth changes. Waves move more rapidly into the Gulf of Maine through the deeper channel to the east of Georges Bank. A shallower region to the west also eases entry and the waves tend to converge in the lee of the bank. Some tsunami energy is reflected by the steep continental rise (Figure 8) but the portion that enters the Gulf is essentially trapped and can set up sustained oscillations that impact the embayments that lead from the Gulf until finally dissipated by friction.

As yet the placement of the eastern boundary of the A grid has not been discussed. As implied by the color contouring of Figure 9, most of the eastern boundary lies in deep water. Though of less concern for waves of Caribbean origin, which arrive from the south, those from the east and southeast can in part enter along the shelf. The fastest waves will, however, be

those traversing deep water so the earliest waves that enter the C grid should be the most accurately represented. Later waves, some of whose paths have taken them along the shelf, where coarser A grid bathymetry may not as accurately reflect the physics, may be less well modeled. In the case of Portland there are no observations for validation but, in comparisons of reference and (coarser) forecast model solutions, it should not come as a surprise if they agree better in the early portion of a simulation.

Another set of considerations comes into play in choosing the placement of the B grid boundary. Portland, in addition to benefiting from the broad shallow shelf of the Gulf of Maine, is further sheltered by the many islands studding Casco Bay. An adequate resolution to represent such islands and entrances leading to the city will, as far as possible, be confined to the innermost C grid. The outer boundary of the B-Grid will be placed well outside this so that it can provide a reasonable transition from the A grid domain to the approaches to the C grid. An extensive B grid encompassing the entirety of Casco Bay has been selected, from near Cape Elizabeth in the south to Cape Small in the northeast.

3.4 Specifics of the model grids

After several rounds of experimentation, the extents and resolutions of the nested grids chosen are as illustrated in Figures 10–12, and Tables 3–4. The first set of grids, released in 2009, are superceded by those discussed in this report. While the previous forecast model grids performed reasonably well, without instability, the more stringent testing protocols now implemented revealed some deficiencies, notably in the periodicity of C-grid oscillations. The problem was traced to the A-grid; too coarse resolution in the forecast model A-grid inadequately resolved waves impinging on the steep continental rise leading to Georges Bank. Ideally, the forecast model A-grid would employ the full 30 arc-sec resolution and extent of the reference model but this would result in run-times far in excess of the target of 10 minutes per 4 hours of simulation. The compromise employs 60 arc-sec resolution and a slightly more northerly (38°N) placement of the forecast model A-grid boundary (Figure 10). At 13.55 minutes, the 10-minute run-time target is not met but the slow progression of the waves over the shallows reduces the urgency compared with other locations.

Another alteration in the grid sets, over those initially released, is in the C-grid. As evident in the aerial views and NOAA chart 13292 (Figures 1–3), the Fore River becomes shallower and more constricted by the western bridges. The earliest reference model efforts included the upper reaches of the Fore River and Presumpscot River Estuary with credible results, but their exclusion in the forecast version lost nothing of importance. The current C-grids of the reference and forecast models (Figure 12) share the same spatial domain and are truncated at the I-295 bridge (centered in the Figure 1 aerial view). This facilitates intercomparison, particularly for measures of inundation. The B-grids are essentially unchanged from the initial release; they have the same extent and are illustrated in Figure 11.

The parent grids were sub-sampled at their nodes, rather than interpolated, with some smoothing and editing where necessary to eliminate erroneous points or grid features that tend to cause model instability. For example, “point” islands where an isolated grid cell stands above water are eliminated, as are narrow channels or inlets one grid unit wide; these tend to resonate in the numerical solution. Large depth changes between adjacent grid cells can also cause numerical problems; customized tools (such as “bathcorr”) are available to correct many of these grid defects. In other situations some “sculpting,” particularly of the lower resolution grids,

was necessary to retain important features such as causeways, jetties and deep-water channels that may have been poorly represented or eliminated by the sub-sampling. This was particularly necessary for the Casco Bay Bridge (Figure 3) which presents a partial barrier to tsunami penetration, and the causeways leading to Mackworth Island and the Spring Point Light.

Details of the model grids are provided in Tables 3–4. The latter lists the maximum depth, the CFL time step requirement that must not be exceeded, and the actual time steps chosen for the reference and forecast model runs. Since, in the current version of MOST, employed by SIFT, the numerical solutions in the three grids proceed simultaneously, there is a requirement that the A and B grid time steps be integer multiples of the (innermost) C grid time step in addition to satisfying the appropriate CFL requirement. For both reference and forecast models the CFL requirement of the C grid was the most stringent. The values chosen are shown in the fifth column of Table 4 and are such that an integer multiple of each time step (18× for the forecast model; 72× for the reference) is identically 30 sec, the chosen output time interval for both models.

3.5 Model run input and output files

In addition to providing the bathymetry file names, the appropriate time step, and A, B grid multiples, the user must provide a number of additional parameters in an input file. These include the friction parameter (n–squared), where n is the Manning Coefficient), a depth threshold to determine when a grid point becomes inundated, and the threshold amplitude at the A grid boundary that will start the model. An upper limit for wave amplitude within the model is specified in order to terminate the run if the wave amplitude grows beyond reasonable expectation. Standard values are used: 0.0009 for the friction parameter and 0.1 m for the inundation threshold. The latter causes the inundation calculation to be avoided for insignificant water encroachments that are probably below the uncertainty in the topographic data. Inundation can, optionally, be ignored in the A and B grids, as is the norm in the (non-nested) MOST model runs that generate the propagation database. When A and B grid inundation is excluded, water depths less than a specified "minimum offshore depth" are treated as land; in effect a "wall" is placed at the corresponding isobath. When invoked, a value of 5 m is applied as the threshold, though A and B inundation is normally permitted as a way to gain some knowledge of tsunami impact beyond the scope of the C grid domain. Other parameter settings allow decimation of the output in space and/or time. As noted earlier, 30-sec output has been the target and output at every spatial node is preferred. These choices limit aliasing in the output fields that may be suggestive of instability, (particularly in graphical output) when none in fact exists.

Finally the input file (supplied in Appendix A) provides options that control the output produced. Output of the three variables: wave amplitude, and the zonal (positive to the east) and meridional (positive to the north) currents can be written (in netCDF format) for any combination of the A, B, and C grids. These files can be very large (6.9GB each for height and the velocity components in an 8-hour run of the reference model; 0.9GB for the forecast model). A separate file, referred to as a "SIFT" file, contains the time series of wave amplitude at each time step at discrete cells of a selected grid. Normally the time series at a "reference" or "warning point," typically the location of a tide gauge, is selected to permit validation in the case of future or historical events. Also output in the SIFT file is the distribution of the overall maximum wave amplitude, velocity and speed in each grid and the inundated area. By contrast with the complete space-time results of a run, the SIFT files (also netCDF) are very compact

(~ 60MB and 7MB for reference and forecast models respectively) and, if more than a single grid point is specified, a broader view of the response can be provided. The input files used in model development employed 30 output locations; 25 of these at points of interest within the C grid.

By default two additional output files are generated. A "listing" file summarizes run specifications, progress, and performance in terms of run time; this file also includes information, should a run not start or terminates early, to assist in determining the cause. Before running, the MOST program may adapt the input grids to conform with underlying expectations. When this occurs it is reported in the listing file and the grid values actually employed are written to new files. In some instances these corrections undo the modelers intent, for example by introducing openings in a narrow jetty. Thus the existence of such output grid files may prompt modeler action, such as widening a jetty, to ensure that non-physical alterations do not occur. A "restart" file is produced so that a run can be resumed, beginning at the time it ended, either normally or by operator intervention.

The input files described above are specific to the model itself. For an actual run, the program must be pointed toward the files that contain the boundary conditions of wave amplitude (HA), and velocity components (UA, VA), to be imposed at the A grid boundary. Time varying conditions are generally extracted as a subset of a basin-wide propagation solution (either a single unit source or several, individually scaled and linearly combined) that mimic a particular event. Alternately a customized source, such as one of those constructed as scenarios for the Lisbon 1755 event, can be employed. These boundary-forcing files typically consist of 24 hr of values (beginning at the time of the earthquake), sampled at 1-min intervals and available on a 16 arc min grid. Occasionally, for more remote seismic sources (or when delayed arrival of secondary waves due to reflections as has been seen at Hawaii), the time span of the propagation run available for forcing is extended beyond one day.

Chapter 4

Model Stability Testing

Before proceeding to an extensive suite of model runs, that explore the threat to Portland from various source regions, the stability of the model is tested in both low and extreme amplitude situations. The former we refer to as "micro-tsunami" source testing, where the boundary forcing is at such a low level (but not precisely zero) that the response is expected to be negligible. These tests can be highly valuable in revealing localized instabilities that may result from undesirable features in the discretized bathymetric representation. Inlets or channels that are only one grid cell wide may "ring" or resonate in a non-physical way in the numerical solution. An instability may not grow large enough to cause the model to fail but, in a run with typical tsunami amplitudes, may be masked by actual wave variability.

Forcing by extreme event scenarios, termed "mega-tsunamis", of magnitude Mw 9.3 are also simulated as part of the testing protocol. In addition to the need to test model stability under such circumstances, there is a parameter in the input file that truncates the run if a prescribed threshold is exceeded. The threshold must be set high enough so that a model run under operational conditions is not unnecessarily terminated.

Both micro- and mega-tsunami trials should be performed for test sources whose waves enter the model domain from different directions since, although stable for one set of incoming waves, an instability may be encountered for another. For communities in the northwest Atlantic, three major regions of seismic activity comprise the threat of tsunami generation, as was illustrated in Figure 4. The Caribbean and, in particular, the Puerto Rico Trench, the Eastern Atlantic near the Gulf of Cadiz, and the South Atlantic where the South Sandwich Trench and Scotia Sea are seismically active. Figure 13 illustrates the propagation patterns for mega-tsunami scenarios in each of these regions. Where possible, these are based on unit source combinations from the propagation database (see Appendix B) as illustrated in Figure 14; the complex faulting of the Gulf of Cadiz (see Figure 15) in the Eastern Atlantic has not as yet been represented as unit sources, largely the result of uncertainty in the mechanism of the major Lisbon Tsunami that originated there in 1755. Three of the proposed sources of this event are employed in testing of the Portland, Maine model. However, as the 1755 tsunami went unobserved on the eastern seaboard of colonial America, it is possible that scenarios of greater impact to Portland might be generated by other eastern Atlantic source locations and orientations.

The micro- and mega-tsunami testing of the forecast (and reference) model is reported in the following sections. Further evidence of stability is provided by the extensive set of scenarios, aimed at exploring the dependence of impact to Portland on source location, described in

section 5.3, and in independent testing by other members of the NCTR group before the model was released for operational use. Table 5 summarizes the synthetic tsunami scenarios tested by the author for this report.

4.1 The "micro-tsunami" tests

Three micro-tsunami test cases were run representing sources in the Caribbean and the Eastern and South Atlantic as detailed in Table 5. Two, AT51B, and SS11B, are based on unit sources in the propagation database (as illustrated in Figure 14 and Appendix B). The third, LI01A, was derived from a reduced slip version of a source (LI01 in Figure 15) from the ComMIT (Titov et al., 2011) database. Several instability-prone features were detected: south of Cottage Cove and between the offshore islands, near Fort Gorges, Long Wharf (west of State Pier), the Casco Bay Bridge, and the north end of the Presumpscot Estuary. Judicious editing of the small-scale features in these areas eliminated the problems. In the B grid a number of the narrow channels in the north and northeast were sources of localized instability. Some editing removed the problem, though some of the highly responsive B-grid areas undoubtedly reflect reality. Harbors with narrow inlets are where instances of unusual wave activity (mentioned in Section 1) have been reported, and the funnel-shape of Penobscot Bay, to the east of the B grid domain, has been identified by Maine's Emergency Management Agency (maine.gov/mema) as being particularly vulnerable to storm surges. Since these areas are not the focus of this study, and would require more detailed bathymetry to accurately represent them, the editing to eliminate their potential to cause instabilities is justifiable. A limited number of grid cells in the outermost (A) grid required correction. Generally these were associated with non-physical features in the DEM, such as where a track of ship-based soundings were improperly merged with other data sources.

The upper panel of Figure 16 illustrates the responses at the Portland tide gauge location for the revised reference (RM, black) and forecast model (FM, red) solutions of the micro-tsunami scenarios. The agreement is best in the early hours of the response; later the solutions diverge somewhat as the waves reflect and interact but do retain similar characteristics. The lower panel of Figure 16 shows the reference model solution to the AT51B scenario for an earlier /it superceded /rm version of the reference model C-grid. A tedious iterative process of grid correction and re-testing with the micro-tsunami sources was required to eliminate such features before the testing of large events could begin.

4.2 The "mega-tsunami" tests

As has been found for other forecast models along the U.S. eastern seaboard, a significant tsunami threat to Portland, Maine is associated with the Puerto Rico Trench, north of that island. A synthetic "mega-tsunami" is simulated by linearly combining 20 unit sources from the propagation database (see Appendix B) and scaling up the slip in each by a factor of 25. As described by Gica et al. (2008), each unit source represents a 100×50 km area of the fault surface with the long axis parallel to the plate boundary. The B row is shallowest, sloping from a nominal depth of 5 km (unless a depth estimate has been provided by the USGS based on the earthquake catalogs), row A is deeper, followed by rows Z, Y, X, ... where appropriate. Thus, the extreme case sources represent 1000-km-long ruptures with a width of 100 km; the corresponding magni-

tude is Mw 9.3. Several mega-tsunami scenarios constructed in this manner are employed, as listed in Table 5 and illustrated in Figure 14. The complex fault lines in the Gulf of Cadiz do not readily lend themselves to unit source representation. Instead, a composite Mw 9.3 scenario is constructed based on two rectangular areas (HS01 and HS02 in Figure 15) that are among the proposed sources for the Lisbon-1755 tsunami (Zitellini et al., 2001). Weights are applied to the HA, UA, VA files to mimic a single source with uniformly distributed slip.

We focus first on the synthetic mega-source AT 48–57 (see Figure 13). Reference and forecast model maximum amplitude (H_{max}) and speed (S_{max}) results for the C-grid are compared in Figures 17 and 18. A common color scale is employed for these and subsequent figures illustrating other synthetic mega-sources. The underlying topography is that of the reference model whose undisturbed MHW coastline is drawn to aid in identifying inundated areas. In Figure 18, and similar figures to follow, vectors are drawn to show the direction, at the time of maximum speed, for a subset of grid cells; a scale vector is drawn in the lower left corner. The lower panel of each figure compares the time series at the Portland tide gauge over the entire 24 hours of the simulation. The time axis is in hours from the time of the initial deformation in the source area but the portion shown begins when the waves arrive at the A-grid boundary. It is notable that several hours elapse between this triggering of the model run and the arrival of the first wave at the tide gauge reference point, consistent with the travel times (Figure 9) from the TTT calculation.

The reference and forecast model time series for wave amplitude (Figure 17) at the Portland tide gauge are in close agreement for the entire simulation though some synchronicity is lost later in the record. Differences are mainly in the form of higher frequency peaks and troughs that are stronger in one series than in the other. Such differences are more evident in the time series of speed at the tide gauge (Figure 18) which is dominated by high frequency variability, likely due to harbor resonances or eddy-like features. In the case of Crescent City, California the harbor resonates strongly in response to tsunami waves making it prone to infrastructure damage more often that other west coast communities of the United States. An illustration of this behavior, in the detided Crescent City tide gauge record following the Kuril Islands event of November 15, 2006, is shown in Figure 19. Differing representations of such resonances by the reference and forecast models can cause mismatches in maxima and minima, both in timing and size, throughout the model domain so a degree of disagreement between the upper panels of figures such as Figures 17 and 18 is to be expected.

Figure 20 provides further information on the inundation associated with mega-source AT 48–57. The red areas in the upper panels indicate grid cells that are above the undisturbed MHW but become inundated *at some time* during the simulation. They generally match those above the waterline in Figures 17 and 18. The lower panel of Figure 20 shows as solid lines (black for the reference and red for the forecast model) the time variation in the inundated area. Dashed lines shows the cumulative build up in the impacted area, as regorted in the SIFT output file. It is notable that for both versions of the model the inundated area does not return to zero. This is the result of cells on land that are local minima of elevation and which, once inundated, have no way to drain as a wave recedes. Cells inundated at the end of the simulated period are highlighted in yellow in the upper panels. By and large these yellow-highlighted areas match in the reference (RM) and forecast model (FM) versions but there are notable areas of disagreement: the upper reaches of the Fore River and the Portland waterfront just upriver of the Casco Bay Bridge. These, together with an area in the northern portion of the C-grid domain, account for much of the excess of inundation displayed for the forecast

model. Some of the difference is due to the coarsening of the resolution that necessitated the "drying" of forecast model cells that remain "wet" (and thus not counted as inundated) in the reference model. To the extent that measures of inundation in the forecast model exceed those from the reference model, the former are more conservative for use in an emergency. For true risk assessment and definition of inundation lines and evacuation routes, however, the greater fidelity of the reference model topography would be preferable.

In forecast model application to other sites, it may be desireable to intentionally set the elevation of some nearshore freshwater lakes or ponds to be just above MHW so that they are counted as being inundated should salt water intrude in the course of a tsunami.

The agreement between the reference and forecast model versions of maximum amplitude and speed distributions, and areas of inundation is good, with similar structures in each. The vector distributions generally agree though in places the maximum is associated with an episode of flood for one model but ebb for the other. Particularly for the earliest waves, the reference model time series (black) and the forecast model version (red) agree well. Later the time series lose synchronicity as differences in reflection and resonant period between models alter patterns of constructive and destructive interference.

Various metrics to compare the reference and forecast model are provided in Tables 6 and 7 for AT 48–57 and the remaining scenarios discussed below. Maximum amplitude and speed at the reference point and throughout the C-grid are reported as are the areas inundated and the amplitude of the leading crest. In the absence of any historical observations, no objective measure of model performance is available and the goal is consistency between the models. Later, in section 5.5, some more detailed graphical intercomparisons of the AT 48–57 scenario are presented. Overlaid with reduced opacity and geo-referenced to Google Earth imagery near the Casco Bay Bridge, the Mackworth Island causeway, and dock areas of the lower Fore River are represented and lead to a brief discussion of the treatment of fine scale features (such as marinas), and structures elevated on pilings (such as State Pier) in the model.

Before discussing other mega-tsunami sources in the vicinity of Puerto Rico, results from the eastern (HS 01–02) and southern Atlantic (SS 01–10) are presented to verify that the agreement between the AT 48–57 solutions holds for other directions of tsunami wave train incidence (Figure 13). Figures 21 and 22 represent an eastern Atlantic source; Figures 23 and 24 represent the more remote South Atlantic. The reference point time series and periodicities, patterns of inundation and regions of greatest wave amplitude and speed are again in good agreement. There is a suggestion of differences in the penetration of waves upriver from the Casco Bay Bridge and in amplitudes for bays and headlands in the southeast of the model domain, but areas of greater concern such as the lower Fore River waterfront (including Mill Cove), Back Cove, and the Mackworth Island causeway are similarly represented.

Metrics derived from the HS 01–02 and SS 01–10 scenarios also appear in Tables 6–7. With the caveat that HS 01–02 may not represent the greatest threat from the eastern Atlantic, it appears that these sources (each a synthetic Mw 9.3 scenario) generate lesser impacts at Portland, Maine than did the Puerto Rico source AT 48–57. We next proceed to examine further mega-tsunami scenarios from the western Atlantic and Caribbean region illustrated in Figure 5.

Sources AT 38–47 and AT 58–67 lie to either side of source AT 48–57. Though not illustrated here, the beam patterns of their energy distributions are less directed toward Portland, Maine. Source AT 38–47 is directed more to the northeast Atlantic while waves from AT 58–67, much of which is comprised of the Cayman Trough, are partially blocked by the Greater Antilles from

emanating into the Atlantic. This expectation of lesser impact is borne out by their reference and forecast model comparison results presented in Figures 25–28 and their associated entries in Tables 6 and 7. The primary goal of these comparisons is also met: a satisfactory level of agreement between the reference and forecast models confirms the utility of the latter for emergency usage.

Two other synthetic mega-tsunami scenarios are also used for this purpose: AT 68–77 and AT 82–91. The first of these lies in the western Caribbean in the Gulf of Honduras. Though tsunamis were generated in this area in 1976 and, more recently, in 2009 the impact was purely local. The other source AT 82–91 comprises unit sources south of Hispaniola and the Muertos Trough south of Puerto Rico. While the greatest impact of such a source would be expected locally, the Windward and Mona Passages to the west and east respectively of Hispaniola could provide greater potential for tsunami waves to emerge into the Atlantic. In Table 7 it is noted that sources within the Caribbean generate wave trains that arrive at Portland with a leading trough; the remainder generate a leading peak. Figures 29–32 (and Tables 6– 7) illustrate the impact to Portland, Maine from these intra-Caribbean sources, as well as providing further evidence for the utility of the forecast model. Neither source generates significant inundation near Portland though, surprisingly, the maximum amplitudes predicted are quite similar. The composite AT 68-77 forcing at the A-grid boundary, based on the propagation database, has a much longer period that that for the other synthetic mega-tsunami scenarios discussed above. The similar periodicity of the greater than expected response at Portland, Maine (Figure 29) suggests that such long waves may be more effective in surmounting Georges Bank.

Other source combinations, to the south of AT 38–47 along the Lesser Antilles,and therefore directed to the east, or along the northern coast of South America and largely screened from the Atlantic, are not considered for purposes of reference to forecast model comparison. Later, in section 5.3 and using the forecast model alone, a broader set of Mw 8.83 scenarios is employed to provide insight into the dependence of impact to Portland on source location and orientation.

A final element of the standard model testing protocol checks for agreement between the reference and forecast model results for a moderate (Mw 7.5) scenario. Unit source AT B52 (see Figure 14) is used for this purpose with the results displayed in Figures 33–34. Satisfactory agreement is again found in the areas of greatest concern; for wave amplitude, the maxima at the Portland tide gauge are greater for the reference model (Figure 33); the converse is true for peaks in speed (Figure 34). Compared to mega-tsunami scenarios, with more extended source lengths, the response of Portland, Maine is more high-frequency in character.

To conclude this chapter, the similarity in solution and lack of instability in micro-tsunami testing and agreement between reference and forecast model results for mega-tsunami scenarios (for diverse source areas throughout the Atlantic and Caribbean), provides confidence in employing the revised forecast model for emergency use in the event of seismically-generated future events. Revisions to the A-grid were responsible for a substantial improvement in the level of agreement over the earlier model release. The reduced resolution in the earlier representation of the steep continental rise south of Georges Bank resulted in differing periodicities in the waves predicted for Portland, Maine. Differences remain, particularly in the predicted amplitudes of later waves, but, in the absence of historical observations, the significance of these cannot be determined. From the metrics presented in Tables 6–7, and from Figure 20, it appears that the forecast model overestimates the inundated area. In the next chapter a broader set of source scenarios, each representing a Mw 8.83 event, are employed to determine

how tsunami impact on Portland might depend on source location. The results indicate that an area near Puerto Rico poses the greatest threat and suggest an additional “stress-test” of the forecast model as reported in Section 5.4. In Section 5.5 some specific areas in the Portland C-grid are examined in closer detail.

Chapter 5

Dependence of Impact on Source Location

5.1 Further testing of the Portland forecast model

In the report to date, the stability of the forecast model for Portland has been demonstrated based on micro-tsunami sources and selected mega-tsunami scenarios. Were observations available, it would be natural to proceed to validate the Portland model with hindcasts of historical events. In the absence of such observations, the outstanding success of the SIFT scheme in more tsunami-prone areas, such as the Pacific Ocean basin, both in hindcast mode and real-time application, must serve as a proxy for Portland-specific observational validation. The SIFT methodology has provided useful and accurate forecasts (in quasi-operational conditions at NCTR during the development phase) for several mild tsunamis in the past five years (Wei et al., 2008), and is presently employed operationally at the warning centers. It performed well during the damaging tsunami that struck Samoa in September 2009 and for the major Chile and Tohoku events of 2010 and 2011.

Before a forecast model is added to SIFT for operational use, it must be exercised with a wide a range of simulated scenarios as possible. Experience by other NCTR forecast model developers has indicated that the MOST model may exhibit instability for some specific combination of event magnitude and location. It would not be good to discover such an issue under emergency conditions. In this section we report on numerous scenarios explored, beyond those discussed above during intercomparison of the reference and forecast versions of the model. In addition to checking that no issues are encountered, these and the additional tests reported below, build up a knowledge base to inform emergency management in the absence of a historical record. This effort is only a "first installment" on a comprehensive risk assessment and validation. In addition to the scenarios run by the author, and reported here, further tests will be made by other members of the group at NCTR, by staff at the Warning Centers, and by others perhaps in training situations. Among the many related tools developed at NCTR is ComMIT (Titov et al., 2011), the Community Model Interface for Tsunami, which provides a highly intuitive graphical environment in which to exercise and explore forecast models for any combination of propagation database unit sources. Were any of these avenues to reveal a problem with the Portland forecast model, its origin (most likely in some quirk of the bathymetric files) would be located and corrected then the revised version re-installed for op-

erational use. The development of the forecast system will be a dynamic process, with new models added (and old ones revisited) for locations of U.S. interest and globally. In the coming years it is expected that further capabilities (for example landslides) will be added as algorithms and methodologies mature.

5.2 Source scenarios

As mentioned earlier, potential sources of seismically-generated tsunami waves that might impact the U.S. east coast, and Portland in particular, lie in the subduction zones of the Atlantic Ocean: the Caribbean and the South Sandwich Arc, east of Drake Passage. Both of these regions are fully represented in the propagation database (see Appendix B) .

The situation with regard to candidate East Atlantic sources is not entirely satisfactory. Those employed earlier in this report were candidate sources for the 1755 Lisbon tsunami. A constraint on such sources, however, is that to conform with observation they should not direct much energy toward North America. While waves were detected in the Caribbean area of the western Atlantic at the time, no observations were reported from colonial population centers of North America (an exception being Bonavista on Newfoundland). The non-existence of reports of the 1755 tsunami in North America has been discussed by Barkan et al. (2009) who also investigated the role of the source orientation on potential impacts to the U.S. Such an approach may be needed to complete a risk assessment and to make stability testing more comprehensive. Clearly relying on East Atlantic sources designed *to not significantly impact* North America is a weakness that must be addressed in future testing and risk assessment.

5.3 Potential impacts to Portland

With that caveat regarding the eastern Atlantic, the forecast model has been applied to a set of 24 magnitude Mw 8.83 scenarios. Those derived from the propagation database employ five A,B unit source pairs with a slip of 10m in each. Eighteen of these are based on AT sources; three from SS. The eastern Atlantic sources (HS 01, HS 02, LI 01 in Figure 15) are used, with appropriate slip values, to provide three further Mw 8.83 scenarios. The forecast model was stable in all cases with summary results shown in Figure 35 and Table 8. Scenario AT 49–53 causes the greatest impact to Portland among those considered with a 54cm peak at the Portland tide gauge. C-grid amplitudes have a maximum of 237cm at the south end of Mill Cove, and the area inundated at some time during the simulation is 2.5 square kilometers (0.7 sq-km along the Fore River).

The inundation panels of Figure 35 show that several Mw 8.83 scenarios provide no threat of inundation to the Portland area. None of the South Atlantic scenarios inundate and, within the Caribbean, only the sources near Panama, the Muertos Trough (adjacent to the Mona Passage) and near Trinidad cause mild impact. Source HS 02 in the eastern Atlantic, perhaps due to its orientation or to limited scattering along its ray path, has the greatest impact of the three on Portland, comparable to some segments of the Puerto Rico trough.

5.4 A stress test for the Portland, Maine forecast model

The prominent high impact associated with Mw 8.83 scenario AT 49–53 (and AT 48–57 among the Mw 9.3 mega-event scenarios) suggest one further "stress test" for the forecast model. Examining individual B-row sources AT 39B – 60B and 82B – 92B, identifies AT 48B as having the greatest potential for impact. Thus, while perhaps physically unrealistic as seismic sources, a set of AT 48B scenarios with slips equivalent to Mw 7.5 – 9.3, are tested. It often is found that individual unit sources can have greater relative impact at a particular far-field location, than a composite source with the same magnitude. The main reason, however, for employing a single unit was to simplify source definition and limit interference in multi-unit composites. For none of these, some admittedly unrealistic, scenarios was the model found to be unstable and metrics of impact are listed in Table 9. The overall maximum of about 500 cm (5 m) within the C-grid seen in Table 9 suggests the choice of 90 m as an appropriate upper limit for wave amplitude, as specified in the Appendix A parameter settings, is more than adequate.

5.5 Inundation and extreme speeds for selected areas

Finally, the potential for inundation or hazardous current speeds is explored for some selected areas using the AT 48–57 scenario. For inundation, based on earlier graphics for the entire C-grid, the areas of most concern for inundation appear to be Mill Cove, an inlet in the Knightville area of South Portland. Resonance in the inlet to the north west of Mackworth Island suggests the causeway linking it to the mainland, with an elevation of only 1m above MHW, may also be at risk of inundation. In Figures 36 and 37 the reference and forecast model representations of these localities are contrasted for the AT 48–57 mega-tsunami scenario. The model results are reduced in opacity, geo-referenced, and overlaid on Google Earth imagery of September, 2014. In these enlarged views the earlier statement of agreement between the reference and forecast models is reinforced.

For high speeds, channels and areas near headlands are most at risk. Among the latter are the sites of the Portland Breakwater and Spring Ledge Lights that bracket the oil tanker jetty. This is the terminus of the Portland-Montreal Pipe Line where up to 200 tankers berth per year. Another site of concern is Ocean Gateway Pier II, completed in 2011, after the initial draft of this report was written. Pier II, elevated on piles above the Fore River just east of State Pier, serves the largest cruise vessels with several thousands of passengers and crew. Strong currents or extreme water level excursions would pose a severe threat to both locations though, with the proximity of Casco Bay, deploying of vessels to sea is probably a viable option. Figure 38 provides a close-up comparison of reference and forecast model representations of speed in this area, again superimposed on Google Earth imagery. With its greater resolution, the reference model suggests a tongue of higher speeds extending westward from the Spring Point Ledge Light. The forecast model has a similar, though less intense feature. A vector overlay in each panel represents the instantaneous pattern of velocity at the time of greatest speed in the vicinity (these times differ by only 7 minutes between models). A scale arrow is drawn to represent a 5-knot current. Apparently eddies shed near the tip of the causeway are responsible for the wave speed maxima which, though substantial near the headlands for this extreme Mw 9.3 scenario, are less severe at the jetty; the rapid directional variability, however, may be problematic. Currents at the cruise ship terminal on the north shore of the Fore River appear more benign.

The model overlay in Figure 38 further suggests that in the vicinity of the oil terminal there is very limited inundation, and the berms surrounding the storage tank farm are likely to be more than adequate for protection during tsunami events. It should be noted that the suggestion in these graphics that marinas and some major piers (for example State Pier) may be inundated is misleading. Substantial docks, if elevated on piles, do not appear in the model grid as impediments to the flow and conclusions as to whether they might be overtopped would require comparison of wave amplitudes to their platform elevation. Less substantial marina docks, though perhaps more vulnerable to tsunami currents cannot be included at the resolution of the forecast model grid.

Inundation may be of greater concern further to the west where the resonant response of Mill Cove may be accompanied with overtopping of the low-lying neck of land and the southern approaches to the Casco Bay Bridge (Figure 36). The limited forecast model resolution of the bridge support structure introduces some uncertainty to the forecast model results further upriver. On the other hand, the similar results from both models in the vicinity of Mackworth Island (Figure 37) suggest vulnerability of the causeway and of the communities near the Martin Point Bridge in the event of a strong tsunami. These comments are somewhat speculative and do not constitute a comprehensive risk assessment. .

Chapter 6

Discussion and Conclusions

The forecast model (and the associated reference model) described in this report will permit Portland to be added to the coastal communities for which forecast capability is available, and as a tool for use in risk assessment. Although no historical observations exist with which to validate the models, their behavior in test scenarios suggest that they produce realistic and consistent results. The forecast model is an optimized version of the reference model that, with reduced spatial resolution and time step, can run within the constraints of an emergency situation while reproducing the main features of the reference model. The forecast model run time of 13.55 min per 4 hr of simulation does not meet the desired standard of 10 min, and the location of Portland deep within the Gulf of Maine means that several hours of simulation are needed before waves reach the harbor. Conversely, this delayed arrival reduces the need for early model run completion. Reports, during an event, of a lack of damaging waves at other communities en route may eliminate the need for a Portland run to be completed.

Considerable effort was involved in eliminating artifacts in the digitized bathymetry that generate instabilities: single point islands, single grid cell wide channels or inlets, and severe depth changes between adjacent points. Nonetheless users should be aware that some combination of incoming waves may trigger a numerical resonance and require adjustment to the bathymetry files. Such discoveries would hopefully be made during use of the model for risk assessment, research, or training rather than under operational conditions (see Appendix C for the latest test results using the operational version of SIFT.)

Portland to date has not experienced a tsunami, though not a stranger to storm surges. The SLOSH model (Sea, Lake, and Overland Surges from Hurricanes) is employed by the National Weather Service in storm surge forecasting (Jelesnianski et al., 1992). Maps of potential hurricane inundation for Portland can be viewed at the Maine Department of Agriculture, Conservation and Forestry webpage (www.maine.gov/dacf/mgs/hazards/phim/) and reveal similar areas of vulnerability to those seen in this report. Real-time storm surge warnings are available through NERACOOS. Though both natural hazards involve water level changes, they differ in the time scales they involve. Tsunamis have the potential to arrive with little warning and the time scales of the water movements may induce extreme current speeds more damaging than those associated with a storm surge of similar elevation.

This report has described the development of forecast and reference models for tsunami impact on Portland, Maine. The final stage of testing is discussed in Appendix C where the correspondence between the development model, and that deployed operationally, is verified. Unlike similar modeling for threatened coastal communities in the Pacific Basin, where tide

gauge observations of historic events are available for model validation, no such cases exist for Portland. However, the Portland models, apart from site-specific bathymetry, employ the same numerical codes and parameters as employed for other communities where success under operational conditions has been demonstrated. Simulations indicate that Portland's protected location within Casco Bay, itself a shielded sub-region of the Gulf of Maine, limits its vulnerability to the most severe, seismically generated, tsunami events that might occur north of Puerto Rico. Nonetheless, the strong directionality that tsunami energy propagation may exhibit, and the potential impact that tsunami-generated currents might have on the marine-intense infrastructure of the area makes the addition of forecast capability by the Tsunami Warning Centers an important element of a comprehensive emergency management plan for Portland. Additionally, used as part of a public awareness and education program, or in risk assessment, the forecast model should assist in making the Portland metropolitan area "TsunamiReady" (tsunamiready.noaa.gov).

Chapter 7

Acknowledgments

Members of the NCTR group provided valuable assistance during the production of this report. In particular Chris Chamberlin and Nick Arcos edited the first draft for content and style; grid stability test animations and the report cover imagery were generated by Jean Newman. Lindsey Wright performed the SIFT testing reported in Appendix C. The modeling could not proceed without the detailed DEM produced at NGDC by the painstaking combination of numerous bathymetric and topographic surveys. Ferret (a product of NOAA's Pacific Marine Environmental Laboratory, freely available at ferret.pmel.noaa.gov/Ferret/.) was employed for analysis and graphics while Google Earth and Google Maps were heavily used to visualize the study area. The image used for Figure 1 was obtained from Wikipedia (Author: "Cyrios", 29 April 2013). This publication is partially funded by the Joint Institute for the Study of the Atmosphere and Ocean (JISAO) under NOAA Cooperative Agreements NA17RJ1232 and NA10OAR4320148. It is JISAO Contribution No. 2086 and PMEL Contribution No. 3387.

Chapter 8

References

Atlantic and Gulf of Mexico Tsunami Hazard Assessment Group (AMTHAG), (2008): Evaluation of Tsunami Sources with the Potential to Impact the U.S. Atlantic and Gulf Coasts – An Updated Report to the Nuclear Regulatory Commission. U.S.G.S. Admin. Report: 300 pp.

Barkan, R, U.S. ten Brink, and Jian Lin, (2009): Far field tsunami simulations of the 1755 Lisbon earthquake: Implications for tsunami hazard to the US East Coast and the Caribbean. *Marine Geology* 264(1), 109-122.

Boston Globe (2008): Massive waves a mystery at Maine harbor. boston.com/news/local/maine/articles/2008/11/04/

Budd, B. (1980): A Local Archive of Top Tides and Tidal Surges for Portland, Maine. Available at NWS, 1 Weather La., Gray, ME 04039.]

Cannon, J.W. (2007): Northern New England Coastal Flooding. *GoMOOS Newsletter*, Spring 2007. gomoos.org/aboutgomoos/coastalfloodwafpreprint.pdf

Census Bureau (2010): Population Change for Metropolitan and Micropolitan Statistical Areas in the United States and Puerto Rico (February 2013 Delineations): 2000 to 2010. URL: www.census.gov/population/www/cen2010/cph-t/CPH-T-5.pdf

Conforti, J.A. (2005): Creating Portland: History and Place in Northern New England. Hanover NH, University Press of New England, 348p.

Cotterly, W. (1996): Hurricanes & Tropical Storms: Their Impact on Maine and Androscoggin County. pivit.net/c̆otterly/hurricane.PDF

DiPhilippo, K. (2007): The Grist Mill and Ship Yard Point. South Portland Historical Society article published June 29, 2007 in the *South Portland Sentry* and archived at sphistory.org .

Driscoll, N.W., Weissel, J.K., and Goff, J.A., (2000): Potential for large-scale submarine slope failure and tsunami generation along the US mid-Atlantic Coast. *Geology 28*, (5), 407-410.

Fine, I. V., A.B. Rabinovich, B.D. Bornhold, R.E. Thomson, and E.A. Kulikov, (2005): The Grand Banks landslide-generated tsunami of November 18, 1929: preliminary analysis and numerical modeling. *Marine Geology*, 215(1), 45-57.

Gica, E., M. Spillane, V.V. Titov, C.D. Chamberlin, and J.C. Newman (2008): Development of the forecast propagation database for NOAA"s Short-term Inundation Forecast for Tsunamis (SIFT). NOAA Tech. Memo. OAR PMEL-139, NTIS: PB2008-109391, 89 pp.

Jelesnianski, C.P., J. Chen and W.A. Shaffer (1992): SLOSH – sea, land, and overland surges from hurricanes. NOAA Tech. Report NWS 48, 71 pp.

Lander, J.F. and P.A. Lockridge (1989): United States tsunamis: (including United States possessions): 1690-1988. US Department of Commerce, NOAA, NESDIS, and NGDC, 1989.

Lim, E., L.A. Taylor, B.W. Eakins, K.S. Carignan, R.R. Warnken, and P.R. Medley (2008): Digital elevation model of Portland, Maine: Procedures, data sources and analysis. ngdc.noaa.gov/mgg/inundation/tsunami/data/portland_me/portland_me.pdf

Monserrat, S., I. Vilibic, and A. B. Rabinovich (2006): Meteotsunamis: atmospherically induced destructive ocean waves in the tsunami frequency band. *Nat. Hazards Earth Syst. Sci.*, 6, 1035âĂŞ1051.

Percival, D.B., D.W. Denbo, M.C. Eble, E. Gica, H.O. Mofjeld, M.C. Spillane, L. Tang, and V.V. Titov (2011): Extraction of tsunami source coefficients via inversion of DART® buoy data. *Nat. Hazards*, 58(1), doi: 10.1007/s11069-010-9688-1, 567 590.

Sallenger, A.H, Jr., J.H.List, G. Gelfenbaum, R.P. Stumpf, and M. Hansen (1995): Large Wave at Daytona Beach, Florida, Explained as a Squall-line Surge. *J. Coastal Res.*, 11(4), 1383-1388.

Spillane, M.C., E. Gica, V.V. Titov, and H.O. Mofjeld (2008): Tsunameter network design for the U.S. DART® arrays in the Pacific and Atlantic Oceans. NOAA Tech. Memo. OAR PMEL-143, 165 pp.

Sweet, W., C. Zervas, and S. Gill. (2009): Elevated East Coast Sea Level Anomaly: June–July 2009. NOAA Tech. Report NOS CO-OPS 051, August 2009.

Sweet, W.V. and J. Park, (2014): From the extreme to the mean: Acceleration and tipping points of coastal inundation from sea level rise. *Earth's Future*, 2(12), 579-600, doi: 10.10022014EF000272.

ten Brink, U.S., Lee, H.J., Geist, E.L., Twichell, D.C., (2009): Assessment of tsunami hazard to the U.S. East Coast using relationships between submarine landslides and earthquakes. *Marine Geology*, 264, 65âĂŞ73

Titov, V., and F.I. González (1997): Implementation and testing of the Method of Splitting Tsunami (MOST) model. NOAA Tech. Memo. ERL PMEL-112, NTIS: PB98-122773, NOAA/Pacific Marine Environmental Laboratory, Seattle, WA, 11 pp.

Titov, V.V., C. Moore, D.J.M. Greenslade, C. Pattiaratchi, R. Badal, C.E. Synolakis, and U. Kânoğlu (2011): A new tool for inundation modeling: Community Modeling Interface for Tsunamis (ComMIT). *Pure Appl. Geophys.*, 168(11), doi: 10.1007/s00024-011-0292-4, 2121 2131.

Titov, V.V., and C.E. Synolakis (1998). Numerical modeling of tidal wave runup. *J. Waterw. Port Coast. Ocean Eng*, 124(4), 157-171.

Ward, S.N., and S. Day (2012). Cumbre Vieja Volcano – Potential collapse and tsunami at La Palma, Canary Islands. *Geophys. Res. Lett.*, 28(17), 3397-3400, DOI: 10.1029/2001GL013110.

Wei, Y., E. Bernard, L. Tang, R. Weiss, V. Titov, C. Moore, M. Spillane, M. Hopkins, and U. Kânoğlu (2008): Real-time experimental forecast of the Peruvian tsunami of August 2007 for U.S. coastlines. *Geophys. Res. Lett.*, 35, L04609, doi: 10.1029/2007GL032250.

Wessel, P. (2008): Analysis of observed and predicted tsunami travel times for the Pacific and Indian Oceans. *Pure Appl. Geophys.*, 166, 301-324, DOI 10.1007/s00024-008-0437-2.

Wigen, S.O. (1989): Report on the Assessment and Documentation of Tsunamis for Eastern Canada. Unpublished Manuscript. Tide and Tsunami Services, Fulford Harbour, B.C., 16 pp.

Zitellini, N., L. A. Mendes, D. Cordoba, J. Danobeitia, R. Nicolich, G. Pellis, A. Ribeiro, R. Sartori, L. Torelli, R. Bartolome, G. Bortoluzzi, A. Calafato, F. Carrilho, L. Casoni, F. Chierici, C. Corela, A. Correggiari, B. Della Vedova, E. Gracia, P. Jornet, M. Landuzzi, M. Ligi, A. Magagnoli, G. Marozzi, L. Matias, D. Penitenti, P. Rodriguez, M. Rovere, P. Terrinha, L. Vigliotti, A. Zahinos Ruiz (2001): Source of the 1755 Lisbon earthquake and tsunami investigated. *Eos, Trans. Am. Geophys. Union*, 82(26) 285-291. DOI: 10.1029/EO082i026p00285-01.

FIGURES

Figure 1: Aerial view looking eastward of Portland, Maine.

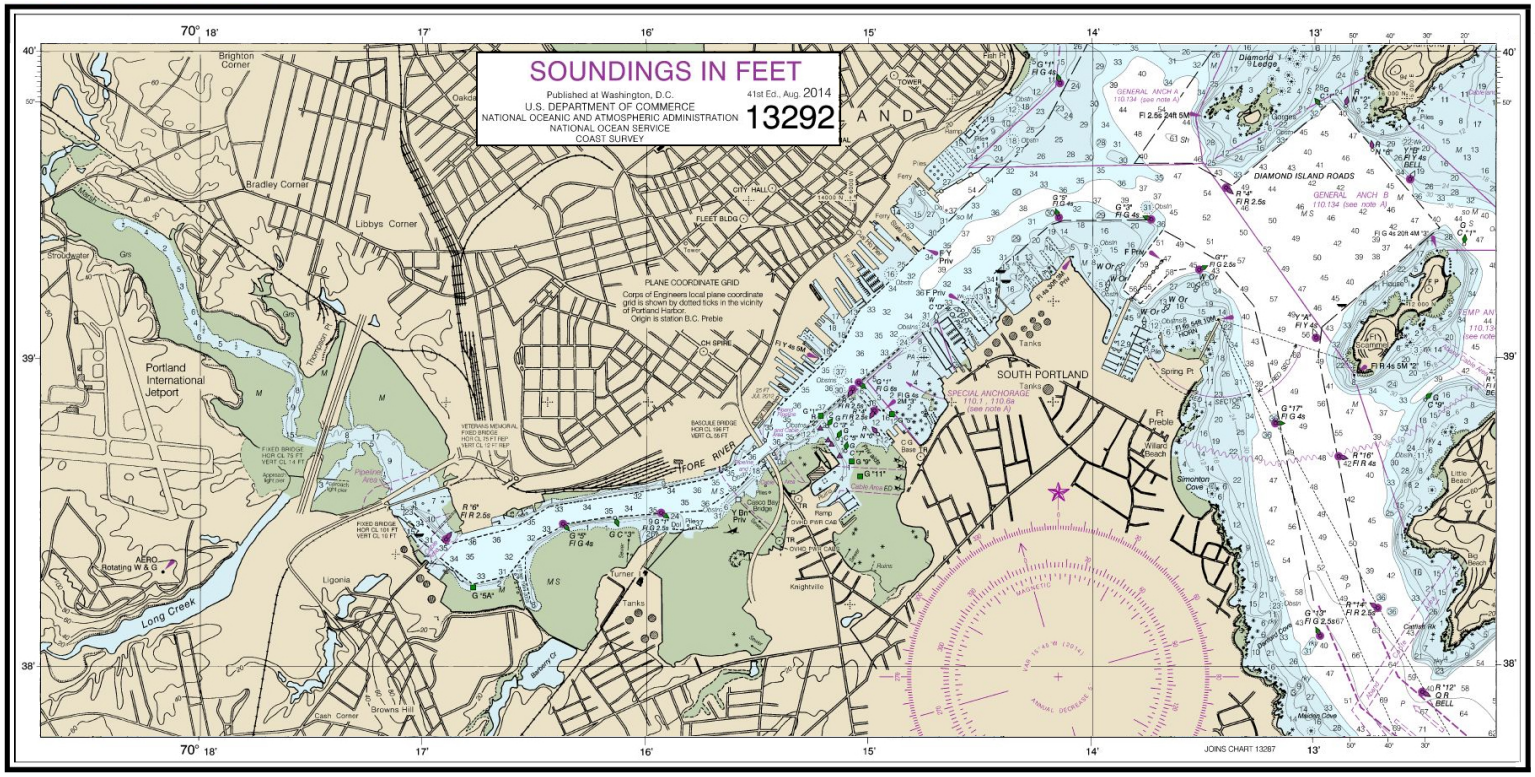

Figure 2: Extract from NOAA Chart 13292 showing the Fore River and entrance to Portland, Maine.

Figure 3: Landmarks of the Portland-South Portland area.

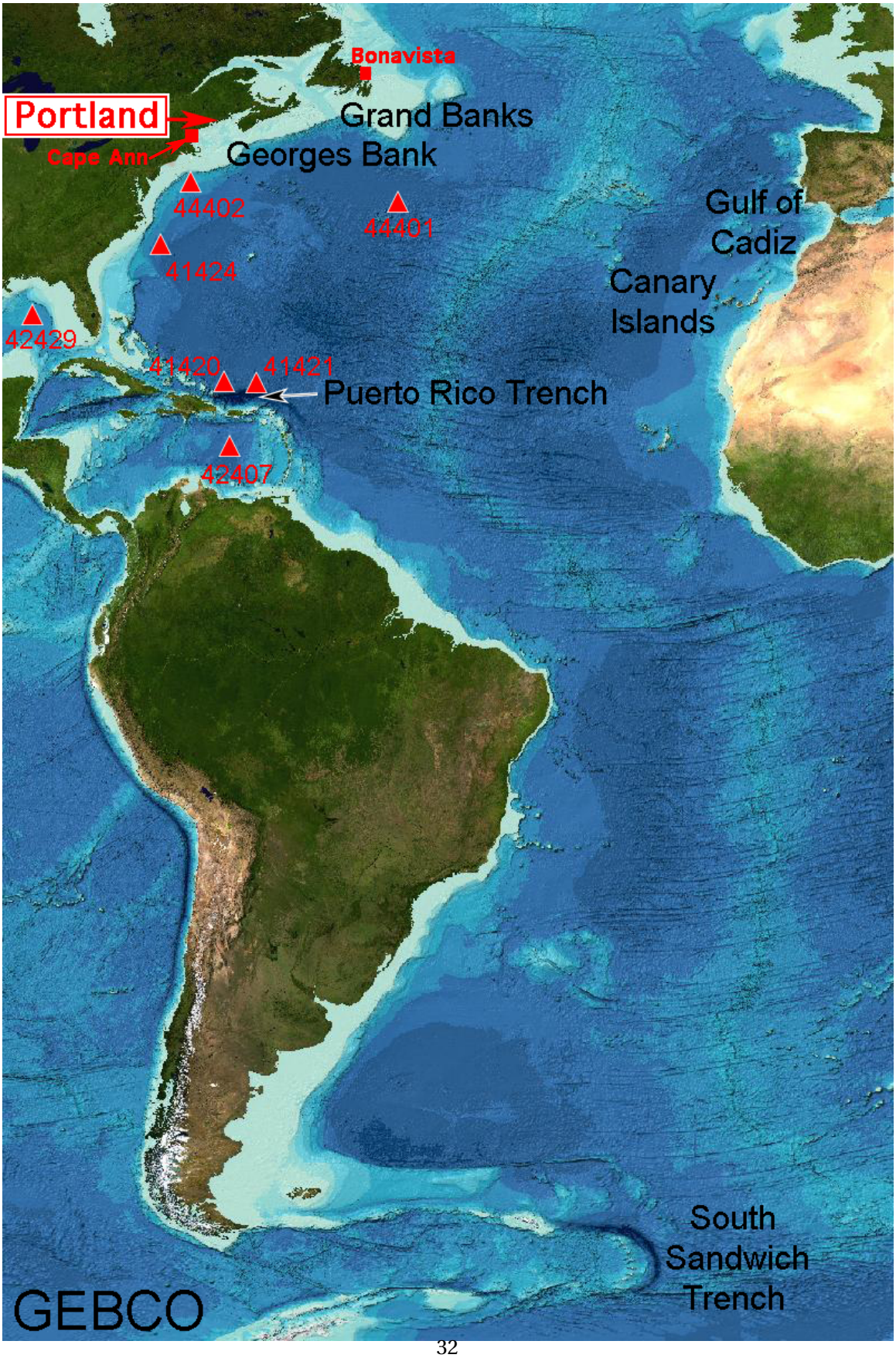

Figure 4: Portland, in relation to potential tsunami sources, and assets for their detection.

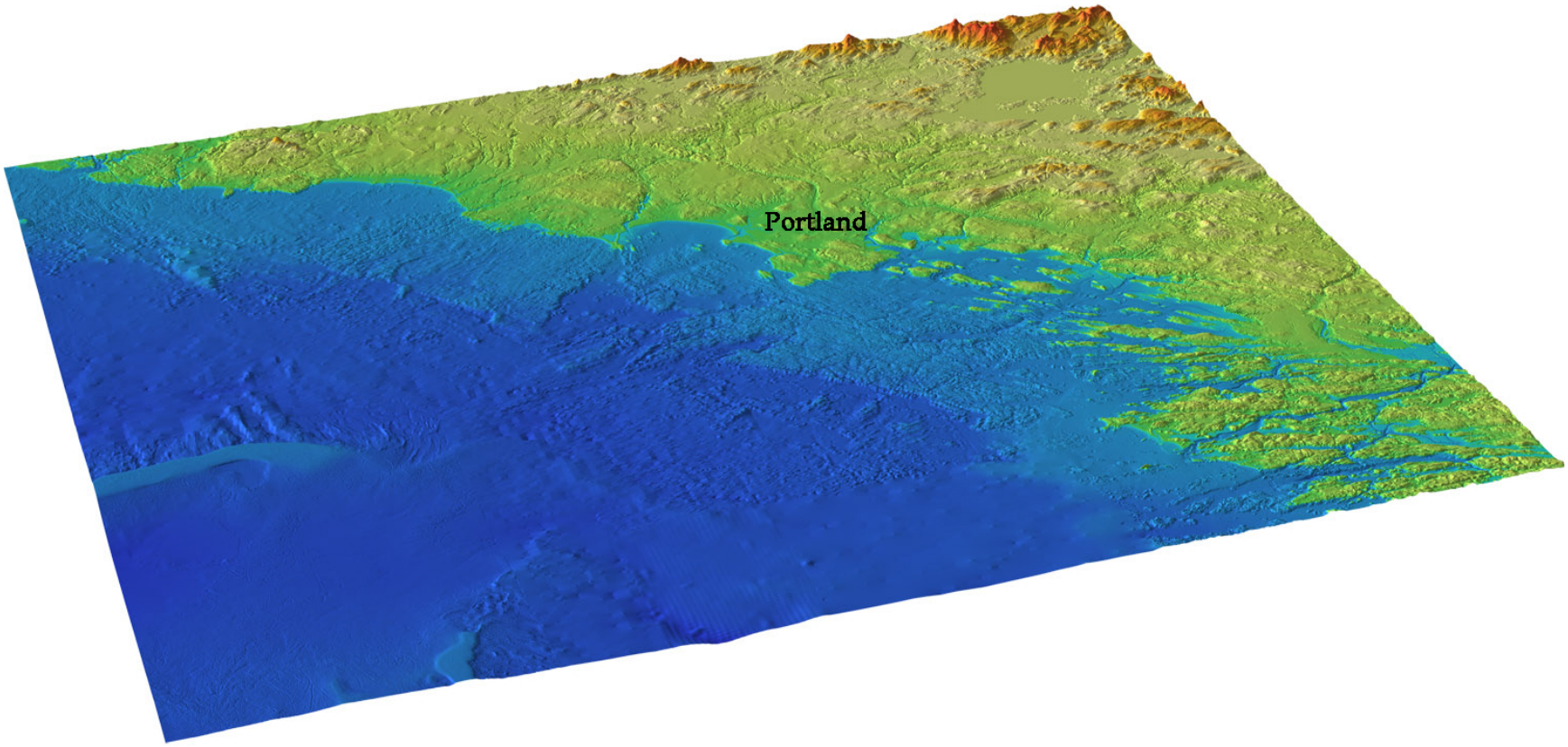

Figure 5: An oblique view of the Portland-area digital elevation model from NGDC.

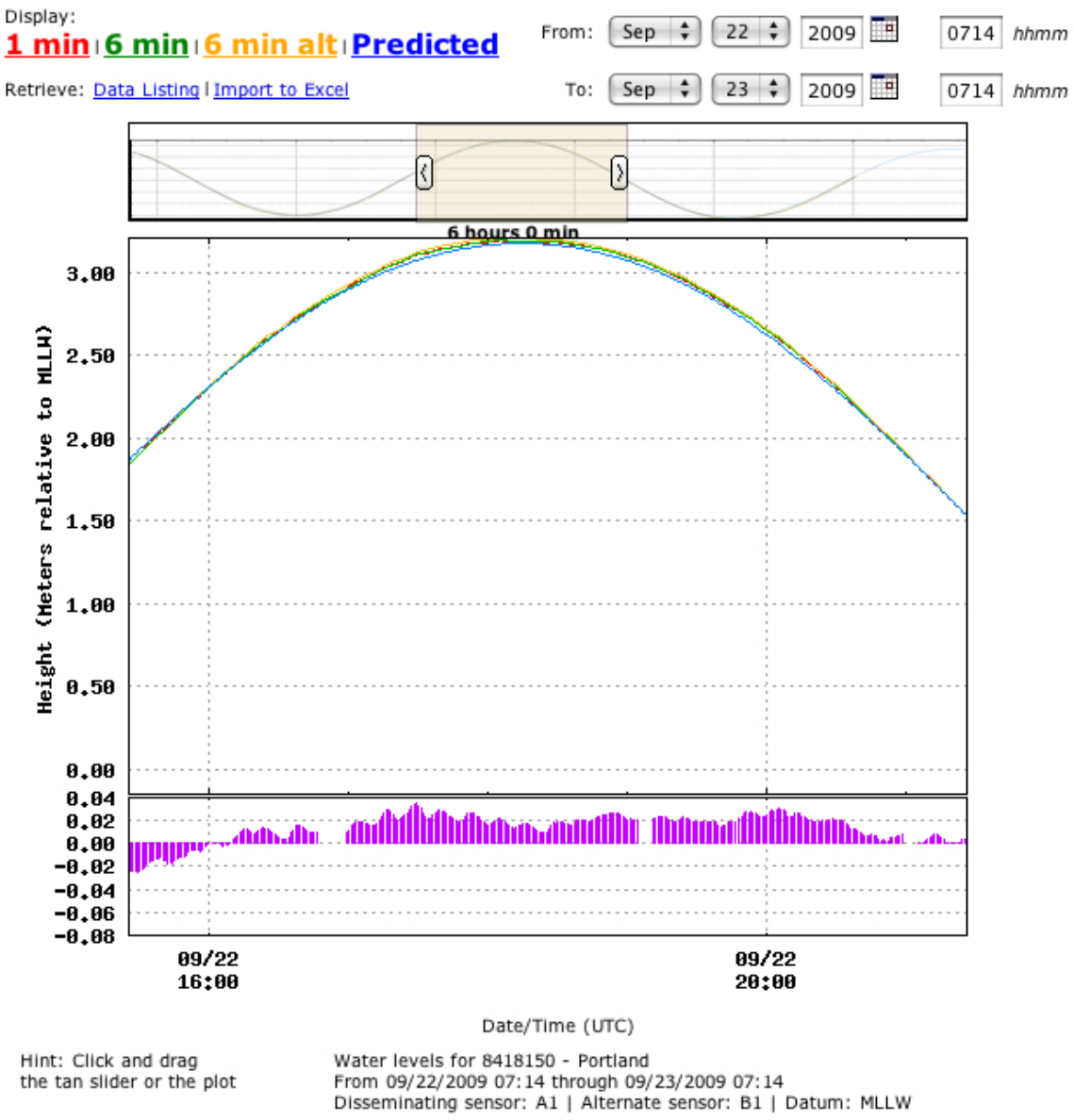

Figure 6: A sample of the record from Portland's tsunami-capable tide gauge.

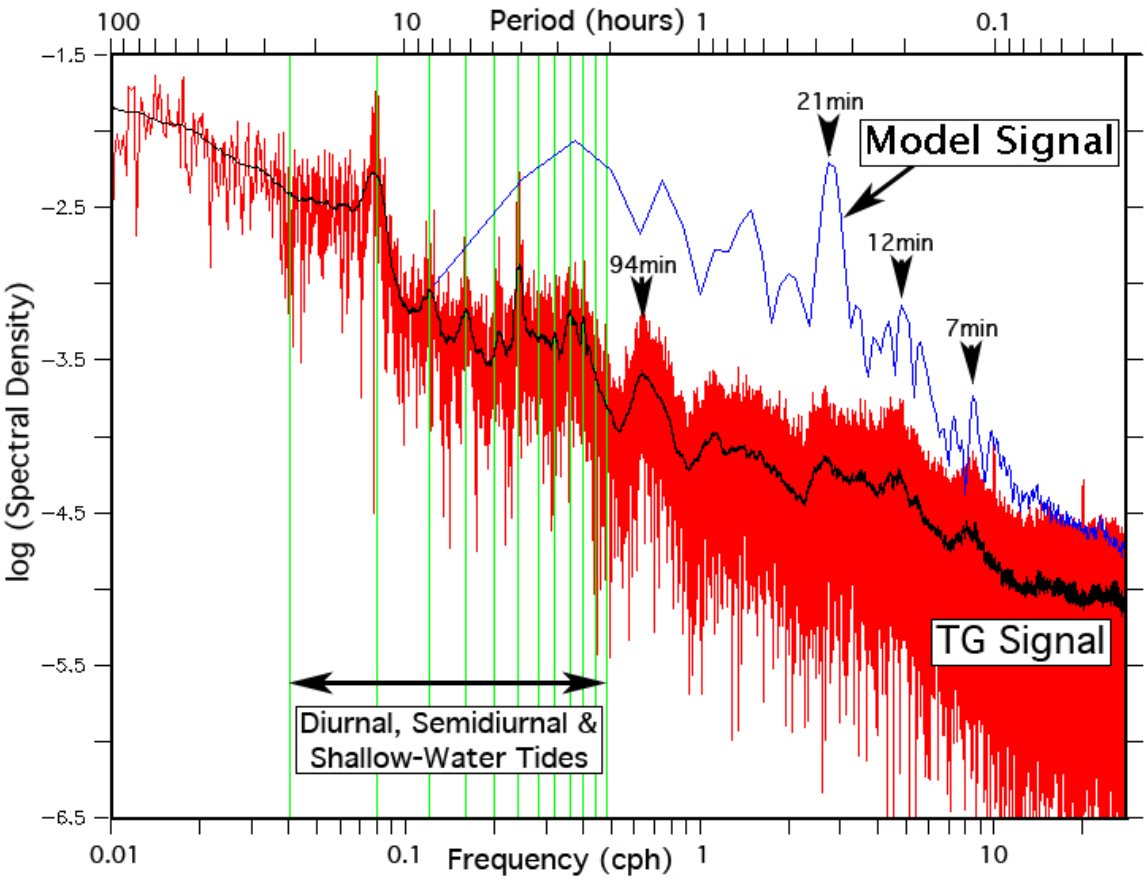

Figure 7: Spectral analysis of de-tided residuals in the Portland tide gauge record.

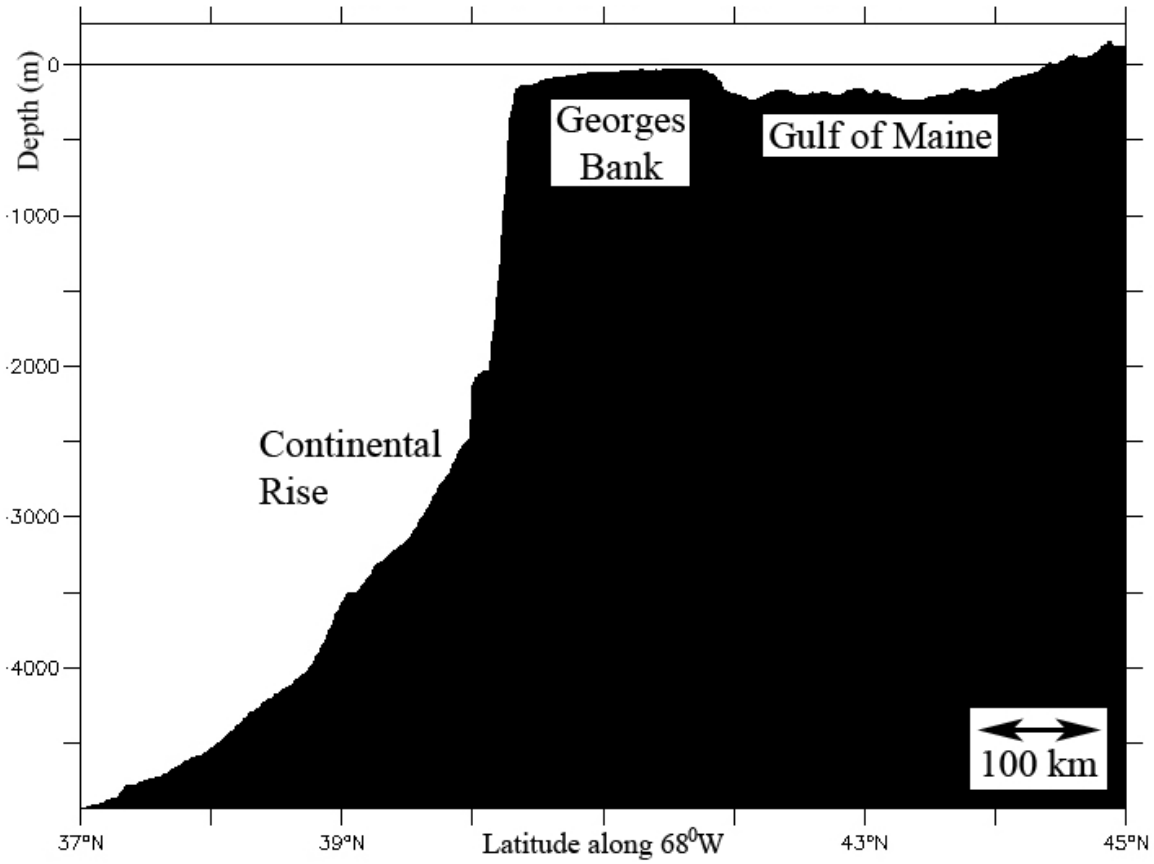

Figure 8: A meridional section of the seafloor south of the Gulf of Maine.

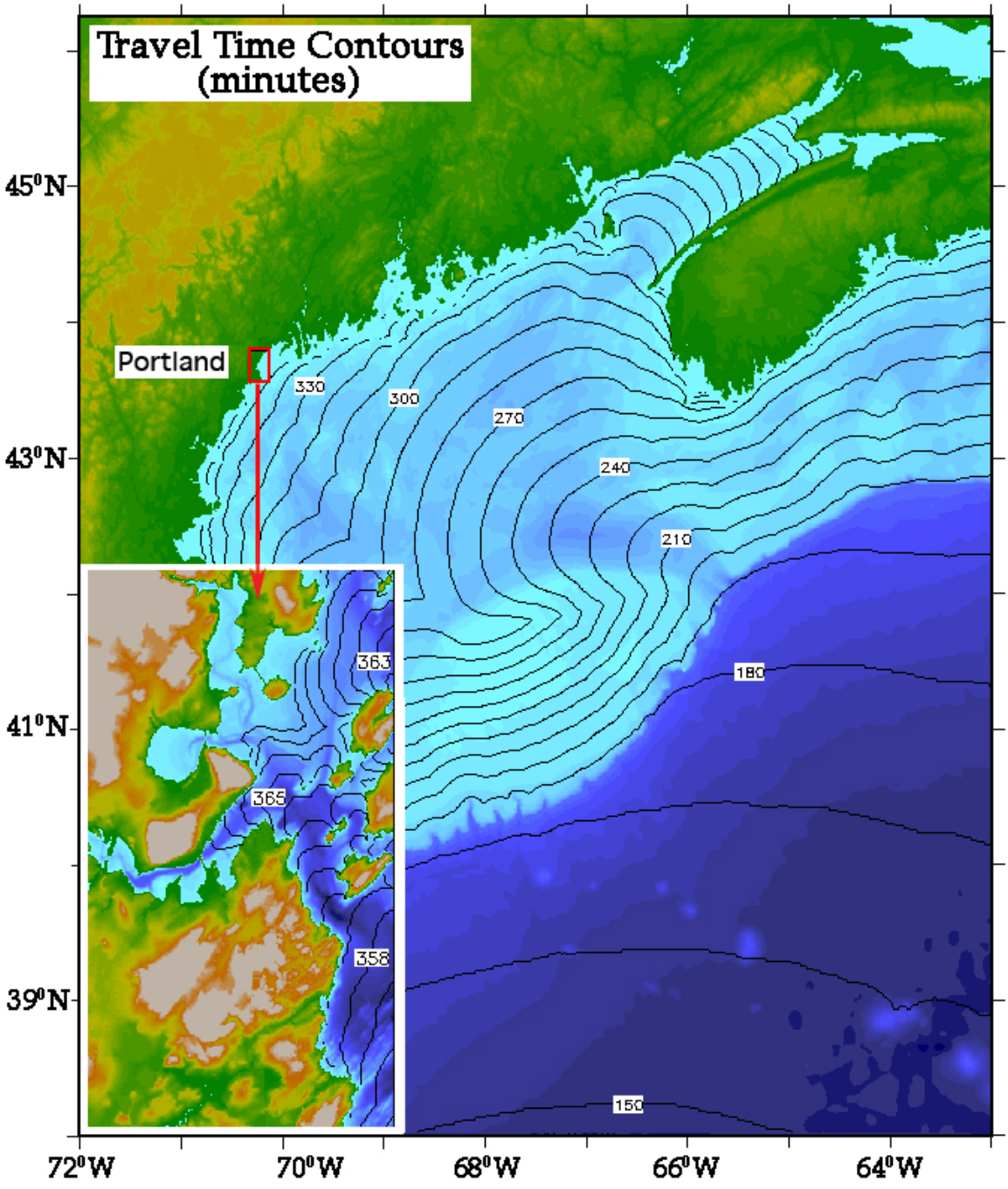

Figure 9: Compression of a wave train as it slows on encountering the continental shelf.

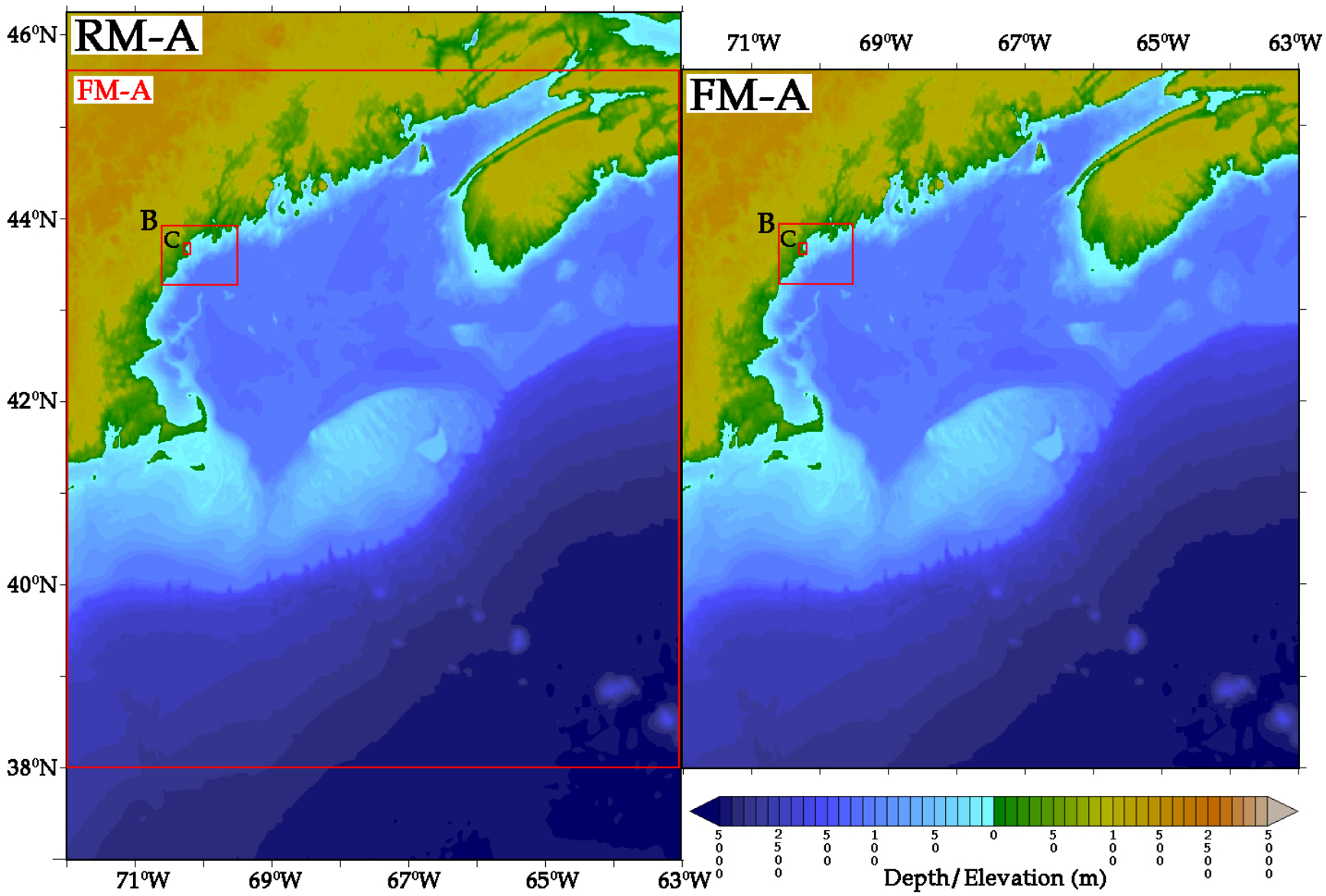

Figure 10: Grid representations for the outermost A-grid of the reference (RM, left panel) and forecast (FM, right panel) models, whose domains differ only in the bounding latitudes. The locations of the nested B and C grid boundaries are marked.

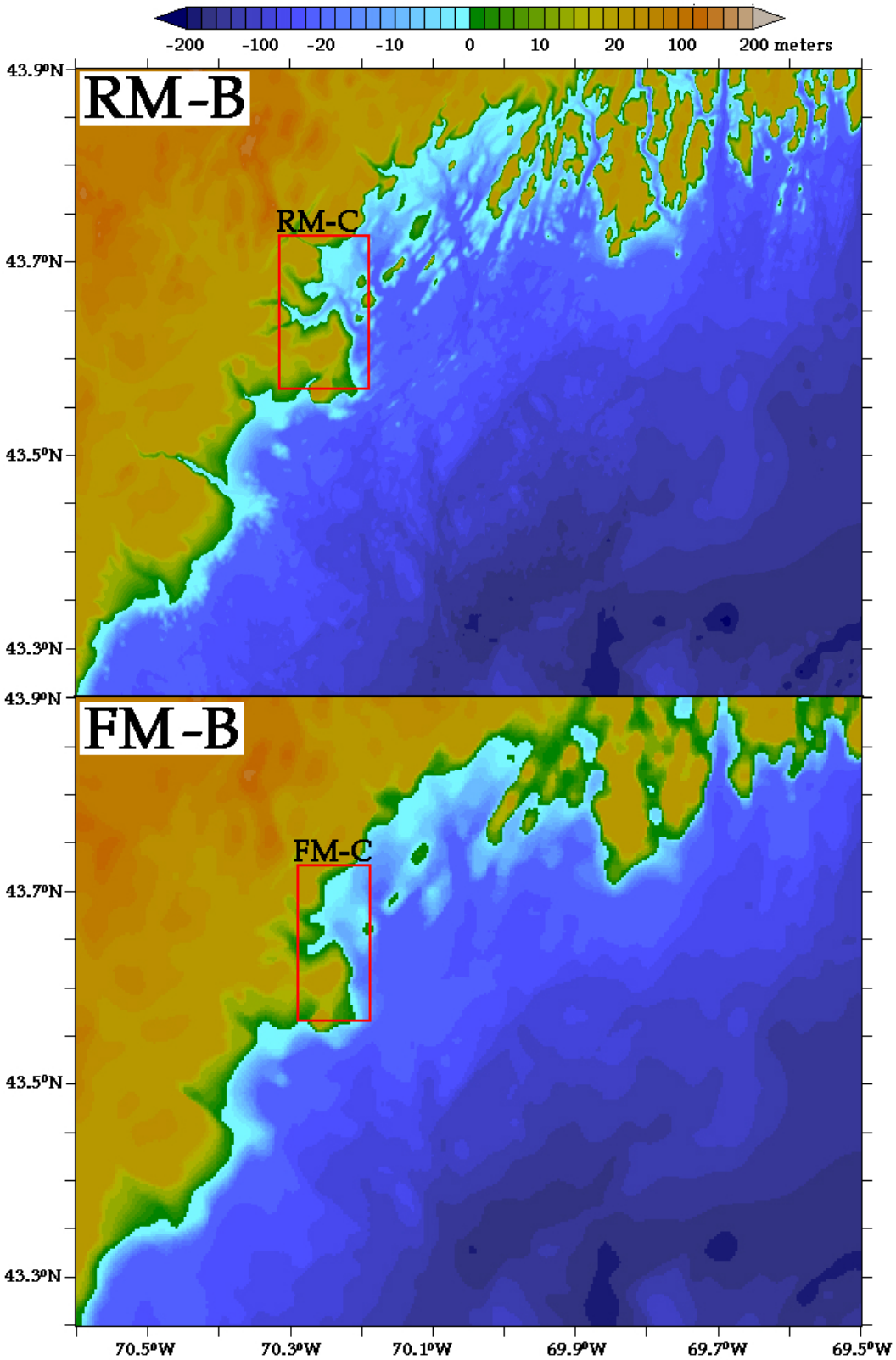

Figure 11: Grid representations for the intermediate B-grid of the reference (RM, upper panel) and forecast (FM, lower panel) models which have the same extent. Red rectangles indicate the location of the C-grids which also have a common extent.

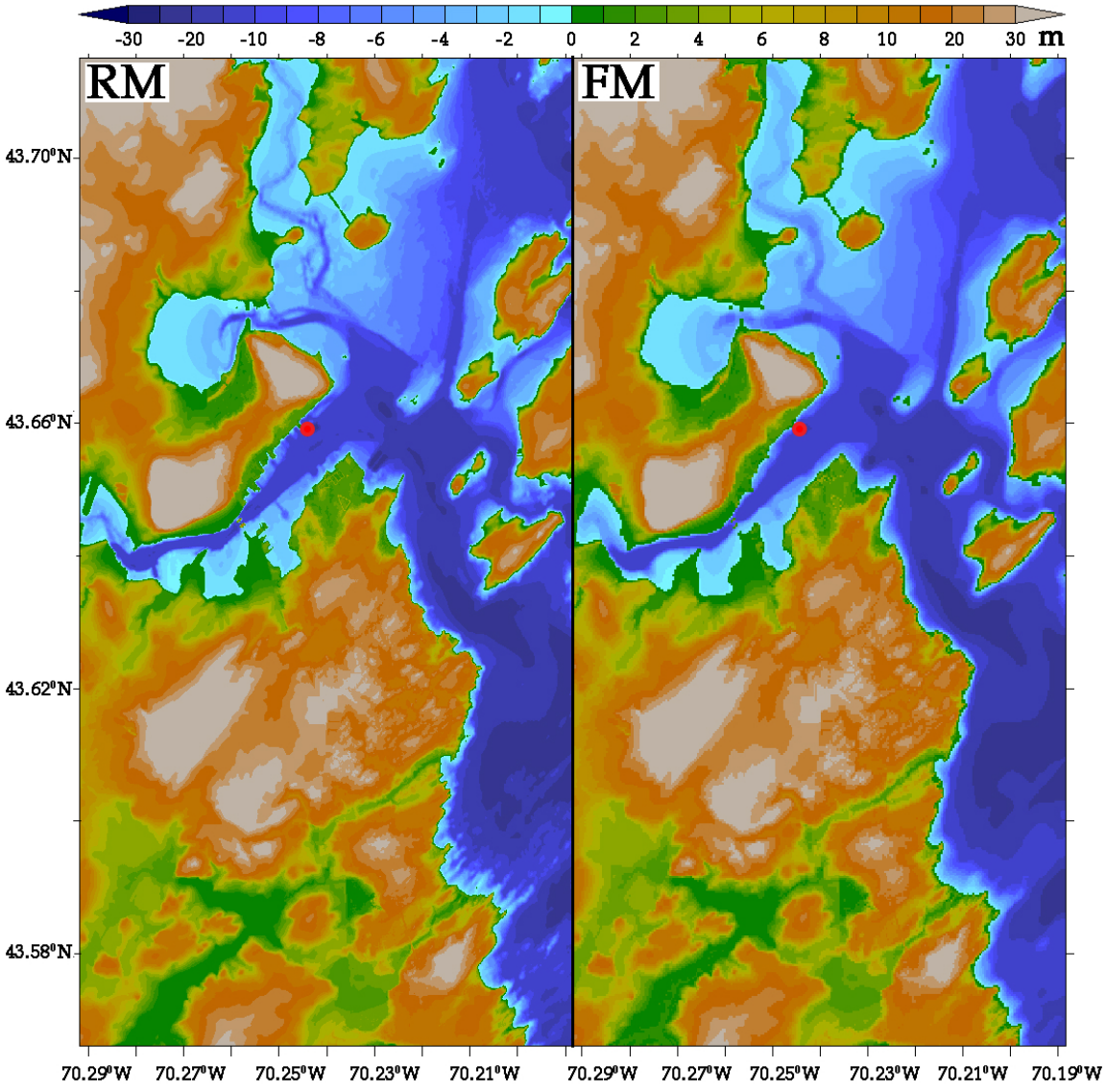

Figure 12: Grid representations for the innermost C-grid of the reference (RM, left panel) and forecast (FM, right panel) models. A red circle marks the location of the Portland tide gauge which is the model reference point.

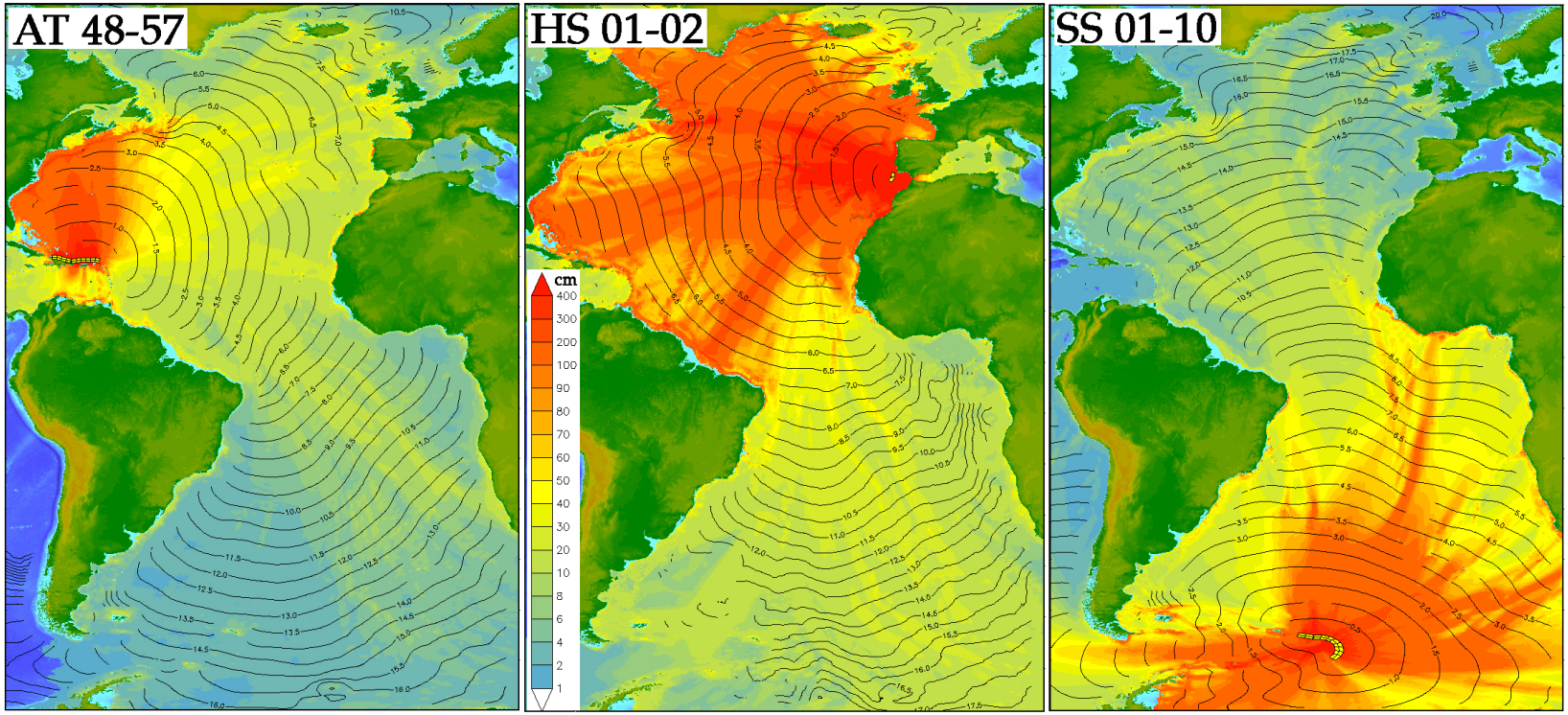

Figure 13: Propagation patterns for three mega-event scenarios, representative of Caribbean, Eastern, and South Atlantic sources. Color-coding, common to all panels, represents the maximum amplitude in the evolution of each tsunami wave train. Travel time contours are at half-hourly intervals. Yellow rectangles mark the sources.

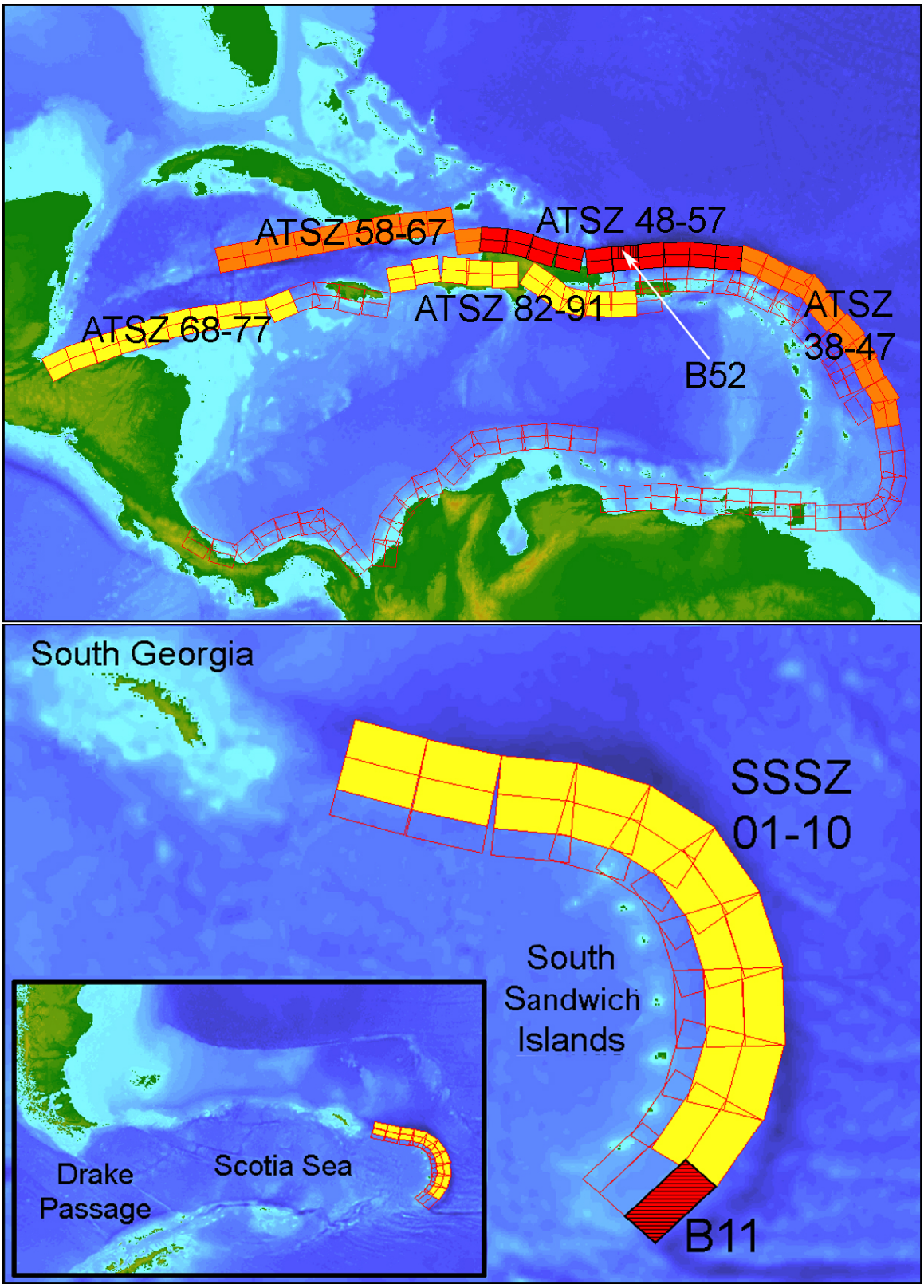

Figure 14: Unit source-based synthetic scenarios employed for Portland, Maine model testing. Twenty-unit mega-event groupings are marked; the singletons (B52 and B11) used in testing are cross-hatched.

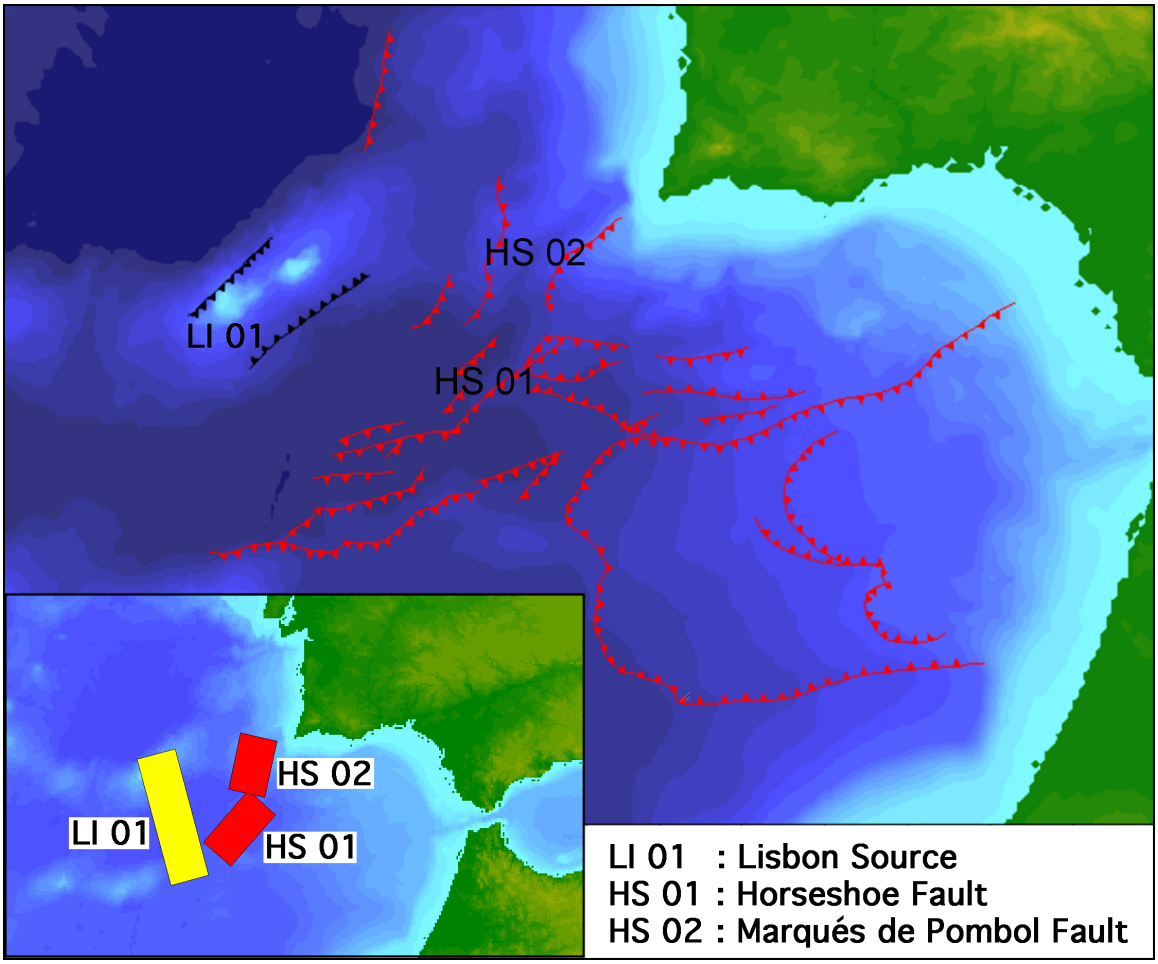

Figure 15: Customized synthetic scenarios used to represent the Eastern Atlantic in Portland, Maine model testing. Those colored red are combined with uniformly distributed slip as a single mega-event source HS 01-02; the L1 01 source, marked in yellow, with a greatly reduced slip, is used in micro-event testing.

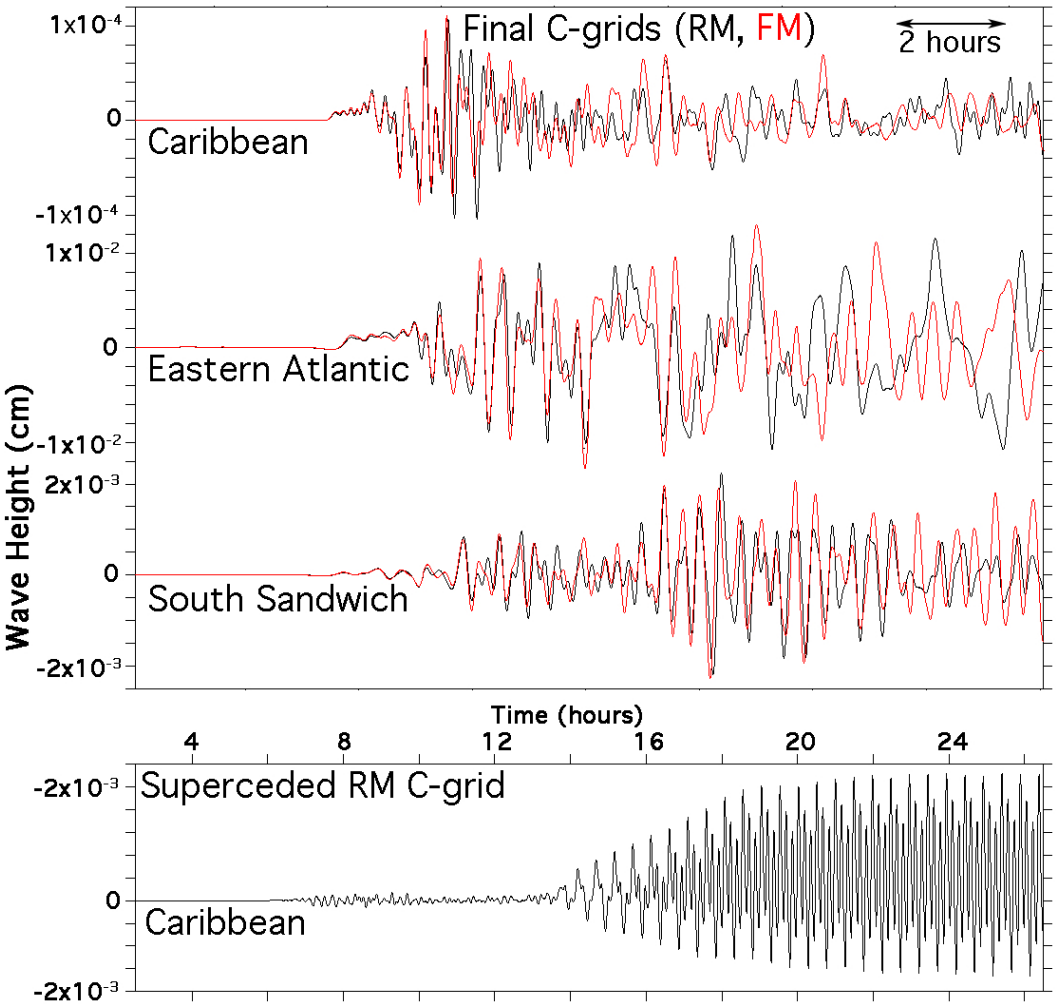

Figure 16: Micro-tsunami testing of the Portland, Maine models. Wave amplitudes at the Portland tide gauge reference point are drawn in the upper panel for the reference (RM, black) and forecast model (FM, red) solutions for the three sources. The lower panel illustrates the appearance of instability in a superceded version of the reference model C-grid.

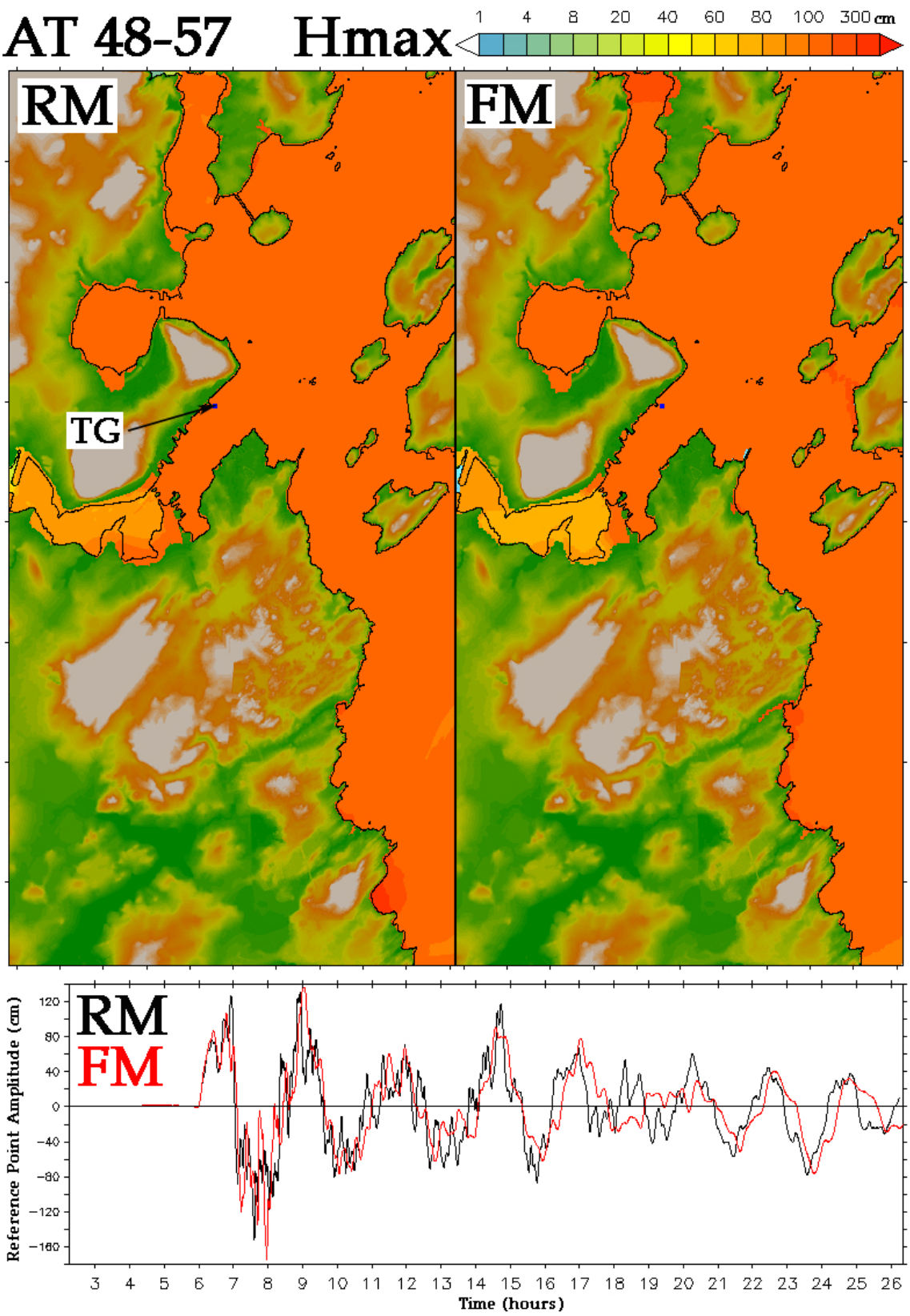

Figure 17: Comparison of maximum amplitude (upper panels) and reference point time series (lower panel) for the Reference (RM) and Forecast Model (FM) simulations of synthetic source AT 48-57. A small blue mark indicates the location of the Portland tide gauge (TG) reference point; the MHW coastline is drawn to delineate areas of inundation.

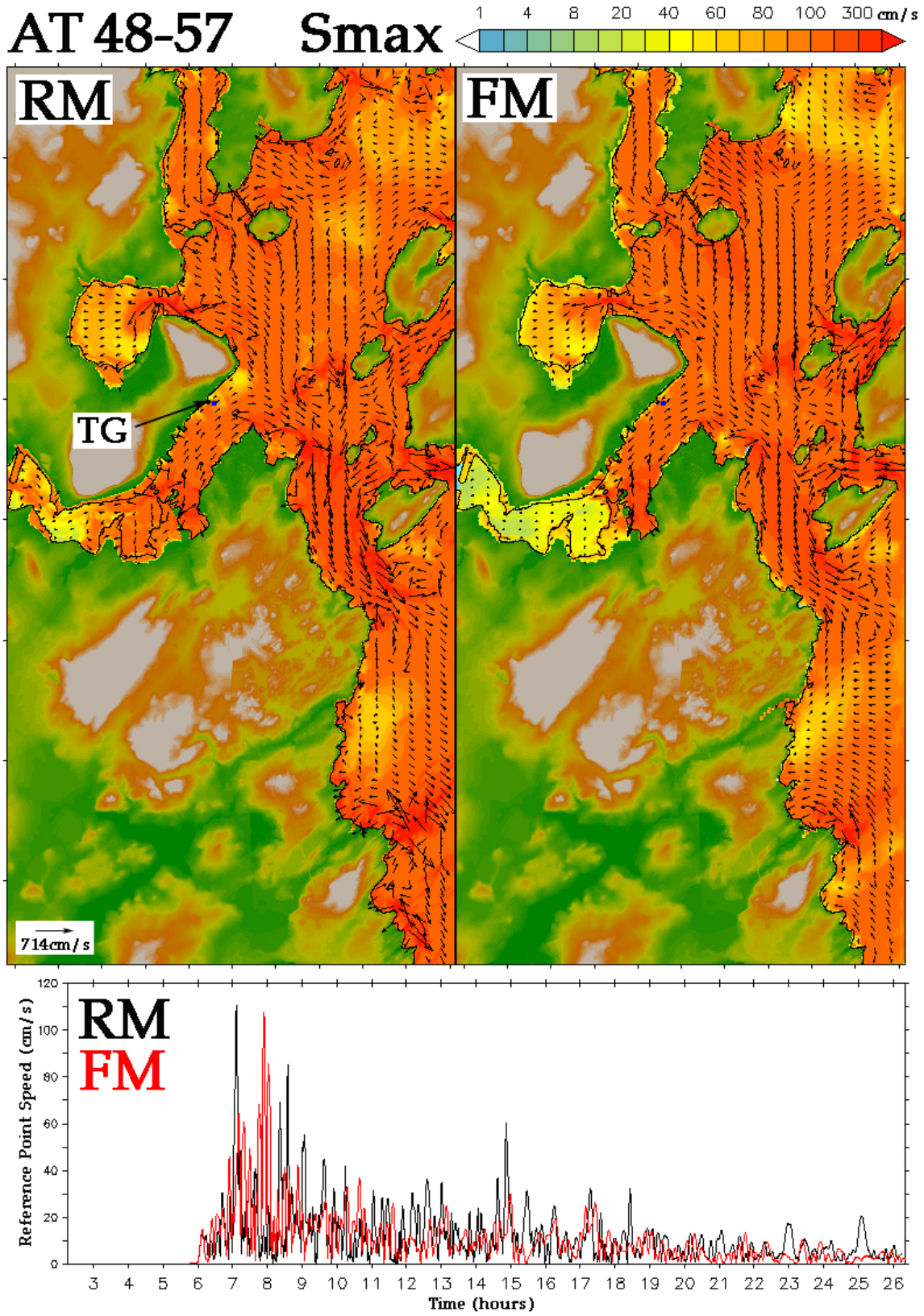

Figure 18: Comparison of maximum speed and direction (upper panels) and reference point time series (lower panel) for the Reference (RM) and Forecast Model (FM) simulations of synthetic source AT 48-57. Velocity vectors are drawn at the time of maximum speed for a subset of grid cells.

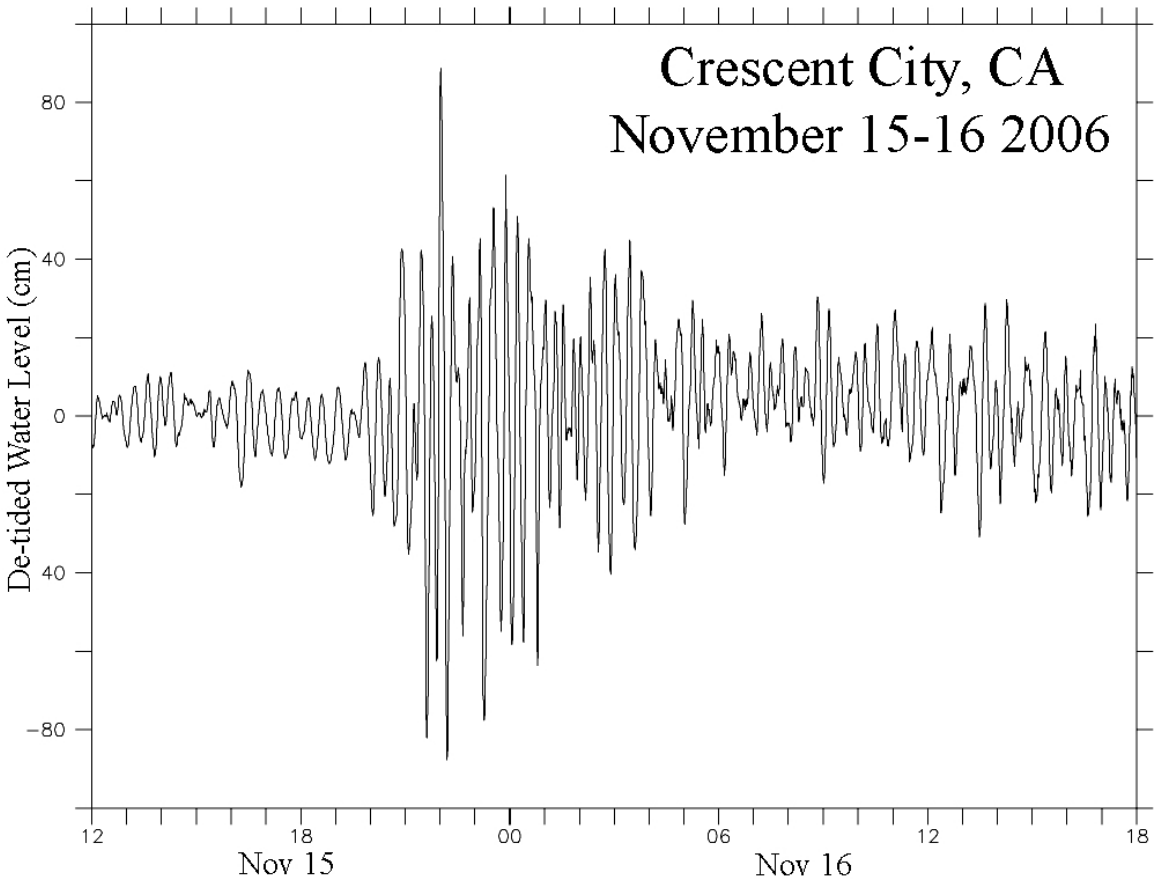

Figure 19: Response of the Crescent City, California tide gauge to forcing by the Kuril Island event of November 2006, illustrating harbor ringing. Similar resonances and reflections within Portland Harbor may extend the duration of a tsunami event there.

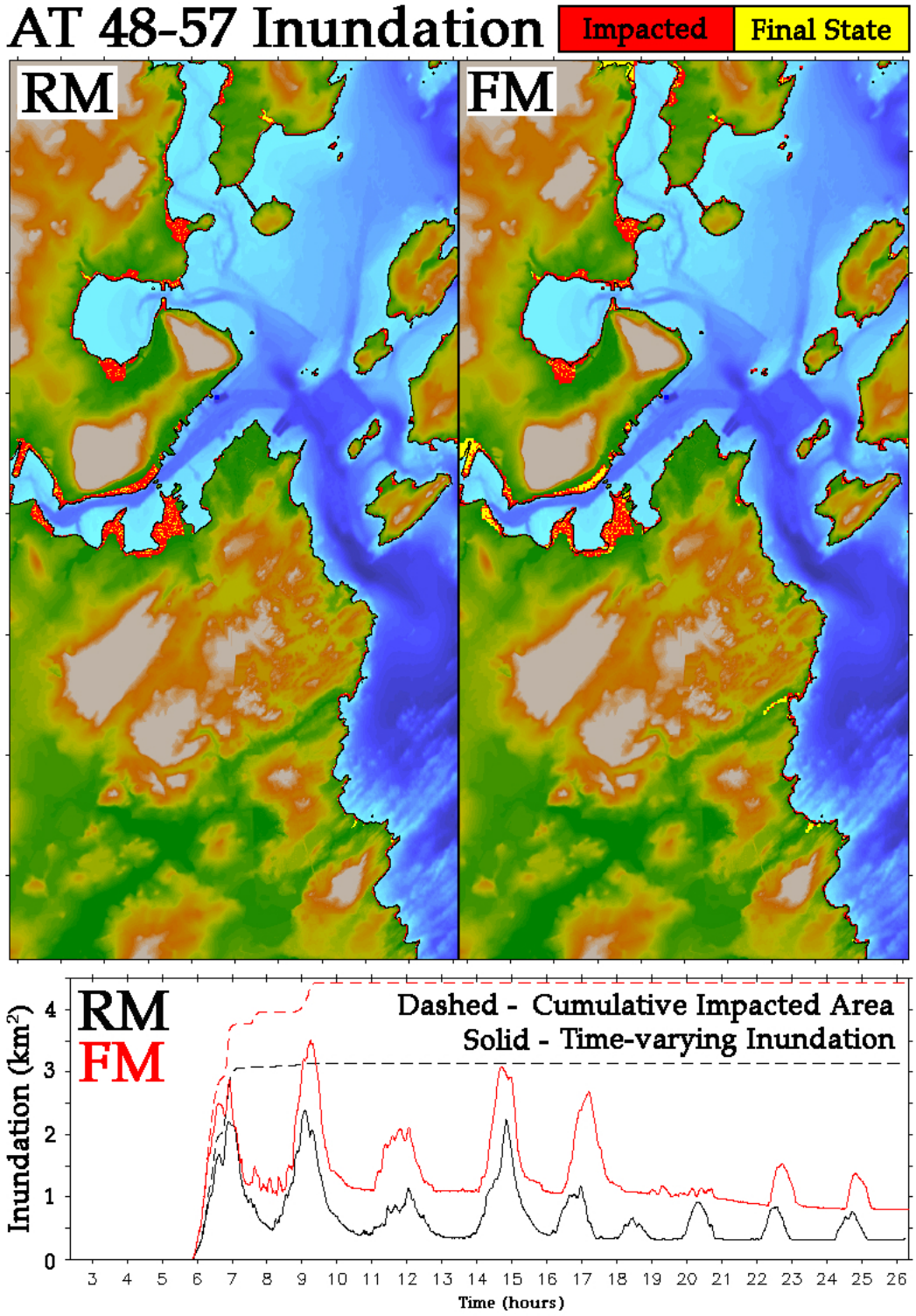

Figure 20: Comparison of impacted cells (upper panels) and inundated area time series (lower panel) for the Reference (RM) and Forecast Model (FM) simulations of synthetic source AT 48-57. Cells colored yellow in the upper panels remain inundated at the end of the simulation. Solid lines in the lower panel show the time variation in inundated area; dashed lines the cumulative area inundated to date.

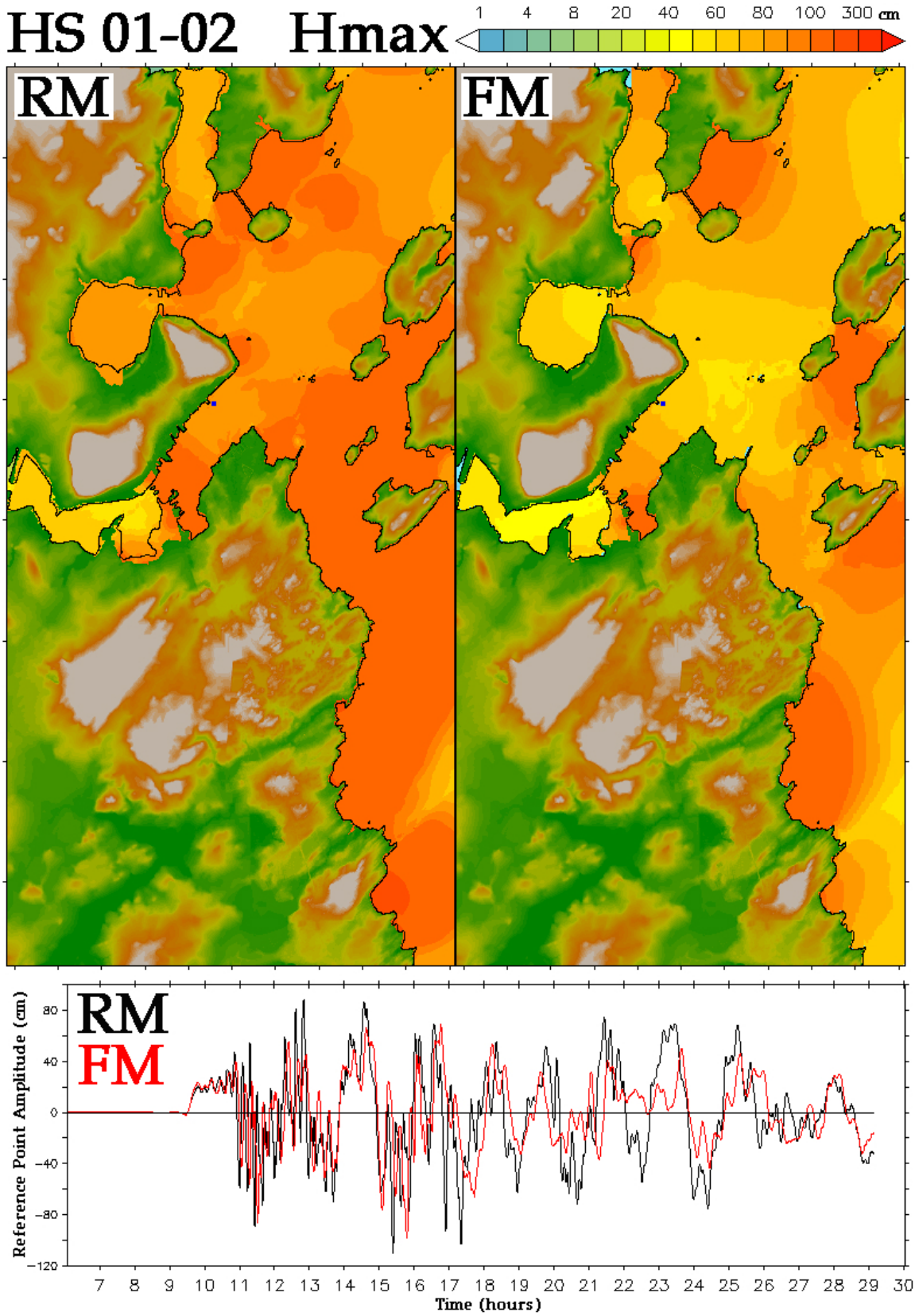

Figure 21: As in Figure 17 but for the HS 01–02 scenario.

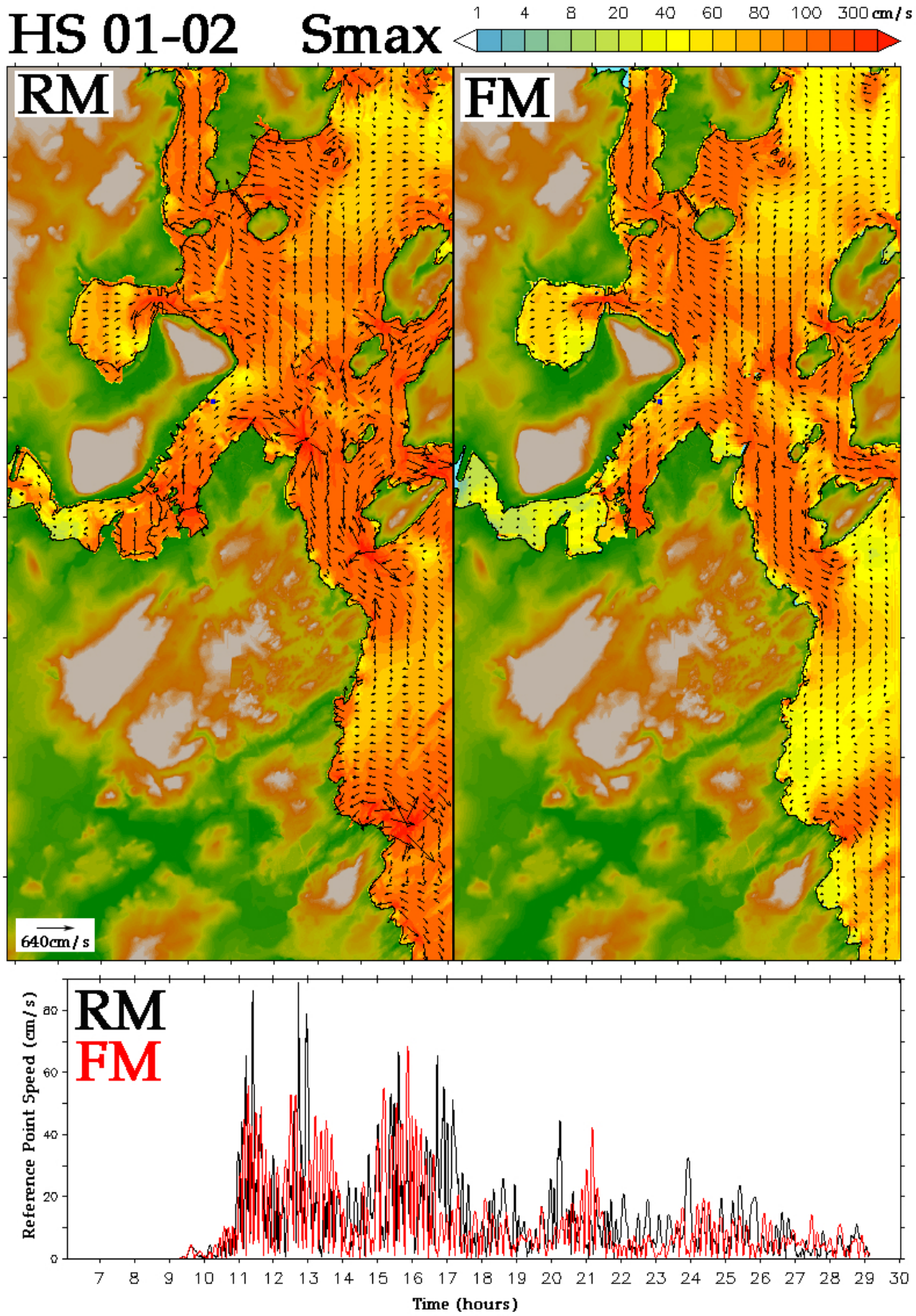

Figure 22: As in Figure 18 but for the HS 01–02 scenario.

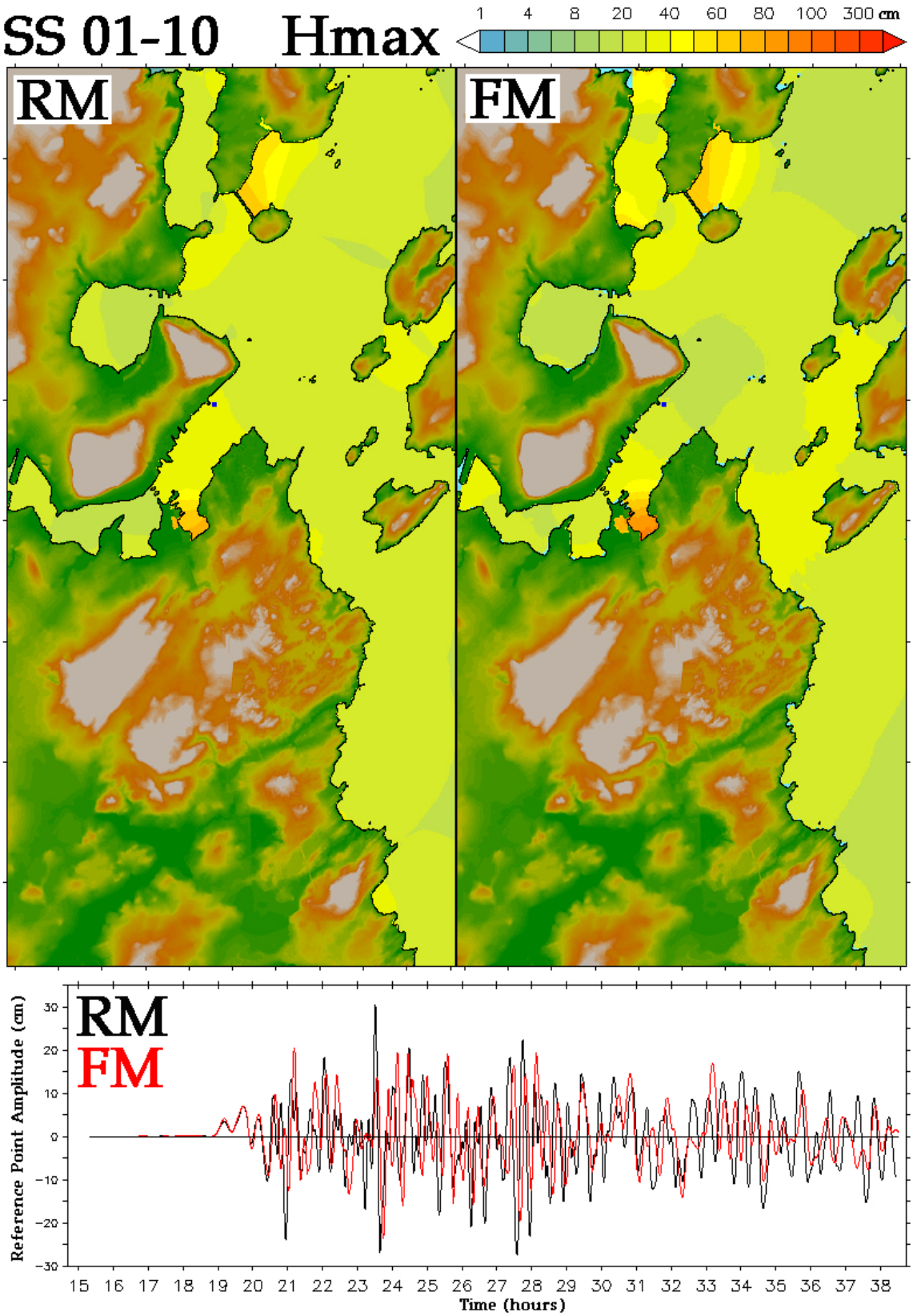

Figure 23: As in Figure 17 but for the SS 01–10 scenario.

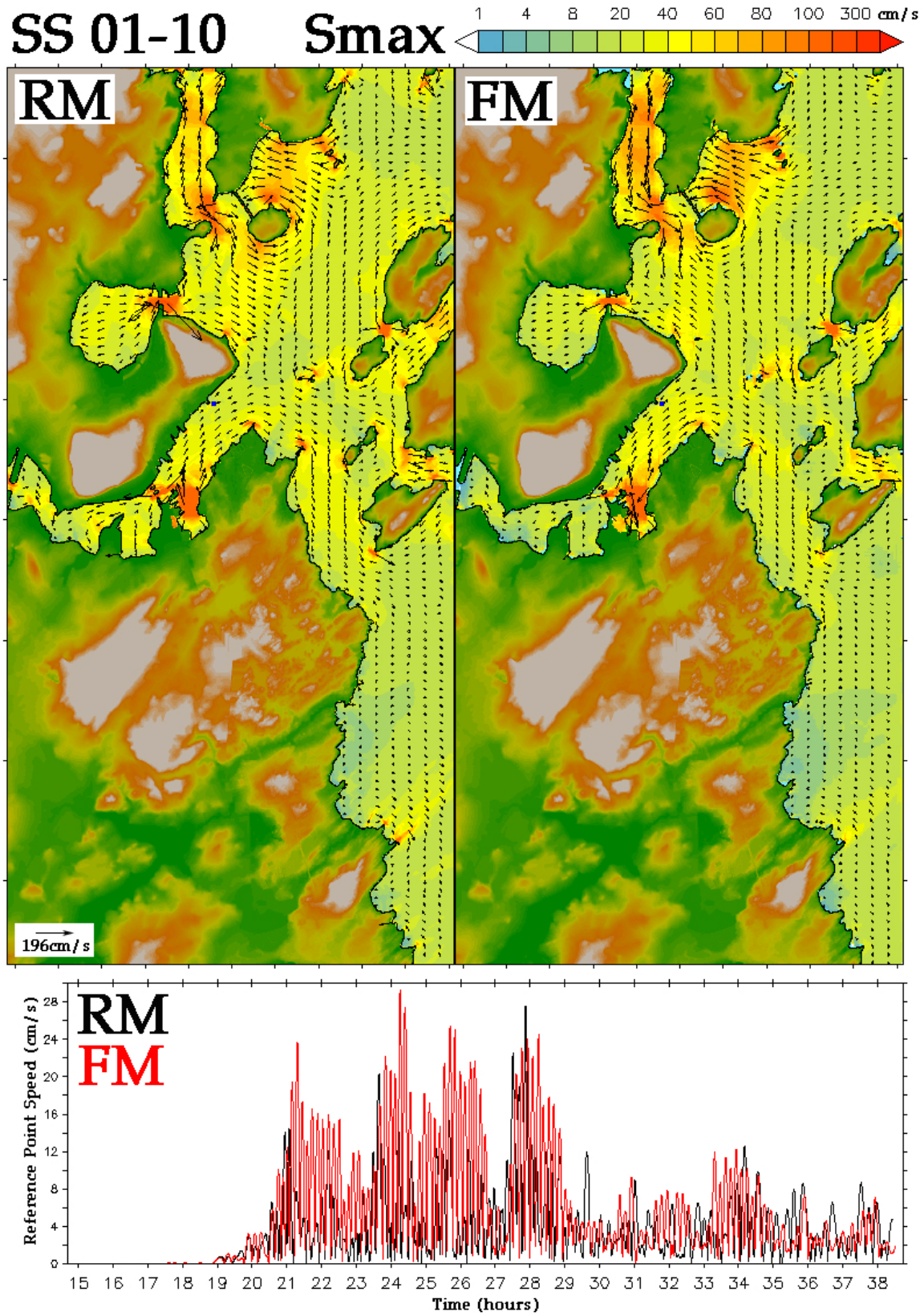

Figure 24: As in Figure 18 but for the SS 01–10 scenario.

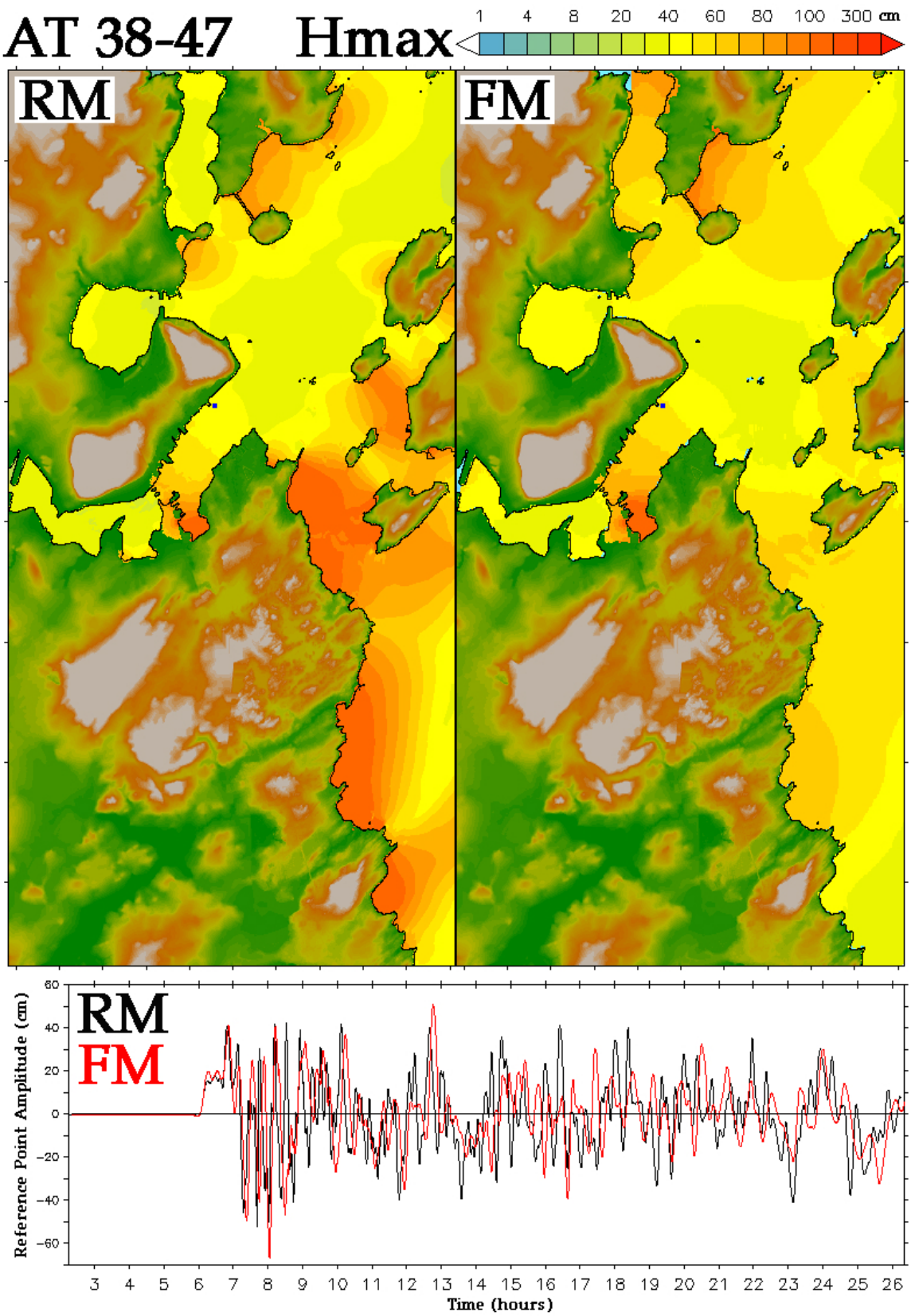

Figure 25: As in Figure 17 but for the AT 38–47 scenario.

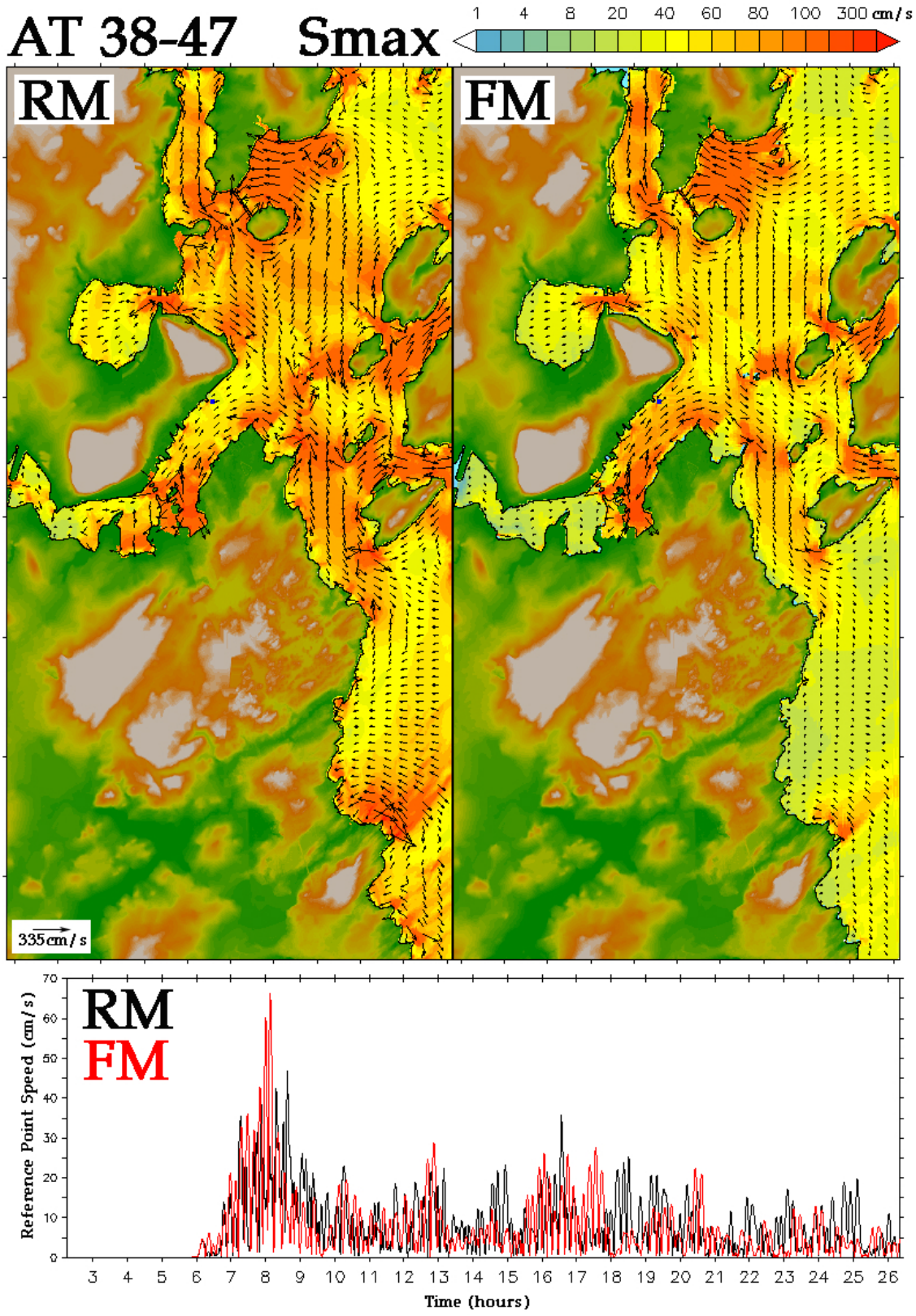

Figure 26: As in Figure 18 but for the AT 38–47 scenario.

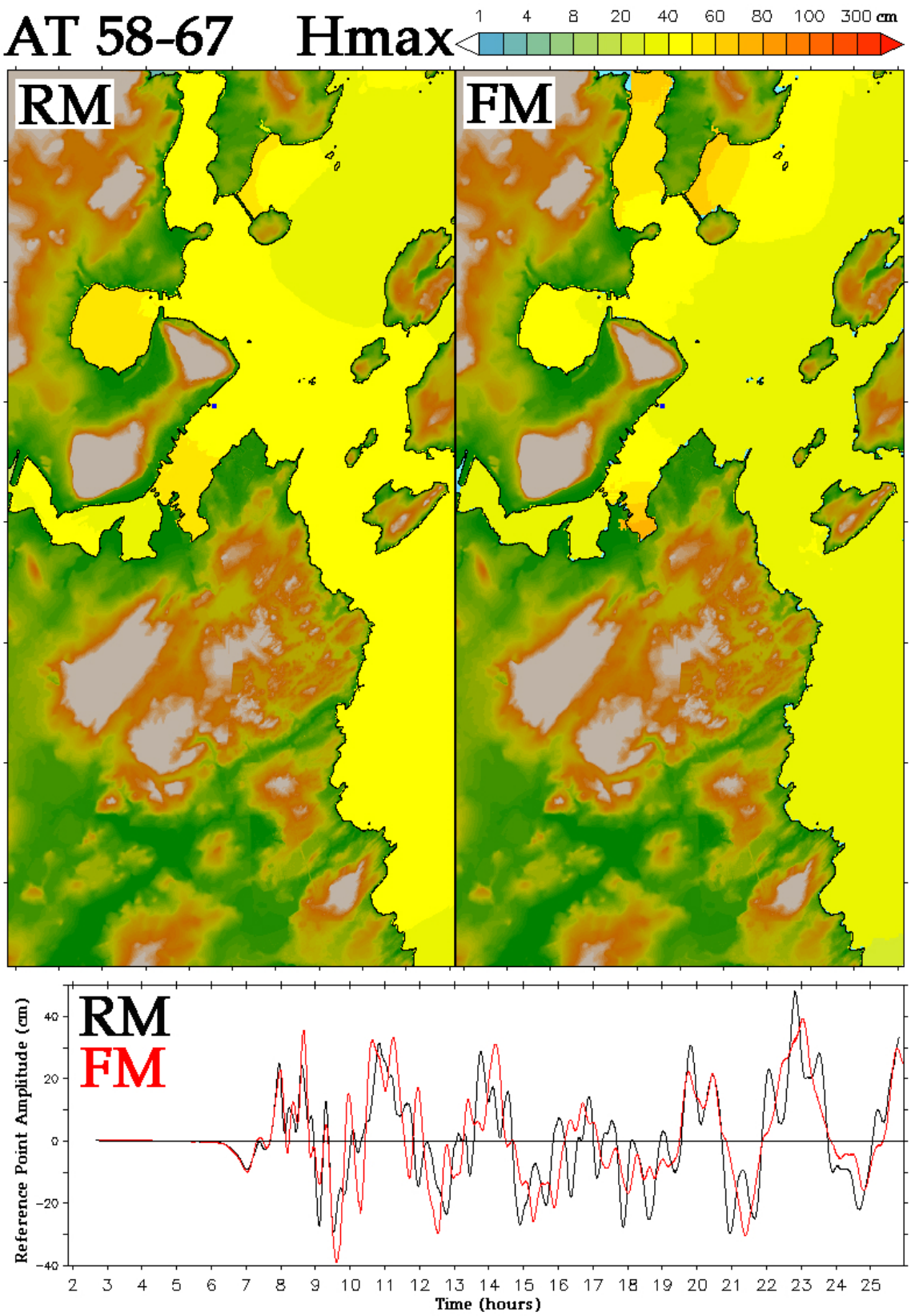

Figure 27: As in Figure 17 but for the AT 58–67 scenario.

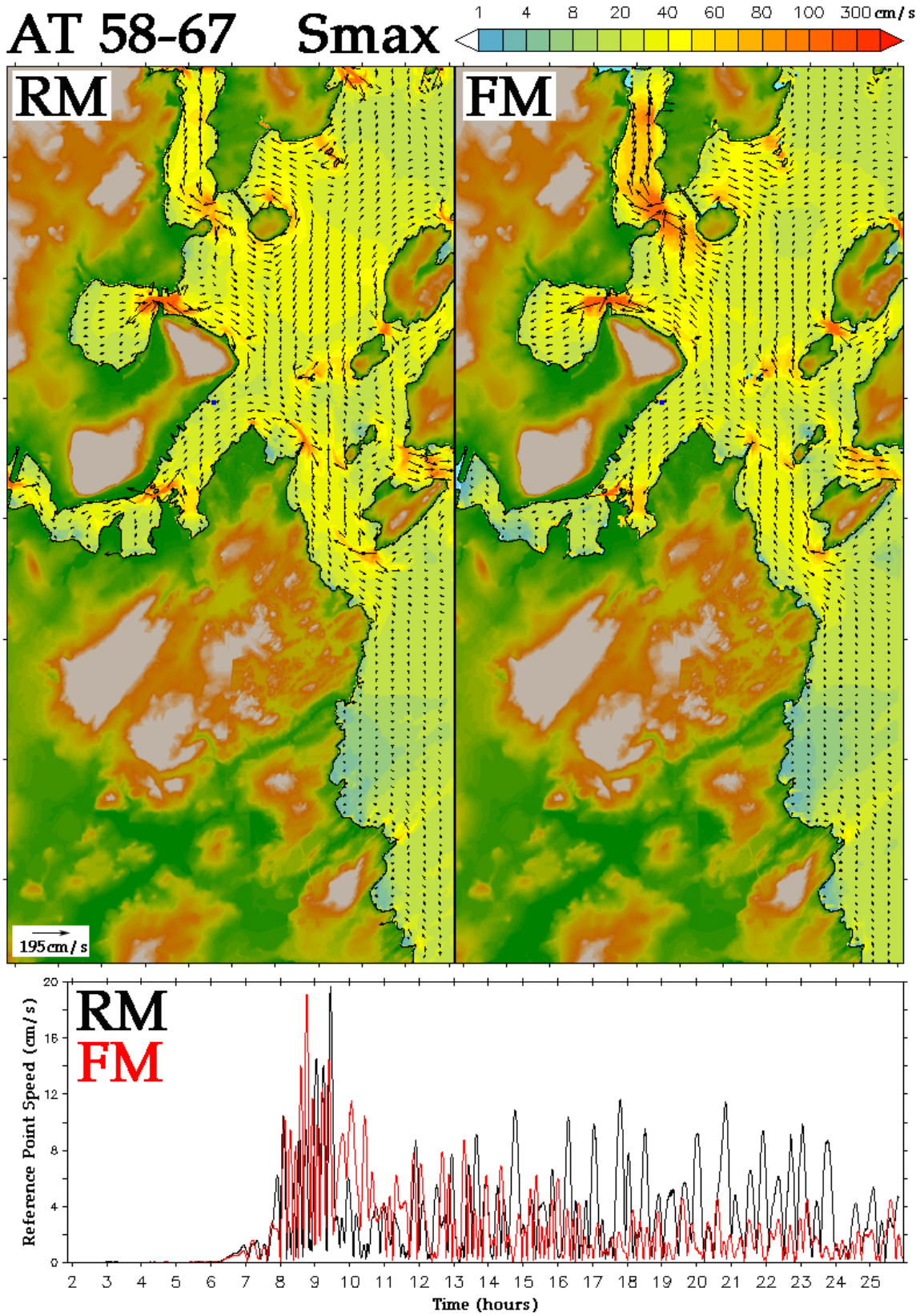

Figure 28: As in Figure 18 but for the AT 58–67 scenario.

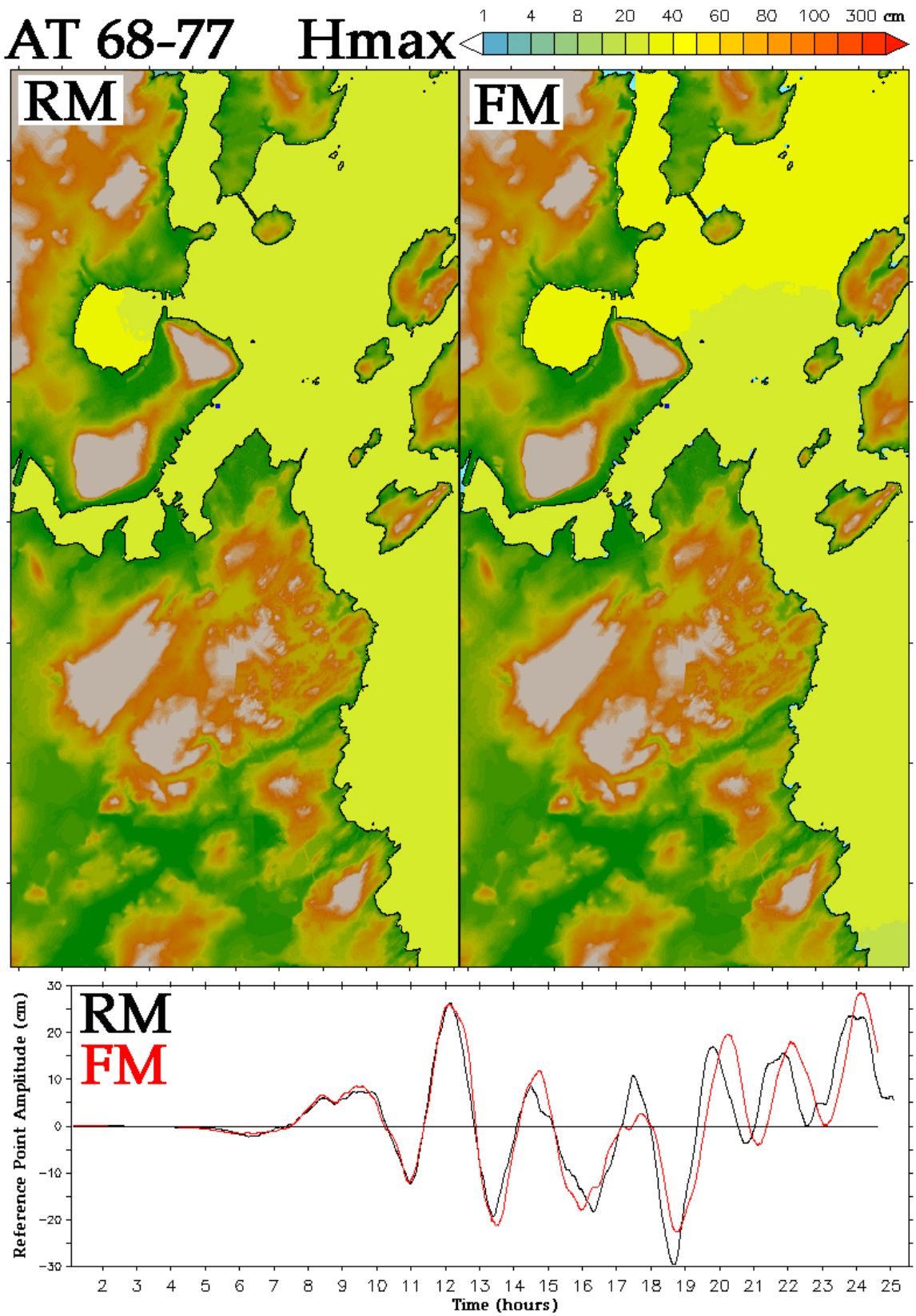

Figure 29: As in Figure 17 but for the AT 68–77 scenario.

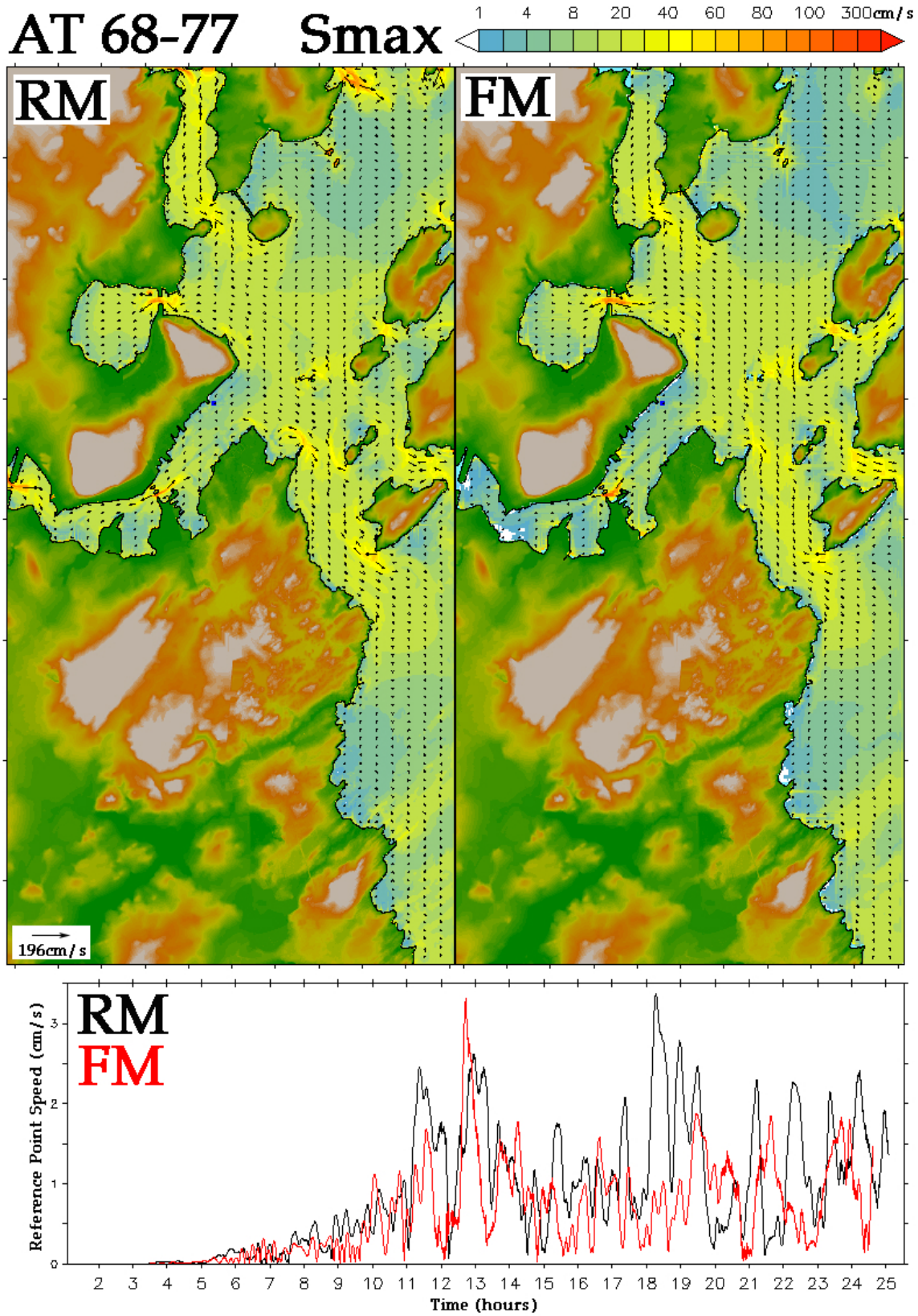

Figure 30: As in Figure 18 but for the AT 68–77 scenario.

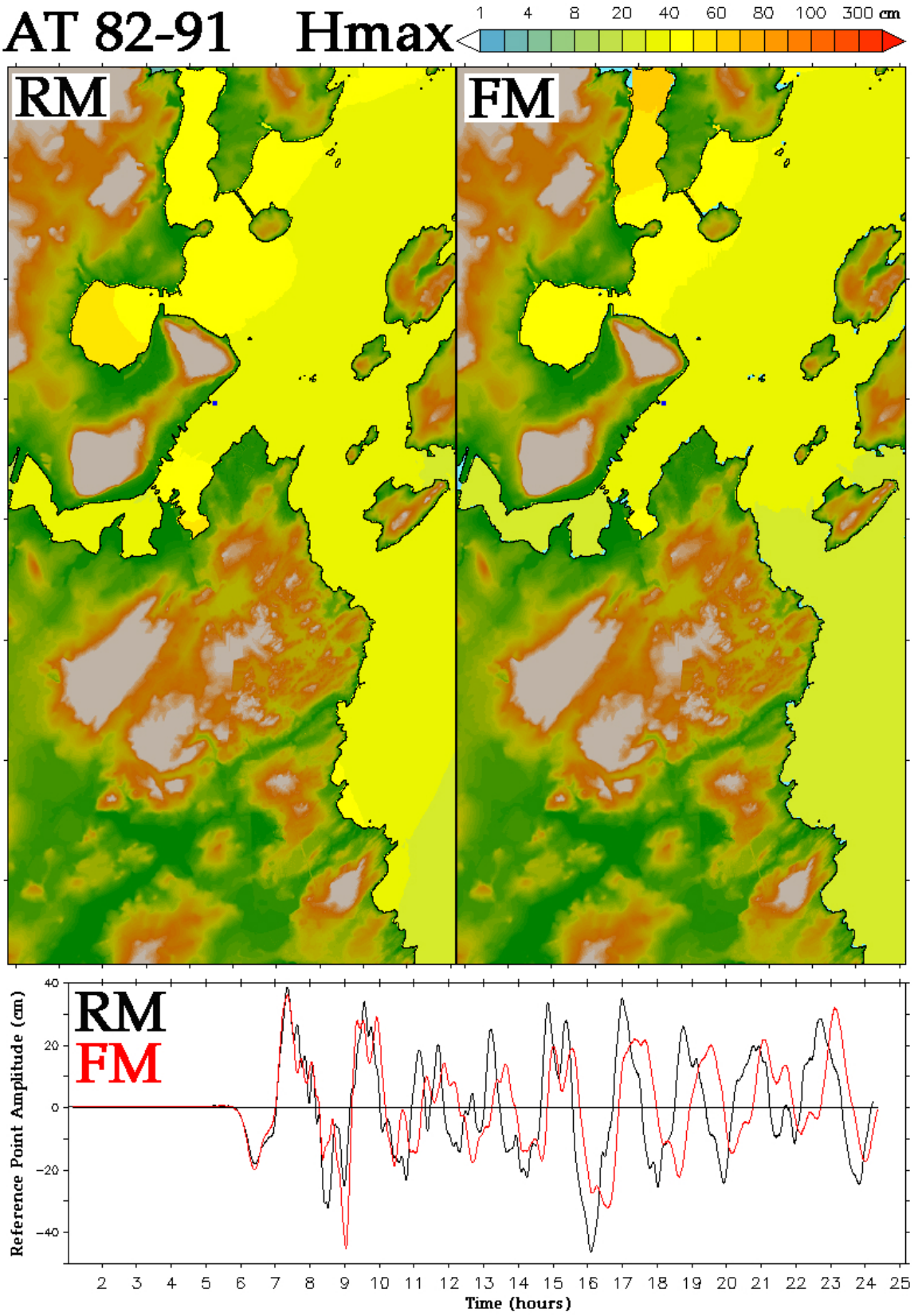

Figure 31: As in Figure 17 but for the AT 82–91 scenario.

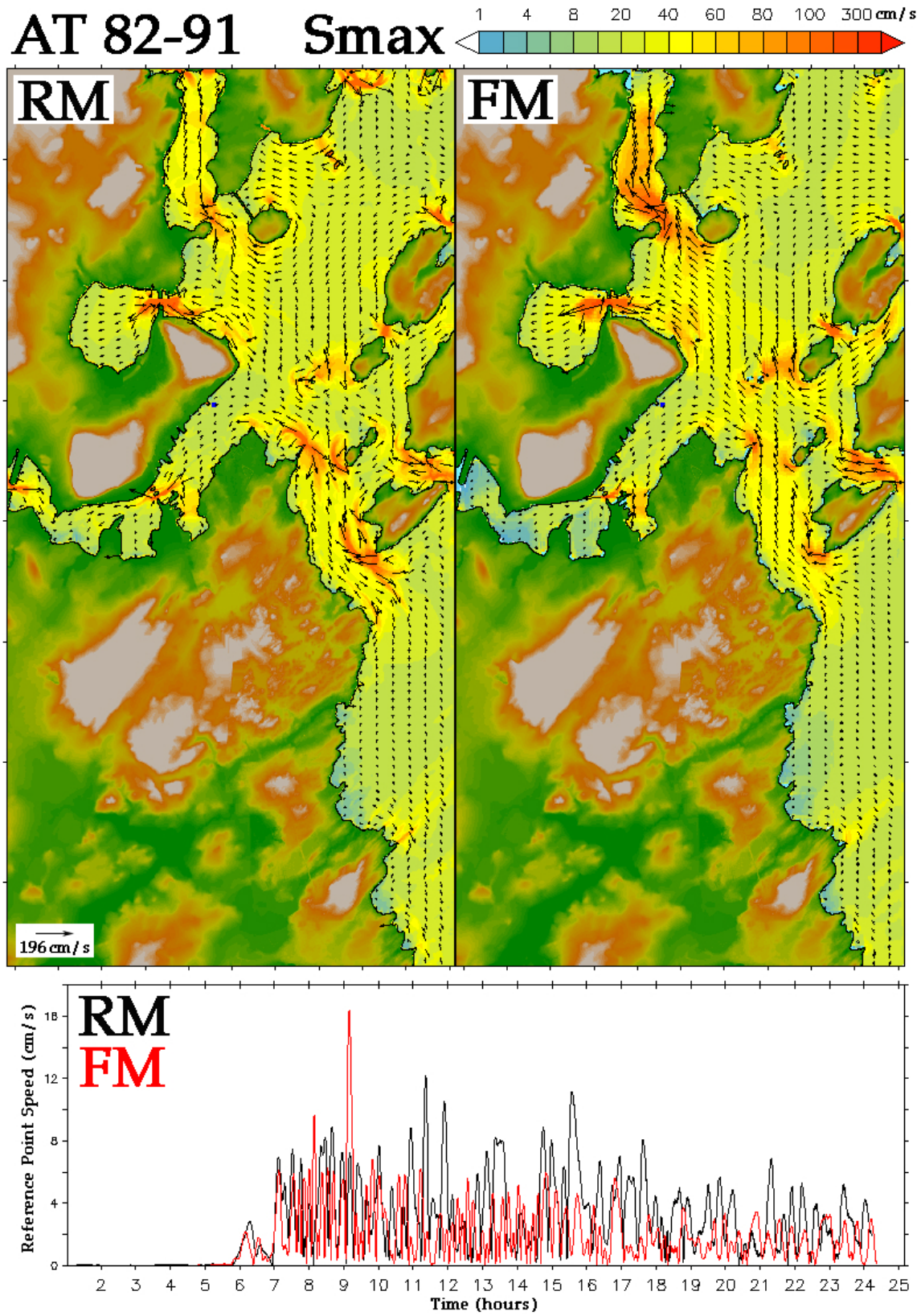

Figure 32: As in Figure 18 but for the AT 82–91 scenario.

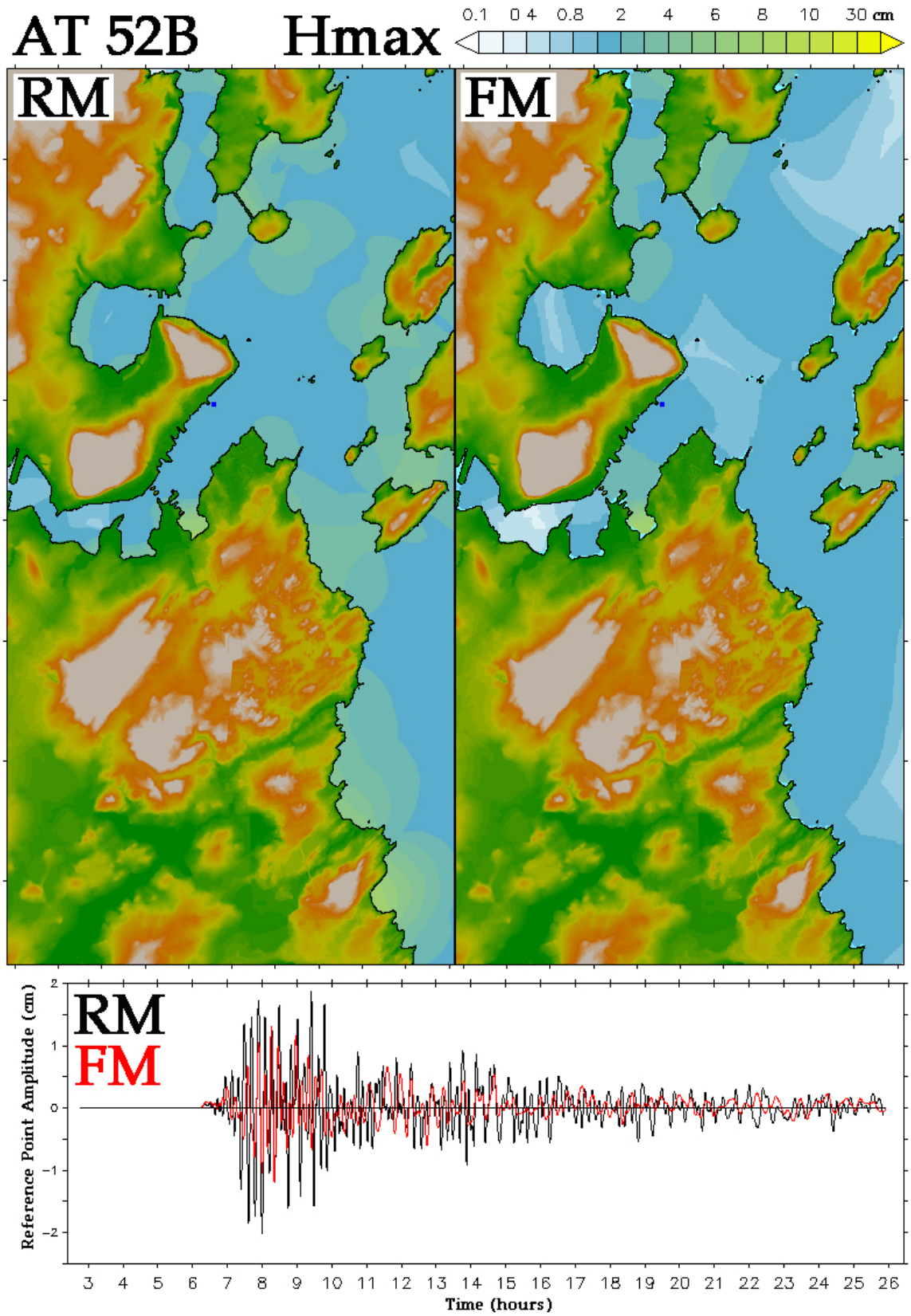

Figure 33: As in Figure 17 but for the AT 52B Mw 7.5 scenario.

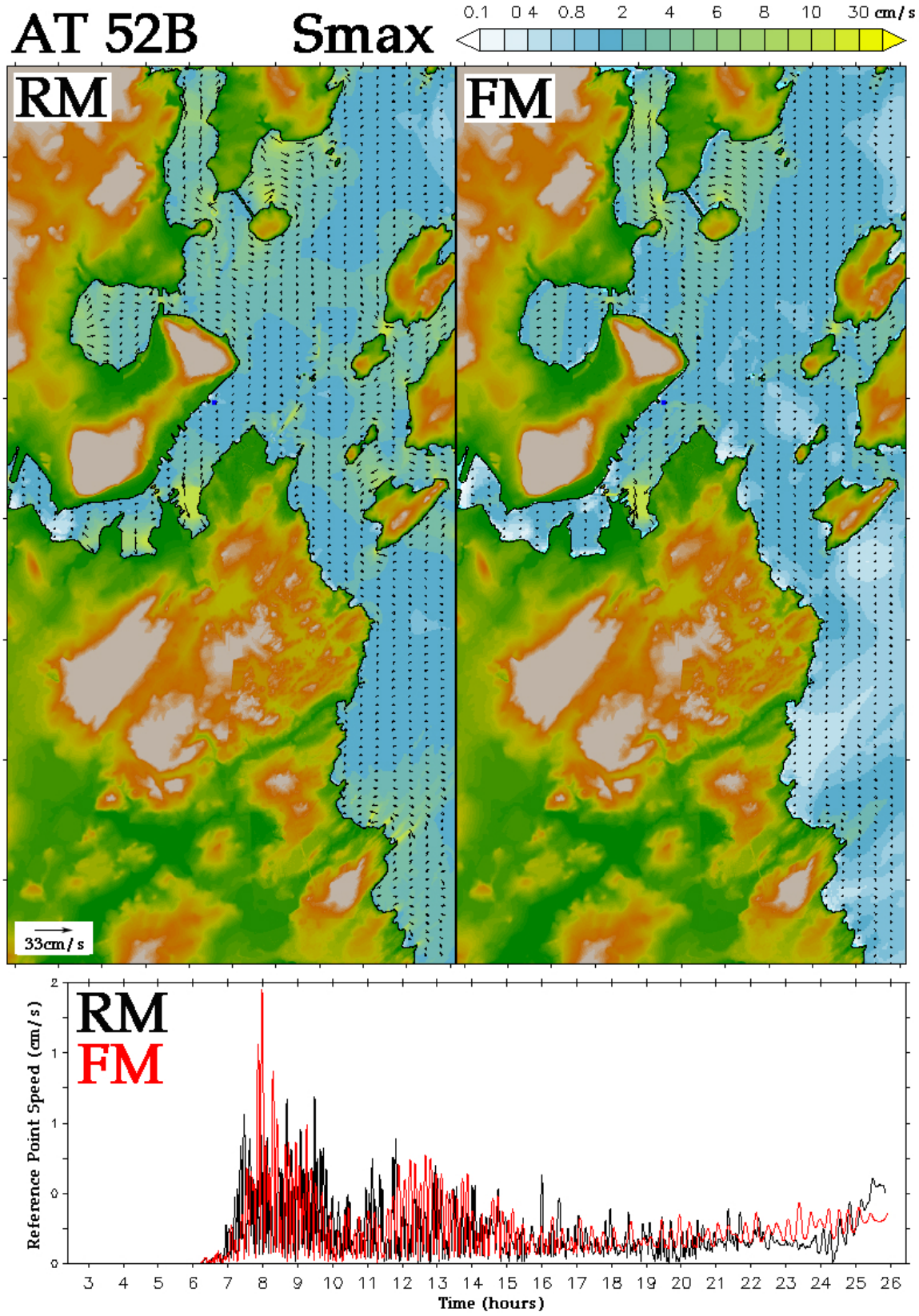

Figure 34: As in Figure 18 but for the AT 52B Mw 7.5 scenario.

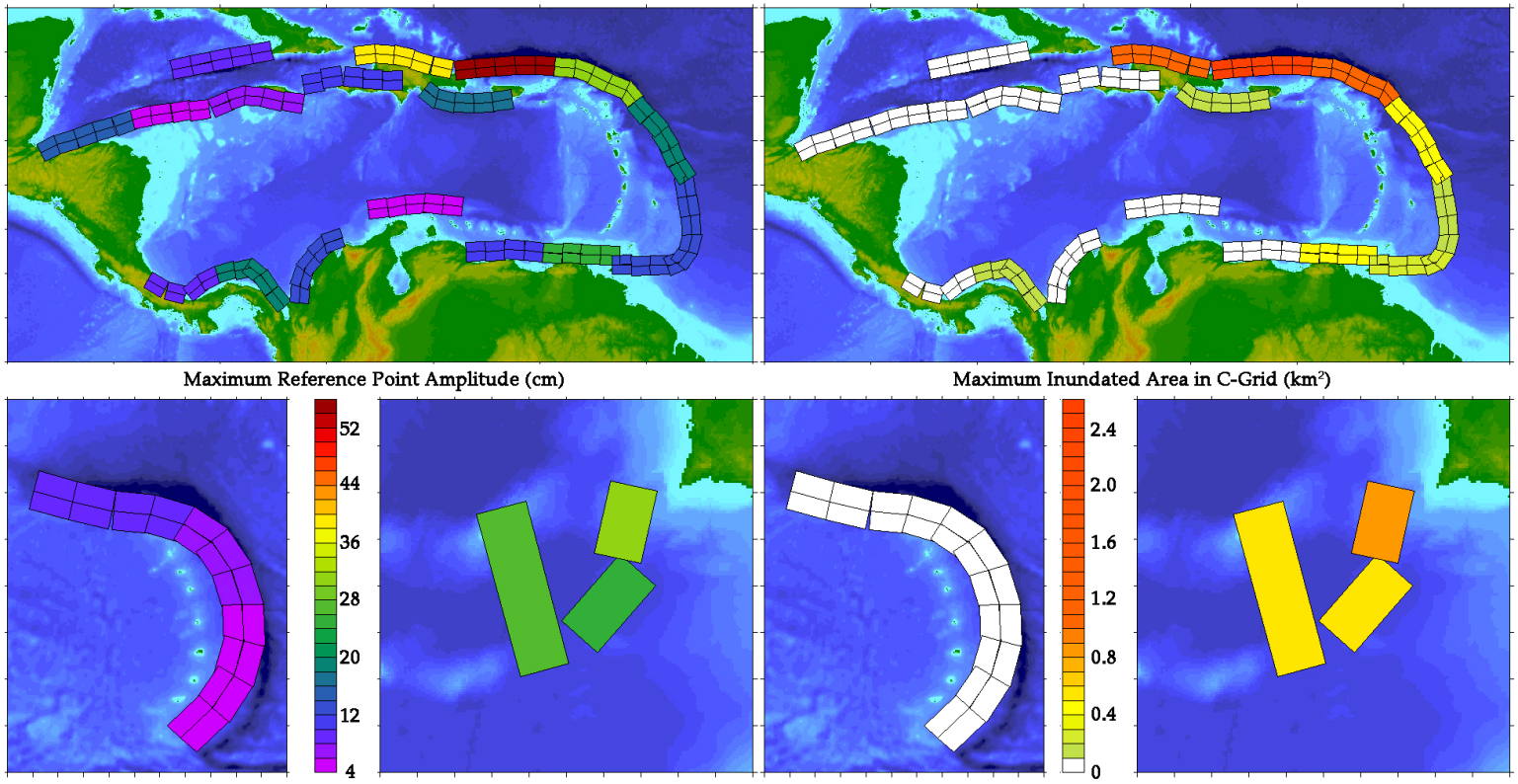

Figure 35: Impact at the Portland, Maine tide gauge for a set of 24 synthetic Mw 8.83 events simulated using the forecast model. The three panels to the left color-code the source groupings by the maximum amplitude (in cm) it generates at Portland tide gauge. The panels to the right are color-coded by the area (sq-kilometers) inundated within the model C-grid; white denotes negligible inundation.

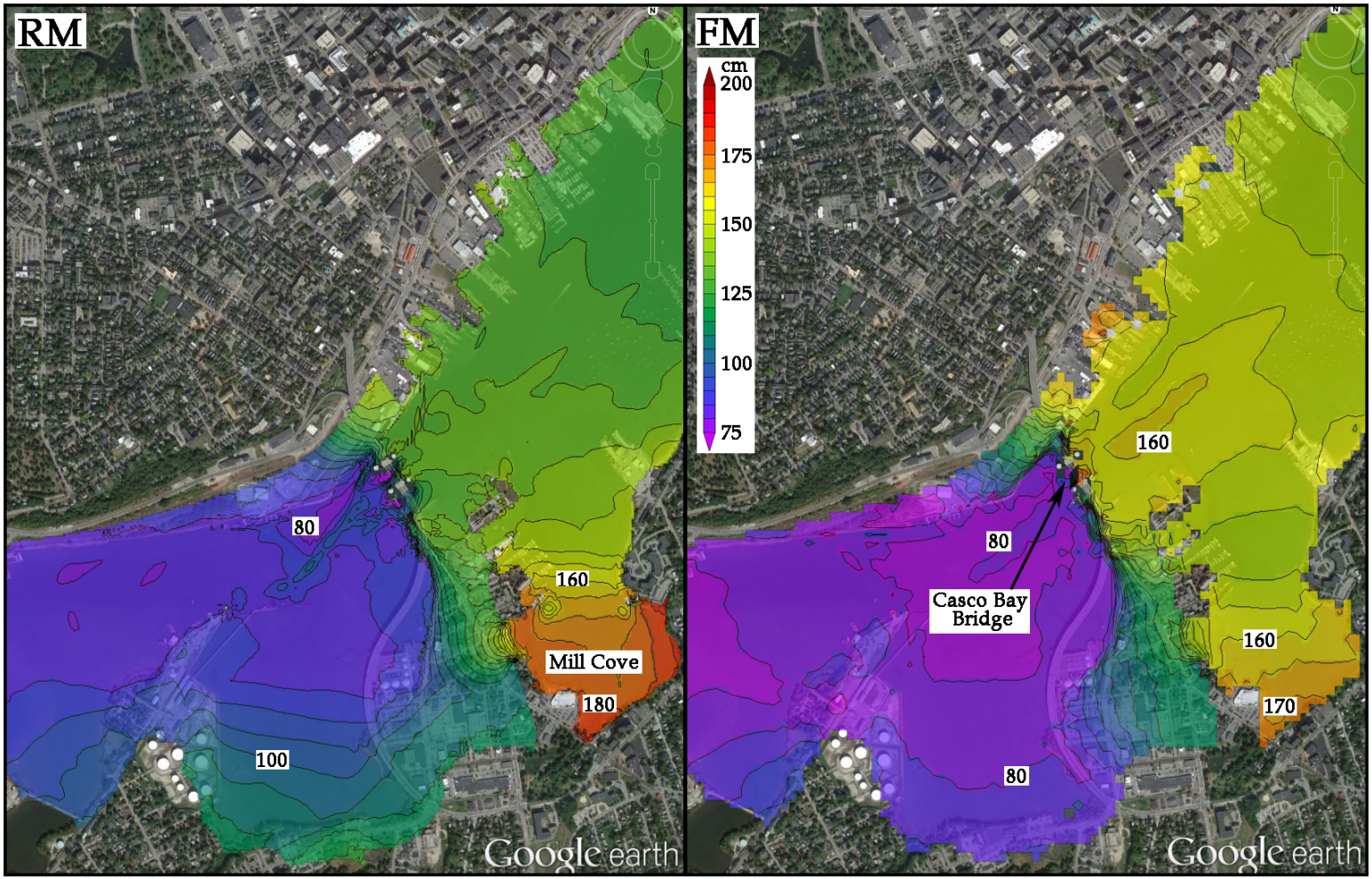

Figure 36: Comparison of Reference (RM) and Forecast Model (FM) representations of maximum wave amplitude in the vicinity of Mill Cove and the Casco Bay Bridge for the AT 48–57 Mw 9.3 scenario. Contour lines are drawn at 5 cm intervals and the model results are geo-referenced to Google Earth imagery from September 2014.

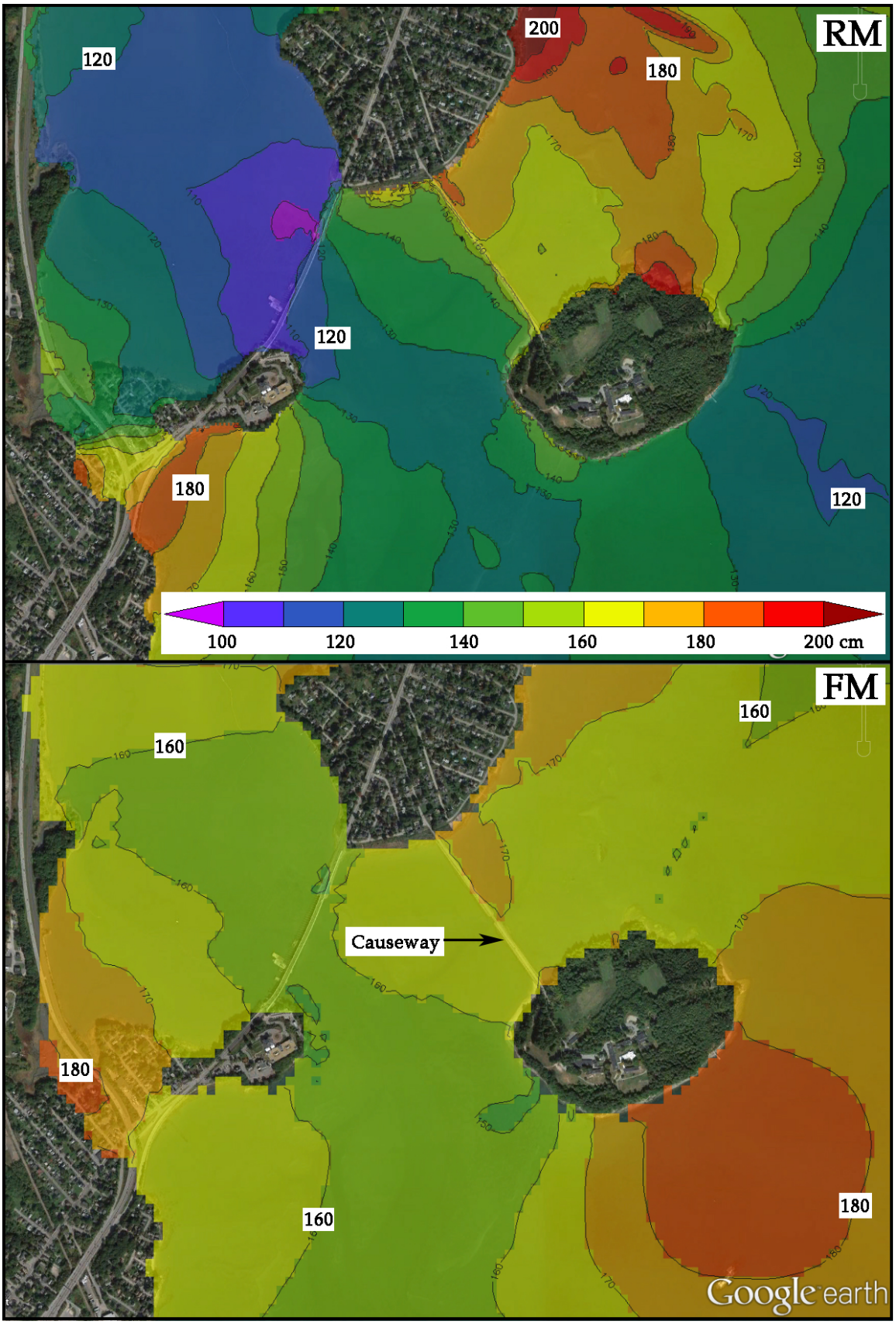

Figure 37: Comparison of Reference (RM) and Forecast Model (FM) representations of maximum wave amplitude near Mackworth Island for the AT 48–57 Mw 9.3 scenario. Contour lines are drawn at 10 cm intervals and the model results are geo-referenced to Google Earth imagery from September 2014.

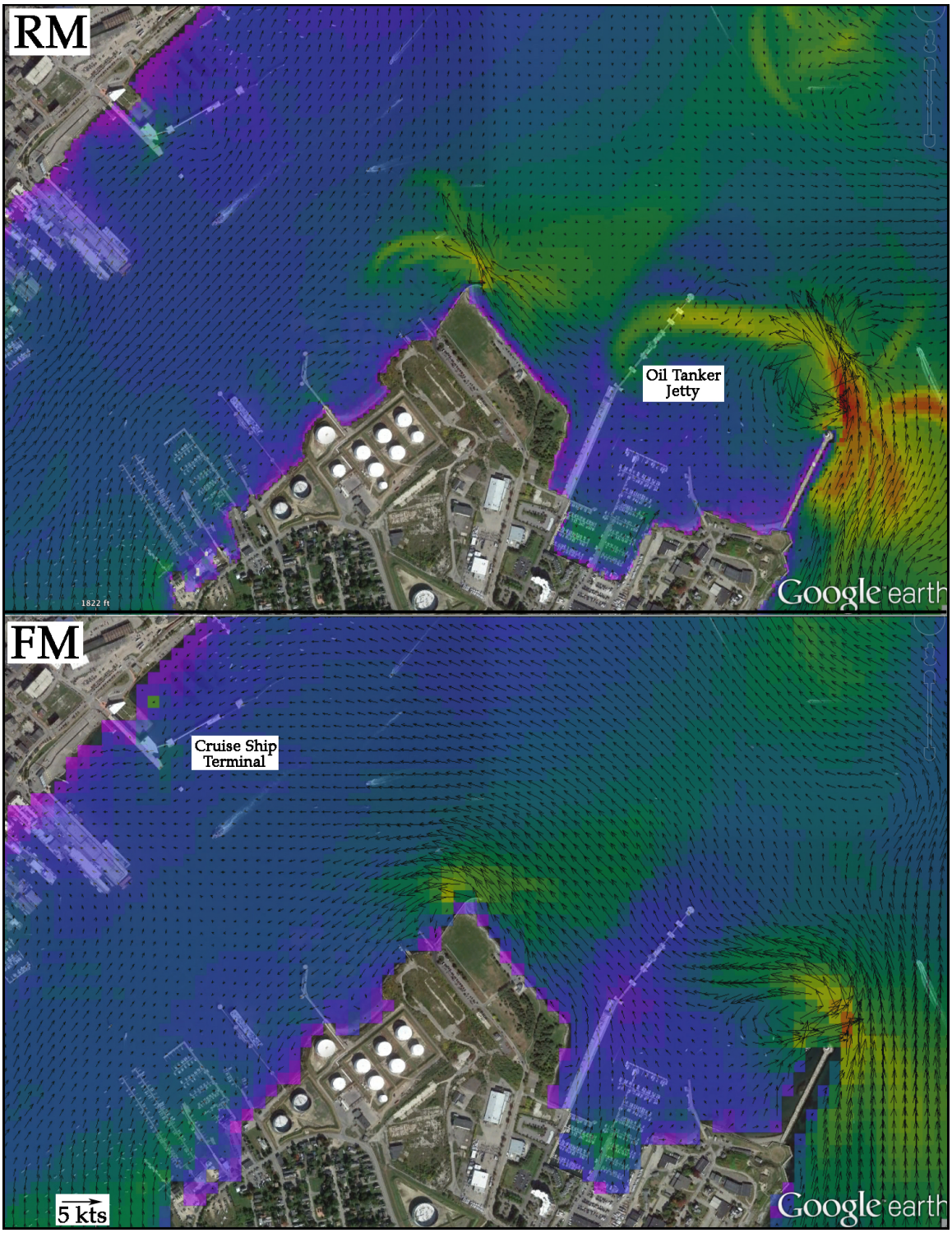

Figure 38: Comparison of Reference (RM) and Forecast Model (FM) representations of maximum speed (cm/s) near in the lower Fore River area for the AT 48–57 Mw 9.3 scenario. Overlaid as vectors (with a common scale vector of 5 knots shown in the lower left) are snapshots of the the velocity at the time of peak speed near the Spring Point Ledge Light, adjacent to the Oil Tanker Jetty of the Portland–Montreal Pipe Line.

TABLES

Grid Area	**Portland, Maine**
Coverage Area	70.74^0 to 69.63^0W, 43.00^0 to 43.99^0N
Coordinate System	Geographic decimal degrees
Horizontal Datum	World Geodetic System 1984 (WGS84)
Vertical Datum	**Mean High Water (MHW)**
Vertical Units	meters
Cell Size	**1/3 arc sec**
Grid Format	ESRI Arc ASCII grid

Table 1: The main features of the Portland, Maine digital elevation model.

<table>
<tr><th colspan="4">Portland, Casco Bay, Maine Station#8418150 43⁰39.4'N, 70⁰14.8W
43.656039,-70.245991</th></tr>
<tr><th colspan="4">Tidal Datum and Range Values (Epoch 1983-2001)</th></tr>
<tr><td>MHHW (Mean Higher High)</td><td>5.626m</td><td rowspan="5">Diurnal Range
3.019m</td><td></td></tr>
<tr><td>MHW (Mean High Water)</td><td>5.493m</td><td rowspan="3">Mean Range
2.781m</td></tr>
<tr><td>MSL (Mean Sea Level)</td><td>4.113m</td></tr>
<tr><td>MLW (Mean Low Water)</td><td>2.712m</td></tr>
<tr><td>MLLW (Mean Lower Low)</td><td>2.607m</td><td></td></tr>
<tr><th colspan="4">Sea Level Trends and Cycles</th></tr>
<tr><td>Long Term SL Trend</td><td colspan="3">Increasing 1.90±0.16mm/year</td></tr>
<tr><td>Seasonal Cycle Range</td><td colspan="3">Minimum -39mm(January); Maximum 32mm(June)</td></tr>
<tr><td>Interannual Variation</td><td colspan="3">Minimum -93mm(1990); Maximum +133mm(2010)</td></tr>
<tr><td>Extremes (to March 2015)</td><td colspan="3">1.554m (30 Nov 1955) to 6.913m (07 Feb1978)</td></tr>
<tr><th colspan="4">Benchmark for Coastal Flooding by Storm Surge (www.neracoos.org)</th></tr>
<tr><td colspan="4">Sea levels of 3.658m (12ft) or more above MLLW</td></tr>
</table>

Table 2: Characteristics of the Portland, Maine tide gauge.

Portland, Maine Reference Model						
Minimum offshore depth: 5.0 m; Water depth for dry land: 0.1m; Friction Coefficient (n^2): 0.0009 CPU time for a 4-hr simulation: 6.4 hr						
Grid	**Zonal Extent**		**Meridional Extent**		**Resolution**	**Grid Points**
A	72.0000ºW	63.0000ºW	37.0000ºN	46.2500ºN	30” x 30”	1081 x 1111
B	70.6000ºW	69.5000ºW	43.2500ºN	43.9000ºN	3” x 3”	1321 x 781
C	70.3139ºW	70.1885ºW	43.5662ºN	43.7150ºN	$^1/_3$” x $^1/_3$”	1117 x 1609

Portland, Maine Forecast Model						
Minimum offshore depth: 1.0 m; Water depth for dry land: 0.1m; Friction Coefficient (n^2): 0.0009 CPU time for a 4-hr simulation: 13.55 min						
Grid	**Zonal Extent**		**Meridional Extent**		**Resolution**	**Grid Points**
A	72.0000ºW	63.0000ºW	38.0000ºN	45.6000ºN	60” x 60”	541 x 457
B	70.6000ºW	69.5000ºW	43.2500ºN	43.9000ºN	12” x 9”	331 x 261
C	70.2917ºW	70.1885ºW	43.5661ºN	43.7150ºN	$^4/_3$” x 1”	280 x 537

Table 3: Specifics of the grids and model parameters employed to model Portland, Maine. Apart from a slight reduction in the western and northern extent of the forecast (FM) model A-grid, the grid extents are the same as those of the Reference (RM) equivalent. Resolution and Grid Point pairings “EWxNS“ list the zonal (east to west) followed by the meridional (north to south) value.

Grid	Filename	Maximum Depth (m)	Minimum CFL (s)	Model Time Step (s)	Water Cells
A	PortlandME_RM_A	5629	3.085	1.6667 (4x)	899892
	PortlandME_FM_A	5621	6.175	5.0 (3x)	191551
B	PortlandME_RM_B	211.1	1.484	0.8333 (2x)	695489
	PortlandME_FM_B	195.8	6.162	5.0 (3x)	56658
C	PortlandME_RM_C	25.01	0.476	0.41667	663989
	PortlandME_FM_C	24.54	1.927	1.66667	54196

Table 4: Grid file names and grid-related parameters. The time steps for the A and B grids must be integer multiples of the basic time step chosen for the C grid.

Scenario Name	Location	Tsunami Source	α (m)
Micro-tsunami Scenario			
AT 52B	Atlantic, North of Puerto Rico	B52	10^{-4}
LI 01A	Eastern Atlantic, Gulf of Cadiz	Ad hoc, non-unit source	0.01
SS B11	South Sandwich Trench	B11	0.01
Mega-tsunami M_W 9.3 Scenarios			
AT 48-57	Atlantic, North of Puerto Rico	A48-A57, B48-A57	25
AT 82-91	Caribbean, South of Hispaniola	A82-A91, B82-B91	25
AT 38-47	Atlantic, East of Puerto Rico	A38-A47, B38-B47	25
AT 58-67	Caribbean, Cayman Trough	A58-A67, B58-B67	25
AT 68-77	Caribbean, Gulf of Honduras	A68-A77, B68-B77	25
SS 01-10	South Sandwich Trench	A01-A10, B01-B10	25
HS 01-02	Eastern Atlantic	Ad hoc, non-unit source combination (see text).	
M_W 7.5 Scenarios			
AT B39--60	Atlantic, near Puerto Rico	Individually, B39--60	1
AT B82--92	Caribbean, near Puerto Rico	Individually, B82--92	1
M_W 8.83 Scenarios			
AT 01 ... 92	Atlantic/Caribbean groupings of five adjacent A,B pairs		10
HS 01	Eastern Atlantic	Combination of A,B,C	22.46
HS 02	Eastern Atlantic	Combination of A,B,C	27.06
LI 01A	Eastern Atlantic	Single 200x80km source	31.25
Forecast Model Stress Test			
AT 48B	Atlantic, North of Puerto Rico	Various α values resulting in M_W Values 7.6 – 9.3	

Table 5: Synthetic tsunami events employed in Portland, Maine model testing. Where available unit sources of the propagation database are employed; ad hoc sources, based on possible scenarios for the Lisbon 1755 tsunami, are used to represent the eastern Atlantic. The three highlighted cases are discussed in Appendix C as part of the test protocol.

Source	Ref. Pt. Max. Amplitude (cm)		Ref. Pt. Max. Speed (cm/s)		C-grid Max. Amplitude (cm)		C-grid Max. Speed (cm/s)	
	RM	FM	RM	FM	RM	FM	RM	FM
AT 48-57	130.7	138.4	111.6	108.3	476.4	317.8	1428	704
HS 01-02	88.3	68.8	89.2	68.7	334.3	183.9	1283	488
SS 01-10	30.6	20.6	27.7	29.3	82.2	103.5	392	295
AT 38-47	42.3	51.1	46.8	66.3	196.3	172.8	671	452
AT 58-67	48.1	39.3	19.7	19.2	72.6	75.7	390	278
AT 68-77	26.4	28.5	3.4	3.3	63.5	44.8	393	208
AT 82-91	38.6	36.4	12.2	16.4	72.6	68.5	391	305

Table 6: Comparison statistics for Reference (RM) and Forecast Model (RM) simulations of mega-tsunami scenarios for Portland, Maine. Maxima of wave amplitude and speed are presented for the tide gauge location which is the reference point, and over the entire C-grid.

Source	First Wave Peak Amplitude (cm)		First Wave Peak Arrival (hours)		Inundated Area (km^2)		Inundation Begins (hours)	
	RM	FM	RM	FM	RM	FM	RM	FM
AT 48-57	75.2	87.0	6.38	6.43	3.14	4.43	5.87	5.87
HS 01-02	19.5	24.1	9.91	9.92	2.55	2.64	12.27	12.27
SS 01-10	3.51	4.33	18.67	18.68	0.47	0.76	20.16	20.20
AT 38-47	15.7	19.6	6.26	6.29	1.22	1.90	6.24	6.22
AT 58-67*	25.2	22.9	7.32	7.36	0.72	1.14	7.13	7.07
AT 68-77*	26.6	26.3	12.32	12.24	0.43	0.76	11.73	11.73
AT 82-91*	38.5	36.5	7.54	7.55	0.65	0.94	7.24	7.22

Table 7: Further comparison statistics from Reference (RM) and Forecast Model (RM) simulations of mega-tsunami scenarios for Portland, Maine: amplitude and arrival time of the first wave peak, inundated area and onset time of inundation. Comparisons are at the reference point; sources marked with an asterisk have a distinct leading trough.

M_w 8.83 Scenarios	Ref. Pt. Max. Amplitude (cm)	C-Grid Max. Amplitude (cm)	Inundation (km^2)
AT 01-05	8.97	14.5	None
AT 05-09	19.4	33.8	0.187
AT 10-14	13.6	20.5	None
AT 17-21	5.36	23.1	0.004
AT 22-26	12.0	18.8	None
AT 25-29	25.9	53.3	0.495
AT 30-34	14.0	36.8	0.220
AT 34-38	12.6	54.0	0.187
AT 39-43	19.4	91.3	0.484
AT 44-48	31.9	110	1.063
AT 49-53	**54.4**	**237**	**2.505**
AT 54-58	39.1	75.3	1.069
AT 63-67	8.18	14.7	None
AT 68-72	14.2	21.3	None
AT 72-76	5.57	7.77	None
AT 77-81	7.50	9.79	None
AT 82-86	11.9	25.9	0.033
AT 88-92	16.4	43.4	0.187
HS 01 (22.46m)	24.5	84.5	0.596
HS 02 (27.06m)	31.8	91.1	0.885
LI 01 (31.25m)	26.1	82.2	0.586
SS 01-05	9.84	52.2	0.067
SS 04-08	7.03	47.6	0.078
SS 07-11	5.68	19.7	None

Table 8: Measures of impact to Portland, Maine from a set of magnitude Mw 8.83 scenarios. With the exception of those in the high-lighted rows (whose slip values are shown in parentheses), all others are based on five A,B pairs from the propagation database with slips of 10m.

Moment Magnitude (M_w)	Ref. Pt. Max. Amplitude (cm)	C-Grid Max. Amplitude (cm)	Inundation (km^2)
9.3	170	516	5.15
9.2	133	402	4.42
9.1	106	354	3.86
9.0	76.9	279	3.43
8.9	68.2	276	3.20
8.8	68.0	267	2.99
8.7	62.2	253	2.71
8.6	54.2	234	2.37
8.5	46.2	201	1.94
8.4	37.3	166	1.49
8.3	28.6	139	1.01
8.2	21.9	106	0.686
8.1	16.4	82.7	0.308
8.0	12.1	64.1	0.090
7.9	8.99	45.6	0.053
7.8	6.58	36.9	0.024
7.7	4.78	25.0	0.009
7.6	3.43	18.7	None
7.5	2.46	13.1	None

Table 9: Dependence of impact to Portland, Maine on moment magnitude in a single unit source rectangle (AT 48B). While unrealistic for the largest events, these scenarios were chosen to "stress-test" the model which was able to accommodate all without failure.

Appendix A

Model input files for Portland, Maine.

As discussed in Section 3.5, input files providing model parameters, the file names of the nested grids, and the output specifications are necessary in order to run the model in either its reference or forecast mode. These files are provided below; each record contains the value(s) and an annotation of purpose.

A.1 Reference model ⋆.in file for Portland, Maine

The following table contains the parameter and file choices used in the input file for the SIFT implementation (most3_facts_nc.in) of the reference model for Portland, Maine. When run on an Intel® Xeon® E5670 2.93GHz processor during development the model simulated 4 hr in 6.4 CPU hr.

0.005	Minimum amp. of input offshore wave (m)
5	Minimum depth of offshore (m)
0.1	Dry land depth of inundation (m)
0.0009	Friction coefficient (n**2)
1	Let A-Grid and B-Grid run up
90.0	Max eta before blow-up (m)
0.4166667	Time step (sec)
103680	Total number of time steps in run
4	Time steps between A-Grid computations
2	Time steps between B-Grid computations
72	Time steps between output steps
72	Time steps before saving first output step
1	Save output every n-th grid point
PortlandME_RM_A.most	A-grid bathymetry file
PortlandME_RM_B.most	B-grid bathymetry file
PortlandME_RM_C.most	C-grid bathymetry file
./	Directory of source files
./	Directory for output files
1 1 1 1	netCDF output for A, B, C, SIFT
1	Number of time series locations
3 517 604	Grid & cell indices for Reference Point

A.2 Forecast model ⋆.in file for Portland, Maine

The following table contains the parameter and file choices used in the input file for the SIFT implementation (most3_facts_nc.in) of the optimized forecast model for Portland, Maine. When run on an Intel® Xeon® E5670 2.93GHz processor the model simulates 4 hours in 13.55 min, in excess of the 10-min target for this metric.

0.001	Minimum amp. of input offshore wave (m)
1	Minimum depth of offshore (m)
0.1	Dry land depth of inundation (m)
0.0009	Friction coefficient (n**2)
1	Let A-Grid and B-Grid run up
90.0	Max eta before blow-up (m)
1.6666667	Time step (sec)
25920	Total number of time steps in run
3	Time steps between A-Grid computations
3	Time steps between B-Grid computations
18	Time steps between output steps
18	Time steps before saving first output step
1	Save output every n-th grid point
PortlandME_FM_A.most	A-grid bathymetry file
PortlandME_FM_B.most	B-grid bathymetry file
PortlandME_FM_C.most	C-grid bathymetry file
./	Directory of source files
./	Directory for output files
1 1 1 1	netCDF output for A, B, C, SIFT
1	Number of time series locations
3 130 202	Grid & cell indices for 289.75597217 43.65921256

Appendix B

Propagation Database: Atlantic Ocean Unit Sources

The NOAA Propagation Database presented in this section is the representation of the database as of March, 2013. This database may have been updated since March, 2013.

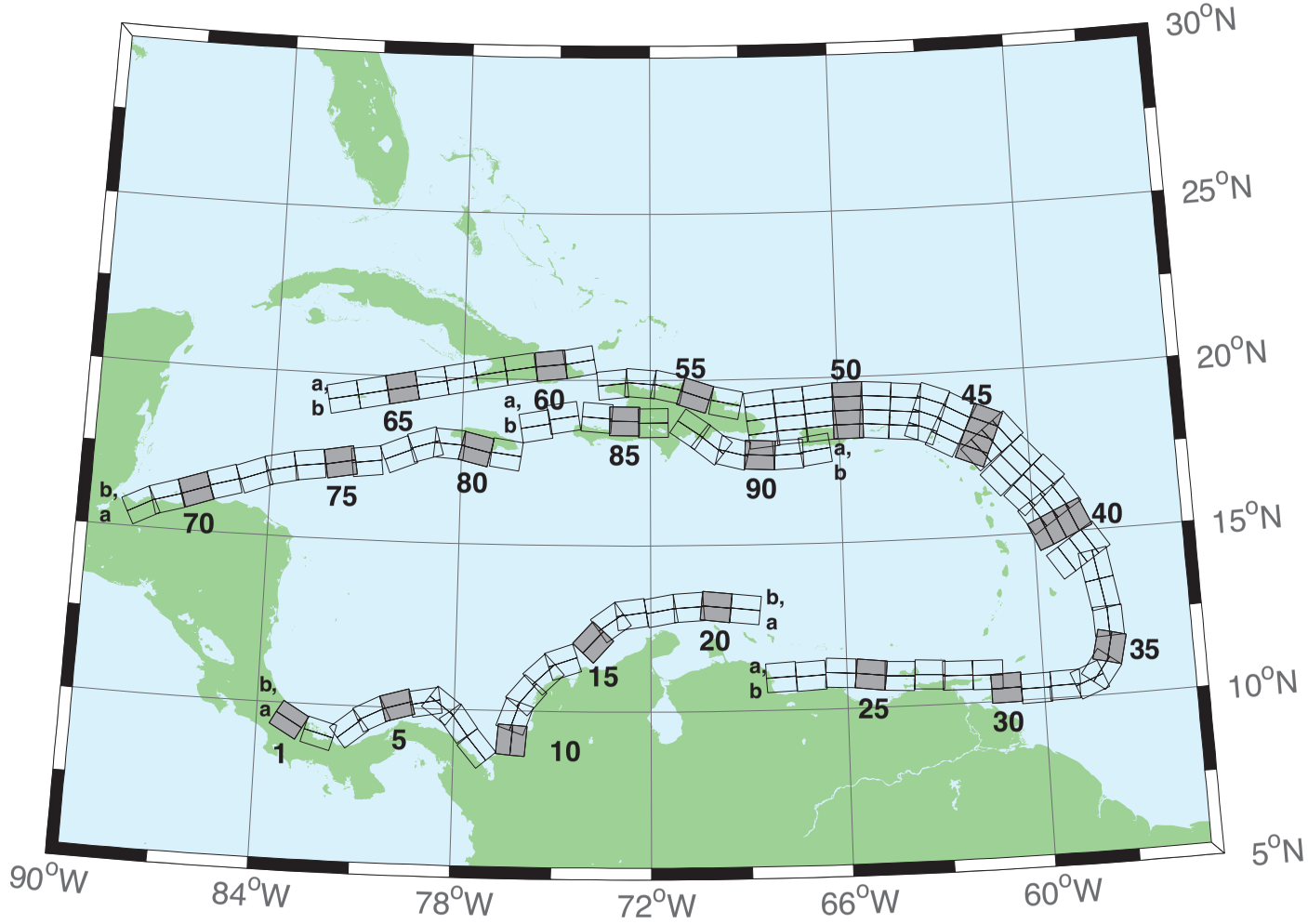

Figure B.1: Atlantic Source Zone unit sources.

Table B.1: Earthquake parameters for Atlantic Source Zone unit sources.

Segment	Description	Longitude(°E)	Latitude(°N)	Strike(°)	Dip(°)	Depth (km)
atsz–1a	Atlantic Source Zone	-83.2020	9.1449	120	27.5	28.09
atsz–1b	Atlantic Source Zone	-83.0000	9.4899	120	27.5	5
atsz–2a	Atlantic Source Zone	-82.1932	8.7408	105.1	27.5	28.09
atsz–2b	Atlantic Source Zone	-82.0880	9.1254	105.1	27.5	5
atsz–3a	Atlantic Source Zone	-80.9172	9.0103	51.31	30	30
atsz–3b	Atlantic Source Zone	-81.1636	9.3139	51.31	30	5
atsz–4a	Atlantic Source Zone	-80.3265	9.4308	63.49	30	30
atsz–4b	Atlantic Source Zone	-80.5027	9.7789	63.49	30	5
atsz–5a	Atlantic Source Zone	-79.6247	9.6961	74.44	30	30
atsz–5b	Atlantic Source Zone	-79.7307	10.0708	74.44	30	5
atsz–6a	Atlantic Source Zone	-78.8069	9.8083	79.71	30	30
atsz–6b	Atlantic Source Zone	-78.8775	10.1910	79.71	30	5
atsz–7a	Atlantic Source Zone	-78.6237	9.7963	127.2	30	30
atsz–7b	Atlantic Source Zone	-78.3845	10.1059	127.2	30	5
atsz–8a	Atlantic Source Zone	-78.1693	9.3544	143.8	30	30
atsz–8b	Atlantic Source Zone	-77.8511	9.5844	143.8	30	5
atsz–9a	Atlantic Source Zone	-77.5913	8.5989	139.9	30	30
atsz–9b	Atlantic Source Zone	-77.2900	8.8493	139.9	30	5
atsz–10a	Atlantic Source Zone	-75.8109	9.0881	4.67	17	19.62
atsz–10b	Atlantic Source Zone	-76.2445	9.1231	4.67	17	5
atsz–11a	Atlantic Source Zone	-75.7406	9.6929	19.67	17	19.62
atsz–11b	Atlantic Source Zone	-76.1511	9.8375	19.67	17	5
atsz–12a	Atlantic Source Zone	-75.4763	10.2042	40.4	17	19.62
atsz–12b	Atlantic Source Zone	-75.8089	10.4826	40.4	17	5
atsz–13a	Atlantic Source Zone	-74.9914	10.7914	47.17	17	19.62
atsz–13b	Atlantic Source Zone	-75.2890	11.1064	47.17	17	5
atsz–14a	Atlantic Source Zone	-74.5666	11.0708	71.68	17	19.62
atsz–14b	Atlantic Source Zone	-74.7043	11.4786	71.68	17	5
atsz–15a	Atlantic Source Zone	-73.4576	11.8012	42.69	17	19.62
atsz–15b	Atlantic Source Zone	-73.7805	12.0924	42.69	17	5
atsz–16a	Atlantic Source Zone	-72.9788	12.3365	54.75	17	19.62
atsz–16b	Atlantic Source Zone	-73.2329	12.6873	54.75	17	5
atsz–17a	Atlantic Source Zone	-72.5454	12.5061	81.96	17	19.62
atsz–17b	Atlantic Source Zone	-72.6071	12.9314	81.96	17	5
atsz–18a	Atlantic Source Zone	-71.6045	12.6174	79.63	17	19.62
atsz–18b	Atlantic Source Zone	-71.6839	13.0399	79.63	17	5
atsz–19a	Atlantic Source Zone	-70.7970	12.7078	86.32	17	19.62
atsz–19b	Atlantic Source Zone	-70.8253	13.1364	86.32	17	5
atsz–20a	Atlantic Source Zone	-70.0246	12.7185	95.94	17	19.62
atsz–20b	Atlantic Source Zone	-69.9789	13.1457	95.94	17	5
atsz–21a	Atlantic Source Zone	-69.1244	12.6320	95.94	17	19.62
atsz–21b	Atlantic Source Zone	-69.0788	13.0592	95.94	17	5
atsz–22a	Atlantic Source Zone	-68.0338	11.4286	266.9	15	17.94
atsz–22b	Atlantic Source Zone	-68.0102	10.9954	266.9	15	5
atsz–23a	Atlantic Source Zone	-67.1246	11.4487	266.9	15	17.94
atsz–23b	Atlantic Source Zone	-67.1010	11.0155	266.9	15	5
atsz–24a	Atlantic Source Zone	-66.1656	11.5055	273.3	15	17.94
atsz–24b	Atlantic Source Zone	-66.1911	11.0724	273.3	15	5
atsz–25a	Atlantic Source Zone	-65.2126	11.4246	276.4	15	17.94
atsz–25b	Atlantic Source Zone	-65.2616	10.9934	276.4	15	5
atsz–26a	Atlantic Source Zone	-64.3641	11.3516	272.9	15	17.94
atsz–26b	Atlantic Source Zone	-64.3862	10.9183	272.9	15	5
atsz–27a	Atlantic Source Zone	-63.4472	11.3516	272.9	15	17.94
atsz–27b	Atlantic Source Zone	-63.4698	10.9183	272.9	15	5
atsz–28a	Atlantic Source Zone	-62.6104	11.2831	271.1	15	17.94
atsz–28b	Atlantic Source Zone	-62.6189	10.8493	271.1	15	5
atsz–29a	Atlantic Source Zone	-61.6826	11.2518	271.6	15	17.94
atsz–29b	Atlantic Source Zone	-61.6947	10.8181	271.6	15	5
atsz–30a	Atlantic Source Zone	-61.1569	10.8303	269	15	17.94
atsz–30b	Atlantic Source Zone	-61.1493	10.3965	269	15	5
atsz–31a	Atlantic Source Zone	-60.2529	10.7739	269	15	17.94

Continued on next page

Table B.1 – continued from previous page

Segment	Description	Longitude(°E)	Latitude(°N)	Strike(°)	Dip(°)	Depth (km)
atsz–31b	Atlantic Source Zone	-60.2453	10.3401	269	15	5
atsz–32a	Atlantic Source Zone	-59.3510	10.8123	269	15	17.94
atsz–32b	Atlantic Source Zone	-59.3734	10.3785	269	15	5
atsz–33a	Atlantic Source Zone	-58.7592	10.8785	248.6	15	17.94
atsz–33b	Atlantic Source Zone	-58.5984	10.4745	248.6	15	5
atsz–34a	Atlantic Source Zone	-58.5699	11.0330	217.2	15	17.94
atsz–34b	Atlantic Source Zone	-58.2179	10.7710	217.2	15	5
atsz–35a	Atlantic Source Zone	-58.3549	11.5300	193.7	15	17.94
atsz–35b	Atlantic Source Zone	-57.9248	11.4274	193.7	15	5
atsz–36a	Atlantic Source Zone	-58.3432	12.1858	177.7	15	17.94
atsz–36b	Atlantic Source Zone	-57.8997	12.2036	177.7	15	5
atsz–37a	Atlantic Source Zone	-58.4490	12.9725	170.7	15	17.94
atsz–37b	Atlantic Source Zone	-58.0095	13.0424	170.7	15	5
atsz–38a	Atlantic Source Zone	-58.6079	13.8503	170.2	15	17.94
atsz–38b	Atlantic Source Zone	-58.1674	13.9240	170.2	15	5
atsz–39a	Atlantic Source Zone	-58.6667	14.3915	146.8	15	17.94
atsz–39b	Atlantic Source Zone	-58.2913	14.6287	146.8	15	5
atsz–39y	Atlantic Source Zone	-59.4168	13.9171	146.8	15	43.82
atsz–39z	Atlantic Source Zone	-59.0415	14.1543	146.8	15	30.88
atsz–40a	Atlantic Source Zone	-59.1899	15.2143	156.2	15	17.94
atsz–40b	Atlantic Source Zone	-58.7781	15.3892	156.2	15	5
atsz–40y	Atlantic Source Zone	-60.0131	14.8646	156.2	15	43.82
atsz–40z	Atlantic Source Zone	-59.6012	15.0395	156.2	15	30.88
atsz–41a	Atlantic Source Zone	-59.4723	15.7987	146.3	15	17.94
atsz–41b	Atlantic Source Zone	-59.0966	16.0392	146.3	15	5
atsz–41y	Atlantic Source Zone	-60.2229	15.3177	146.3	15	43.82
atsz–41z	Atlantic Source Zone	-59.8473	15.5582	146.3	15	30.88
atsz–42a	Atlantic Source Zone	-59.9029	16.4535	137	15	17.94
atsz–42b	Atlantic Source Zone	-59.5716	16.7494	137	15	5
atsz–42y	Atlantic Source Zone	-60.5645	15.8616	137	15	43.82
atsz–42z	Atlantic Source Zone	-60.2334	16.1575	137	15	30.88
atsz–43a	Atlantic Source Zone	-60.5996	17.0903	138.7	15	17.94
atsz–43b	Atlantic Source Zone	-60.2580	17.3766	138.7	15	5
atsz–43y	Atlantic Source Zone	-61.2818	16.5177	138.7	15	43.82
atsz–43z	Atlantic Source Zone	-60.9404	16.8040	138.7	15	30.88
atsz–44a	Atlantic Source Zone	-61.1559	17.8560	141.1	15	17.94
atsz–44b	Atlantic Source Zone	-60.8008	18.1286	141.1	15	5
atsz–44y	Atlantic Source Zone	-61.8651	17.3108	141.1	15	43.82
atsz–44z	Atlantic Source Zone	-61.5102	17.5834	141.1	15	30.88
atsz–45a	Atlantic Source Zone	-61.5491	18.0566	112.8	15	17.94
atsz–45b	Atlantic Source Zone	-61.3716	18.4564	112.8	15	5
atsz–45y	Atlantic Source Zone	-61.9037	17.2569	112.8	15	43.82
atsz–45z	Atlantic Source Zone	-61.7260	17.6567	112.8	15	30.88
atsz–46a	Atlantic Source Zone	-62.4217	18.4149	117.9	15	17.94
atsz–46b	Atlantic Source Zone	-62.2075	18.7985	117.9	15	5
atsz–46y	Atlantic Source Zone	-62.8493	17.6477	117.9	15	43.82
atsz–46z	Atlantic Source Zone	-62.6352	18.0313	117.9	15	30.88
atsz–47a	Atlantic Source Zone	-63.1649	18.7844	110.5	20	22.1
atsz–47b	Atlantic Source Zone	-63.0087	19.1798	110.5	20	5
atsz–47y	Atlantic Source Zone	-63.4770	17.9936	110.5	20	56.3
atsz–47z	Atlantic Source Zone	-63.3205	18.3890	110.5	20	39.2
atsz–48a	Atlantic Source Zone	-63.8800	18.8870	95.37	20	22.1
atsz–48b	Atlantic Source Zone	-63.8382	19.3072	95.37	20	5
atsz–48y	Atlantic Source Zone	-63.9643	18.0465	95.37	20	56.3
atsz–48z	Atlantic Source Zone	-63.9216	18.4667	95.37	20	39.2
atsz–49a	Atlantic Source Zone	-64.8153	18.9650	94.34	20	22.1
atsz–49b	Atlantic Source Zone	-64.7814	19.3859	94.34	20	5
atsz–49y	Atlantic Source Zone	-64.8840	18.1233	94.34	20	56.3
atsz–49z	Atlantic Source Zone	-64.8492	18.5442	94.34	20	39.2
atsz–50a	Atlantic Source Zone	-65.6921	18.9848	89.59	20	22.1
atsz–50b	Atlantic Source Zone	-65.6953	19.4069	89.59	20	5
atsz–50y	Atlantic Source Zone	-65.6874	18.1407	89.59	20	56.3

Continued on next page

Table B.1 – continued from previous page

Segment	Description	Longitude(°E)	Latitude(°N)	Strike(°)	Dip(°)	Depth (km)
atsz–50z	Atlantic Source Zone	-65.6887	18.5628	89.59	20	39.2
atsz–51a	Atlantic Source Zone	-66.5742	18.9484	84.98	20	22.1
atsz–51b	Atlantic Source Zone	-66.6133	19.3688	84.98	20	5
atsz–51y	Atlantic Source Zone	-66.4977	18.1076	84.98	20	56.3
atsz–51z	Atlantic Source Zone	-66.5353	18.5280	84.98	20	39.2
atsz–52a	Atlantic Source Zone	-67.5412	18.8738	85.87	20	22.1
atsz–52b	Atlantic Source Zone	-67.5734	19.2948	85.87	20	5
atsz–52y	Atlantic Source Zone	-67.4781	18.0319	85.87	20	56.3
atsz–52z	Atlantic Source Zone	-67.5090	18.4529	85.87	20	39.2
atsz–53a	Atlantic Source Zone	-68.4547	18.7853	83.64	20	22.1
atsz–53b	Atlantic Source Zone	-68.5042	19.2048	83.64	20	5
atsz–53y	Atlantic Source Zone	-68.3575	17.9463	83.64	20	56.3
atsz–53z	Atlantic Source Zone	-68.4055	18.3658	83.64	20	39.2
atsz–54a	Atlantic Source Zone	-69.6740	18.8841	101.5	20	22.1
atsz–54b	Atlantic Source Zone	-69.5846	19.2976	101.5	20	5
atsz–55a	Atlantic Source Zone	-70.7045	19.1376	108.2	20	22.1
atsz–55b	Atlantic Source Zone	-70.5647	19.5386	108.2	20	5
atsz–56a	Atlantic Source Zone	-71.5368	19.3853	102.6	20	22.1
atsz–56b	Atlantic Source Zone	-71.4386	19.7971	102.6	20	5
atsz–57a	Atlantic Source Zone	-72.3535	19.4838	94.2	20	22.1
atsz–57b	Atlantic Source Zone	-72.3206	19.9047	94.2	20	5
atsz–58a	Atlantic Source Zone	-73.1580	19.4498	84.34	20	22.1
atsz–58b	Atlantic Source Zone	-73.2022	19.8698	84.34	20	5
atsz–59a	Atlantic Source Zone	-74.3567	20.9620	259.7	20	22.1
atsz–59b	Atlantic Source Zone	-74.2764	20.5467	259.7	20	5
atsz–60a	Atlantic Source Zone	-75.2386	20.8622	264.2	15	17.94
atsz–60b	Atlantic Source Zone	-75.1917	20.4306	264.2	15	5
atsz–61a	Atlantic Source Zone	-76.2383	20.7425	260.7	15	17.94
atsz–61b	Atlantic Source Zone	-76.1635	20.3144	260.7	15	5
atsz–62a	Atlantic Source Zone	-77.2021	20.5910	259.9	15	17.94
atsz–62b	Atlantic Source Zone	-77.1214	20.1638	259.9	15	5
atsz–63a	Atlantic Source Zone	-78.1540	20.4189	259	15	17.94
atsz–63b	Atlantic Source Zone	-78.0661	19.9930	259	15	5
atsz–64a	Atlantic Source Zone	-79.0959	20.2498	259.2	15	17.94
atsz–64b	Atlantic Source Zone	-79.0098	19.8236	259.2	15	5
atsz–65a	Atlantic Source Zone	-80.0393	20.0773	258.9	15	17.94
atsz–65b	Atlantic Source Zone	-79.9502	19.6516	258.9	15	5
atsz–66a	Atlantic Source Zone	-80.9675	19.8993	258.6	15	17.94
atsz–66b	Atlantic Source Zone	-80.8766	19.4740	258.6	15	5
atsz–67a	Atlantic Source Zone	-81.9065	19.7214	258.5	15	17.94
atsz–67b	Atlantic Source Zone	-81.8149	19.2962	258.5	15	5
atsz–68a	Atlantic Source Zone	-87.8003	15.2509	62.69	15	17.94
atsz–68b	Atlantic Source Zone	-88.0070	15.6364	62.69	15	5
atsz–69a	Atlantic Source Zone	-87.0824	15.5331	72.73	15	17.94
atsz–69b	Atlantic Source Zone	-87.2163	15.9474	72.73	15	5
atsz–70a	Atlantic Source Zone	-86.1622	15.8274	70.64	15	17.94
atsz–70b	Atlantic Source Zone	-86.3120	16.2367	70.64	15	5
atsz–71a	Atlantic Source Zone	-85.3117	16.1052	73.7	15	17.94
atsz–71b	Atlantic Source Zone	-85.4387	16.5216	73.7	15	5
atsz–72a	Atlantic Source Zone	-84.3470	16.3820	69.66	15	17.94
atsz–72b	Atlantic Source Zone	-84.5045	16.7888	69.66	15	5
atsz–73a	Atlantic Source Zone	-83.5657	16.6196	77.36	15	17.94
atsz–73b	Atlantic Source Zone	-83.6650	17.0429	77.36	15	5
atsz–74a	Atlantic Source Zone	-82.7104	16.7695	82.35	15	17.94
atsz–74b	Atlantic Source Zone	-82.7709	17.1995	82.35	15	5
atsz–75a	Atlantic Source Zone	-81.7297	16.9003	79.86	15	17.94
atsz–75b	Atlantic Source Zone	-81.8097	17.3274	79.86	15	5
atsz–76a	Atlantic Source Zone	-80.9196	16.9495	82.95	15	17.94
atsz–76b	Atlantic Source Zone	-80.9754	17.3801	82.95	15	5
atsz–77a	Atlantic Source Zone	-79.8086	17.2357	67.95	15	17.94
atsz–77b	Atlantic Source Zone	-79.9795	17.6378	67.95	15	5
atsz–78a	Atlantic Source Zone	-79.0245	17.5415	73.61	15	17.94

Continued on next page

Table B.1 – continued from previous page

Segment	Description	Longitude(°E)	Latitude(°N)	Strike(°)	Dip(°)	Depth (km)
atsz–78b	Atlantic Source Zone	-79.1532	17.9577	73.61	15	5
atsz–79a	Atlantic Source Zone	-78.4122	17.5689	94.07	15	17.94
atsz–79b	Atlantic Source Zone	-78.3798	18.0017	94.07	15	5
atsz–80a	Atlantic Source Zone	-77.6403	17.4391	103.3	15	17.94
atsz–80b	Atlantic Source Zone	-77.5352	17.8613	103.3	15	5
atsz–81a	Atlantic Source Zone	-76.6376	17.2984	98.21	15	17.94
atsz–81b	Atlantic Source Zone	-76.5726	17.7278	98.21	15	5
atsz–82a	Atlantic Source Zone	-75.7299	19.0217	260.1	15	17.94
atsz–82b	Atlantic Source Zone	-75.6516	18.5942	260.1	15	5
atsz–83a	Atlantic Source Zone	-74.8351	19.2911	260.8	15	17.94
atsz–83b	Atlantic Source Zone	-74.7621	18.8628	260.8	15	5
atsz–84a	Atlantic Source Zone	-73.6639	19.2991	274.8	15	17.94
atsz–84b	Atlantic Source Zone	-73.7026	18.8668	274.8	15	5
atsz–85a	Atlantic Source Zone	-72.8198	19.2019	270.6	15	17.94
atsz–85b	Atlantic Source Zone	-72.8246	18.7681	270.6	15	5
atsz–86a	Atlantic Source Zone	-71.9143	19.1477	269.1	15	17.94
atsz–86b	Atlantic Source Zone	-71.9068	18.7139	269.1	15	5
atsz–87a	Atlantic Source Zone	-70.4738	18.8821	304.5	15	17.94
atsz–87b	Atlantic Source Zone	-70.7329	18.5245	304.5	15	5
atsz–88a	Atlantic Source Zone	-69.7710	18.3902	308.9	15	17.94
atsz–88b	Atlantic Source Zone	-70.0547	18.0504	308.4	15	5
atsz–89a	Atlantic Source Zone	-69.2635	18.2099	283.9	15	17.94
atsz–89b	Atlantic Source Zone	-69.3728	17.7887	283.9	15	5
atsz–90a	Atlantic Source Zone	-68.5059	18.1443	272.9	15	17.94
atsz–90b	Atlantic Source Zone	-68.5284	17.7110	272.9	15	5
atsz–91a	Atlantic Source Zone	-67.6428	18.1438	267.8	15	17.94
atsz–91b	Atlantic Source Zone	-67.6256	17.7103	267.8	15	5
atsz–92a	Atlantic Source Zone	-66.8261	18.2536	262	15	17.94
atsz–92b	Atlantic Source Zone	-66.7627	17.8240	262	15	5

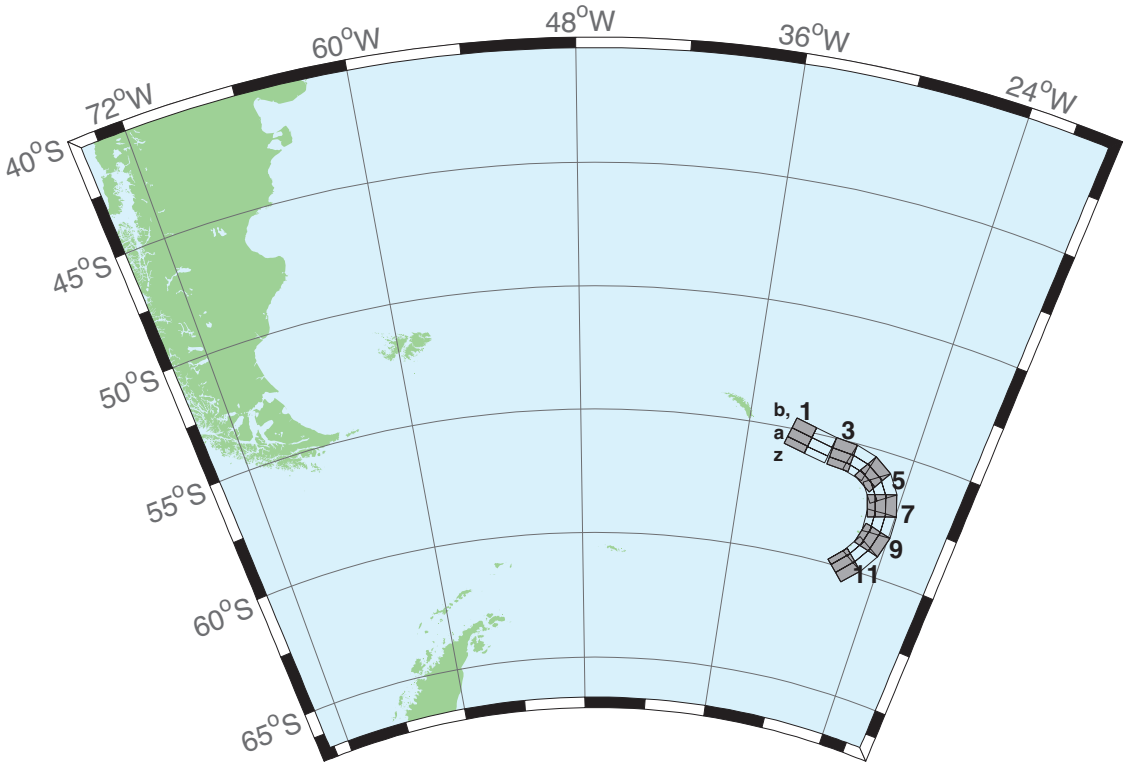

Figure B.2: South Sandwich Islands Subduction Zone.

Table B.2: Earthquake parameters for South Sandwich Islands Subduction Zone unit sources.

Segment	Description	Longitude(°E)	Latitude(°N)	Strike(°)	Dip(°)	Depth (km)
sssz–1a	South Sandwich Islands Subduction Zone	-32.3713	-55.4655	104.7	28.53	17.51
sssz–1b	South Sandwich Islands Subduction Zone	-32.1953	-55.0832	104.7	9.957	8.866
sssz–1z	South Sandwich Islands Subduction Zone	-32.5091	-55.7624	104.7	46.99	41.39
sssz–2a	South Sandwich Islands Subduction Zone	-30.8028	-55.6842	102.4	28.53	17.51
sssz–2b	South Sandwich Islands Subduction Zone	-30.6524	-55.2982	102.4	9.957	8.866
sssz–2z	South Sandwich Islands Subduction Zone	-30.9206	-55.9839	102.4	46.99	41.39
sssz–3a	South Sandwich Islands Subduction Zone	-29.0824	-55.8403	95.53	28.53	17.51
sssz–3b	South Sandwich Islands Subduction Zone	-29.0149	-55.4468	95.53	9.957	8.866
sssz–3z	South Sandwich Islands Subduction Zone	-29.1353	-56.1458	95.53	46.99	41.39
sssz–4a	South Sandwich Islands Subduction Zone	-27.8128	-55.9796	106.1	28.53	17.51
sssz–4b	South Sandwich Islands Subduction Zone	-27.6174	-55.5999	106.1	9.957	8.866
sssz–4z	South Sandwich Islands Subduction Zone	-27.9659	-56.2744	106.1	46.99	41.39
sssz–5a	South Sandwich Islands Subduction Zone	-26.7928	-56.2481	123.1	28.53	17.51
sssz–5b	South Sandwich Islands Subduction Zone	-26.4059	-55.9170	123.1	9.957	8.866
sssz–5z	South Sandwich Islands Subduction Zone	-27.0955	-56.5052	123.1	46.99	41.39
sssz–6a	South Sandwich Islands Subduction Zone	-26.1317	-56.6466	145.6	23.28	16.11
sssz–6b	South Sandwich Islands Subduction Zone	-25.5131	-56.4133	145.6	9.09	8.228
sssz–6z	South Sandwich Islands Subduction Zone	-26.5920	-56.8194	145.6	47.15	35.87
sssz–7a	South Sandwich Islands Subduction Zone	-25.6787	-57.2162	162.9	21.21	14.23
sssz–7b	South Sandwich Islands Subduction Zone	-24.9394	-57.0932	162.9	7.596	7.626
sssz–7z	South Sandwich Islands Subduction Zone	-26.2493	-57.3109	162.9	44.16	32.32
sssz–8a	South Sandwich Islands Subduction Zone	-25.5161	-57.8712	178.2	20.33	15.91
sssz–8b	South Sandwich Islands Subduction Zone	-24.7233	-57.8580	178.2	8.449	8.562
sssz–8z	South Sandwich Islands Subduction Zone	-26.1280	-57.8813	178.2	43.65	33.28
sssz–9a	South Sandwich Islands Subduction Zone	-25.6657	-58.5053	195.4	25.76	15.71
sssz–9b	South Sandwich Islands Subduction Zone	-24.9168	-58.6127	195.4	8.254	8.537
sssz–9z	South Sandwich Islands Subduction Zone	-26.1799	-58.4313	195.4	51.69	37.44
sssz–10a	South Sandwich Islands Subduction Zone	-26.1563	-59.1048	212.5	32.82	15.65
sssz–10b	South Sandwich Islands Subduction Zone	-25.5335	-59.3080	212.5	10.45	6.581
sssz–10z	South Sandwich Islands Subduction Zone	-26.5817	-58.9653	212.5	54.77	42.75
sssz–11a	South Sandwich Islands Subduction Zone	-27.0794	-59.6799	224.2	33.67	15.75
sssz–11b	South Sandwich Islands Subduction Zone	-26.5460	-59.9412	224.2	11.32	5.927
sssz–11z	South Sandwich Islands Subduction Zone	-27.4245	-59.5098	224.2	57.19	43.46

Appendix C

SIFT Testing

C.1 Purpose

Forecast models are tested with synthetic tsunami events covering a range of tsunami source locations. Testing is also done with selected historical tsunami events when available.

The purpose of forecast model testing is three-fold. The first objective is to assure that the results obtained with NOAA's tsunami forecast system, which has been released to the Tsunami Warning Centers for operational use, are identical to those obtained by the researcher during the development of the forecast model. The second objective is to test the forecast model for consistency, accuracy, time efficiency, and quality of results over a range of possible tsunami locations and magnitudes. The third objective is to identify bugs and issues in need of resolution by the researcher who developed the Forecast Model or by the forecast software development team before the next version release to NOAA's two Tsunami Warning Centers.

Local hardware and software applications, and tools familiar to the researcher(s), are used to run the Method of Splitting Tsunamis (MOST) model during the forecast model development. The test results presented in this report lend confidence that the model performs as developed and produces the same results when initiated within the forecast application in an operational setting as those produced by the researcher during the forecast model development. The test results assure those who rely on the Portland tsunami forecast model that consistent results are produced irrespective of system.

C.2 Testing Procedure

The general procedure for forecast model testing is to run a set of synthetic tsunami scenarios through the forecast system application and compare the results with those obtained by the researcher during the forecast model development and presented in the Tsunami Forecast Model Report. Specific steps taken to test the model include:

- Identification of testing scenarios, including the standard set of synthetic events and customized synthetic scenarios that may have been used by the researcher(s) in developing the forecast model.
- Creation of new events to represent customized synthetic scenarios used by the researcher(s) in developing the forecast model, if any.

- Submission of test model runs with the forecast system, and export of the results from A, B, and C grids, along with time series.
- Recording applicable metadata, including the specific version of the forecast system used for testing.
- Examination of forecast model results from the forecast system for instabilities in both time series and plot results.
- Comparison of forecast model results obtained through the forecast system with those obtained during the forecast model development.
- Summarization of results with specific mention of quality, consistency, and time efficiency.
- Reporting of issues identified to modeler and forecast software development team.
- Retesting the forecast models in the forecast system when reported issues have been addressed or explained.

Synthetic model runs were tested on a DELL PowerEdge R510 computer equipped with two Xeon E5670 processors at 2.93 GHz, each with 12 MBytes of cache and 32GB memory. The processors are hex core and support hyperthreading, resulting in the computer performing as a 24 processor core machine. Additionally, the testing computer supports 10 Gigabit Ethernet for fast network connections. This computer configuration is similar or the same as the configurations of the computers installed at the Tsunami Warning Centers so the compute times should only vary slightly.

C.3 Results

The Portland forecast model was tested with NOAA‘s tsunami forecast system version 3.2.

The Portland, Maine forecast model was tested with three synthetic scenarios. Test results from the forecast system and comparisons with the results obtained during the forecast model development are shown numerically in Table C.1 and graphically in Figures 1–3 (to be compared with Figures 25, 17, and 23 respectively). The results show that the forecast model is stable and robust, with consistent and high quality results across geographically distributed tsunami sources and mega-event tsunami magnitudes. The model run time (wall clock time) was under 28 minutes for 12 hours of simulation time, and under 9 minutes for 4 hours. This run time is under the 10 minute run time for 4 hours of simulation time and that satisfies time efficiency requirements.

Three synthetic events were run on the Portland forecast model. The modeled scenarios were stable for all cases tested, with no instabilities or ringing. Results show that the largest modeled height was 138.4 cm and originated in the Caribbean (ATSZ 48-57) source. Amplitudes less than 100 cm were recorded for two test sources. The smallest signal of 20.57 cm was recorded for the far field South Sandwich Islands (SSSZ 1-10) source. Direct comparisons, of output from the forecast tool with results from available development synthetic events, demonstrated that the wave patterns were similar in shape and amplitude with only slight differences.

Note: The maximum and minimum amplitudes are from time series plots in the report.

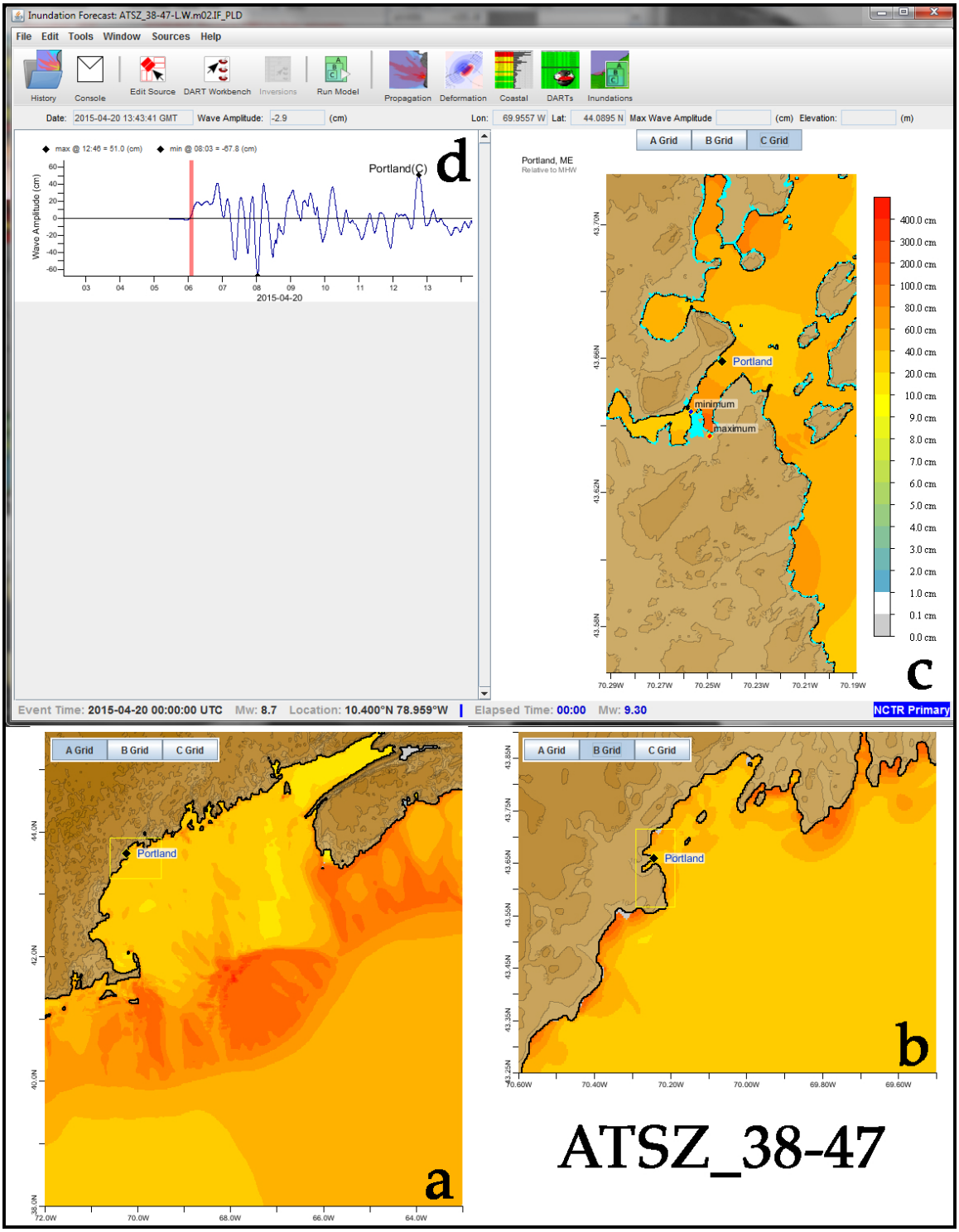

Figure C.1: Response of the Portland forecast model to synthetic scenario ATSZ 38–47 ($\alpha = 25$) using SIFT version 3.2. Panels (a), (b), and (c) counterclockwise from the lower left show the maximum sea surface elevation in the A, B, and C grids, respectively with a common color scale. The time series at the Portland tide gauge warning point is shown in panel (d). The results obtained during development are displayed in Figure 25.

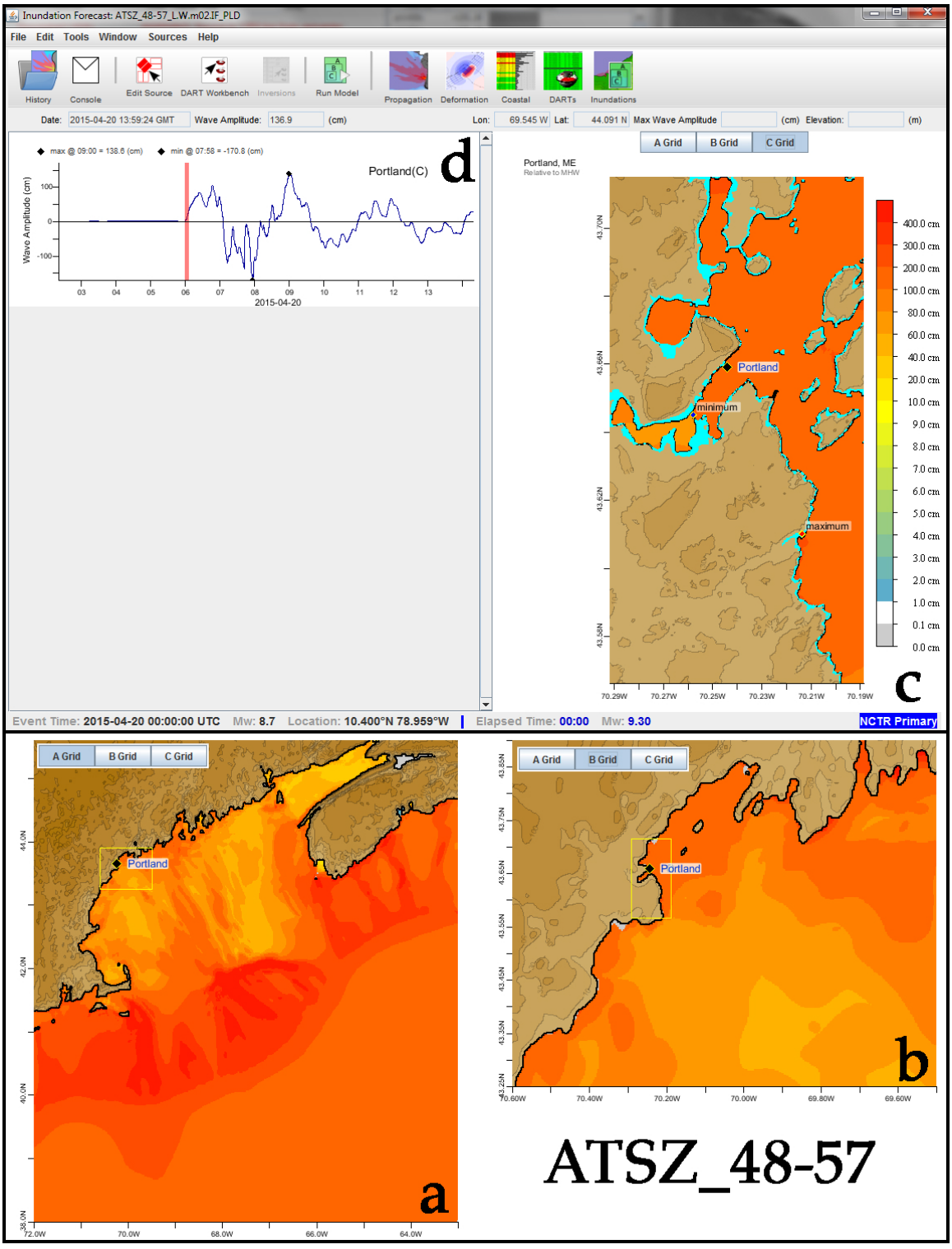

Figure C.2: As in Figure C.3 but for the synthetic scenario ATSZ 48–57 ($\alpha = 25$). The results obtained during development are displayed in Figure 17.

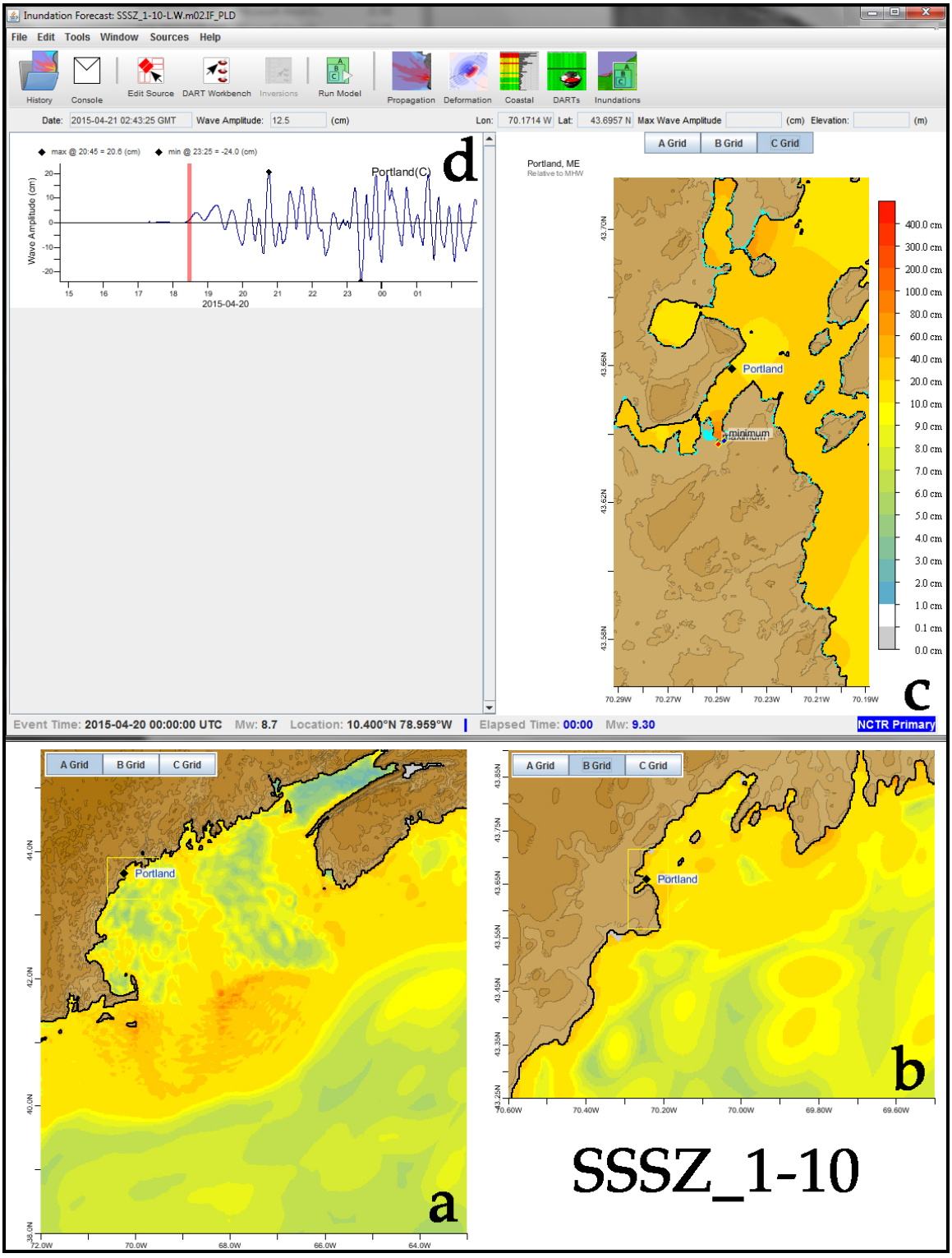

Figure C.3: As in Figure C.3 but for the synthetic scenario SSSZ 1–10 (α = 25). The results obtained during development are displayed in Figure 23.

Scenario Name	Source Zone	Tsunami Source	α [μ]	SIFT Max (cm)	Development Max (cm)	SIFT Min (cm)	Development Min (cm)	SIFT C Grid Max (cm)	Development C Grid Max (cm)	SIFT C Grid Min (cm)	Development C Grid Min (cm)	SIFT Flooded Area (km2)	Development Flooded Area (km2)
Mega-tsunami Scenarios													
ATSZ 38-47	Caribbean	A38-47, B38-47	25	51.0	51.08	-67.8	-66.9	174.5	172.8	-192.1	-190.4	1.883	1.897
ATSZ 48-57	Caribbean	A48-57, B48-57	25	138.6	138.4	-170.8	-174.3	321.9	317.8	-778.8	-763.9	4.426	4.430
SSSZ 1-10	South Sandwich Islands	A1-10, B1-10	25	20.6	20.57	-24.0	-23.7	103.9	103.5	-90.8	-90.43	0.767	0.761

Table C.1: Table of maximum and minimum amplitudes (cm) at the Portland, Maine warning point for synthetic and historical events tested using SIFT 3.2 and those obtained during development.

Glossary

Arrival time The time when the first tsunami wave is observed at a particular location, typically given in local and/or universal time, but also commonly noted in minutes or hours relative to the time of the earthquake.

Bathymetry The measurement of water depth of an undisturbed body of water.

Cascadia Subduction Zone Fault that extends from Cape Mendocino in Northern California northward to mid-Vancouver Island Canada. The fault marks the convergence boundary where the Juan de Fuca tectonic plate is being subducted under the margin of the North America plate.

Current speed The scalar rate of water motion measured as distance/time.

Current velocity Movement of water expressed as a vector quantity. Velocity is the distance of movement per time coupled with direction of motion.

Digital Elevation Model (DEM) A digital representation of bathymetry or topography based on regional survey data or satellite imagery. Data are arrays of regularly spaced elevations referenced to a map projection of the geographic coordinate system.

Epicenter The point on the surface of the earth that is directly above the focus of an earthquake.

Focus The point beneath the surface of the earth where a rupture or energy release occurs due to a buildup of stress or the movement of earth's tectonic plates relative to one another.

Inundation The horizontal inland extent of land that a tsunami penetrates, generally measured perpendicularly to a shoreline.

Marigram Tide gauge recording of wave level as a function of time at a particular location. The instrument used for recording is termed a marigraph.

Moment Magnitude (M_W) The magnitude of an earthquake on a logarithmic scale in terms of the energy released. Moment magnitude is based on the size and characteristics of a fault rupture as determined from long-period seismic waves.

Method of Splitting Tsunamis (MOST) A suite of numerical simulation codes used to provide estimates of the three processes of tsunami evolution: tsunami generation, propagation, and inundation.

Near–field A particular location at which the earth's deformation due to energy release affects the modeling solution.

Propagation database A basin-wide database of pre-computed water elevations and flow velocities at uniformly spaced grid points throughout the world oceans. Values are computed from tsunamis generated by earthquakes with a fault rupture at any one of discrete 100 × 50 km unit sources along worldwide subduction zones.

Runup Vertical difference between the elevation of tsunami inundation and the sea level at the time of a tsunami. Runup is the elevation of the highest point of land inundated by a tsunami as measured relative to a stated datum, such as mean sea level.

Short-term Inundation Forecasting for Tsunamis (SIFT) A tsunami forecast system that integrates tsunami observations in the deep-ocean with numerical models to provide an estimate of tsunami wave arrival and amplitude at specific coastal locations while a tsunami propagates across an ocean basin.

Subduction zone A submarine region of the earth's crust at which two or more tectonic plates converge to cause one plate to sink under another, overriding plate. Subduction zones are regions of high seismic activity.

Synthetic event Hypothetical events based on computer simulations or theory of possible or even likely future scenarios.

Tidal wave Term frequently used incorrectly as a synonym for tsunami. A tsunami is unrelated to the predictable periodic rise and fall of sea level due to the gravitational attractions of the moon and sun: the tide.

Tide The predictable rise and fall of a body of water (ocean, sea, bay, etc.) due to the gravitational attractions of the moon and sun.

Tide gauge An instrument for measuring the rise and fall of a column of water over time at a particular location.

Tele–tsunami or distant tsunami or far–field tsunami Most commonly, a tsunami originating from a source greater than 1000 km away from a particular location. In some contexts, a tele-tsunami is one that propagates through deep-ocean before reaching a particular location without regard to distance separation.

Travel time The time it takes for a tsunami to travel from the generating source to a particular location.

tsunami A Japanese term that literally translates to "harbor wave." Tsunamis are a series of long–period shallow water waves that are generated by the sudden displacement of water due to subsea disturbances such as earthquakes, submarine landslides, or volcanic eruptions. Less commonly, meteoric impact to the ocean or meteorological forcing can generate a tsunami.

Tsunami Hazard Assessment A systematic investigation of seismically active regions of the world oceans to determine their potential tsunami impact at a particular location.

Numerical models are typically used to characterize tsunami generation, propagation, and inundation, and to quantify the risk posed to a particular community from tsunamis generated in each source region investigated.

Tsunami Propagation The directional movement of a tsunami wave outward from the source of generation. The speed at which a tsunami propagates depends on the depth of the water column in which the wave is traveling. Tsunamis travel at a speed of 700 km/hr (450 mi/hr) over the average depth of 4000 m in the open deep Pacific Ocean.

Tsunami source Location of tsunami origin, most typically an underwater earthquake epicenter. Tsunamis are also generated by submarine landslides, underwater volcanic eruptions, or, less commonly, by meteoric impact of the ocean.

Wave amplitude The maximum vertical rise or drop of a column of water as measured from wave crest (peak) or trough to a defined mean water level state.

Wave crest or peak The highest part of a wave or maximum rise above a defined mean water level state, such as mean lower low water.

Wave height The vertical difference between the highest part of a specific wave (crest) and it's corresponding lowest point (trough).

Wavelength The horizontal distance between two successive wave crests or troughs.

Wave period The length of time between the passage of two successive wave crests or troughs as measured at a fixed location.

Wave trough The lowest part of a wave or the maximum drop below a defined mean water level state, such as mean lower low water.